ผลของตัวทำละลายที่มีต่อรอยต่อของเส้นใยนาโนไททาเนียมไดออกไซด์-พอลิไวนิลไพโรลิโดน/พอลิอะคริโลไนไตรล์ที่ยืดหยุ่นได้

นางสาวเวโรนิก้า วิโนโต้

วิทยานิพนธ์นี้เป็นส่วนหนึ่งของการศึกษาตามหลักสูตรปริญญาวิศวกรรมศาสตรมหาบัณฑิต
สาขาวิชาวิศวกรรมเคมี ภาควิชาวิศวกรรมเคมี
คณะวิศวกรรมศาสตร์ จุฬาลงกรณ์มหาวิทยาลัย
ปีการศึกษา 2557

Effect of solvent on interface of TiO_2-PVP/PAN flexible nanofibers

Miss Veronica Winoto

A Thesis Submitted in Partial Fulfillment of the Requirements
for the Degree of Master of Engineering Program in Chemical Engineering
Department of Chemical Engineering
Faculty of Engineering
Chulalongkorn University
Academic Year 2014

Thesis Title	Effect of solvent on interface of TiO_2-PVP/PAN flexible nanofibers
By	Miss Veronica Winoto
Field of Study	Chemical Engineering
Thesis Advisor	Associate Professor Varong Pavarajarn, Ph.D.

Accepted by the Faculty of Engineering, Chulalongkorn University in Partial Fulfillment of the Requirements for the Master's Degree

.....Dean of the Faculty of Engineering
(Professor Bundhit Eua-arporn, Ph.D.)

THESIS COMMITTEE

.....Chairman
(Associate Professor Tawatchai Charinpanitkul, D.Eng.)

.....Thesis Advisor
(Associate Professor Varong Pavarajarn, Ph.D.)

.....Examiner
(Assistant Professor Apinan Soottitantawat, D.Eng.)

.....External Examiner
(Associate Professor Panu Danwanichakul, Ph.D.)

เวโรนิก้า วิโนโต้ : ผลของตัวทำละลายที่มีต่อรอยต่อของเส้นใยนาโนไททาเนียมไดออกไซด์-พอลิไวนิลไพโรลิโดน/พอลิอะคริโลไนไตรล์ที่ยืดหยุ่นได้ (Effect of solvent on interface of TiO_2-PVP/PAN flexible nanofibers) อ.ที่ปรึกษาวิทยานิพนธ์หลัก: รศ. ดร.วรงค์ ปวราจารย์, 186 หน้า.

การเตรียมตัวเร่งปฏิกิริยาเส้นใยนาโนแบบแกนร่วม ไททาเนียมไดออกไซด์-พอลิไวนิลไพโรลิโดน/พอลิอะคริโลไนไตรล์ที่ยืดหยุ่นได้ ด้วยกระบวนการโซล-เจลร่วมด้วยกระบวนการอิเล็กโตรสปินนิ่ง (การปั่นเส้นใยด้วยไฟฟ้าสถิต) ใช้สารพอลิอะคริโลไนไตรล์ที่ละลายในสารไดเมทิลฟอร์มาไมด์ในการเตรียมสารละลายพอลิเมอร์ส่วนแกน ในส่วนของสารละลายเปลือกหุ้มนั้นใช้สารพอลิไวนิลไพโรลิโดนเป็นพอลิเมอร์ โดยมีไททาเนียมเตตระไอโซโพรพอกไซด์เป็นสารตั้งต้นไททาเนีย สำหรับตัวทำละลายของสารละลายเปลือกหุ้มนั้นจะเลือกใช้ตัวทำละลายสองชนิด ได้แก่ สารไดเมทิลฟอร์มาไมด์และเอทานอล สารพอลิอะคริโลไนไตรล์นั้นมีข้อจำกัดในแง่ของตัวทำละลาย การเปลี่ยนตัวทำละลายมีผลต่อโครงสร้างและคุณสมบัติของตัวเร่งปฏิกิริยาเส้นใยนาโนแบบยืดหยุ่นได้ ในงานวิจัยนี้ศึกษาการเปลี่ยนแปลงที่เกิดขึ้นต่อโครงสร้างของตัวเร่งปฏิกิริยา โดยการเปลี่ยนความเข้มข้นของสารพอลิไวนิลไพโรลิโดน การเปลี่ยนปริมาตรของไททาเนียมเตตระไอโซโพรพอกไซด์ การเปลี่ยนแปลงระยะเวลาในการบ่มเจลของไททาเนีย และศักย์ไฟฟ้าในกระบวนการอิเล็กโตรสปินนิ่งของตัวทำละลายทั้งสองชนิด เครื่องมือที่ใช้ในการวิเคราะห์โครงสร้างทางสัณฐานวิทยาและคุณสมบัติของตัวเร่งปฏิกิริยาเส้นใยนาโนแบบยืดหยุ่นในงานวิจัยนี้คือ เครื่องมือวิเคราะห์สารด้วยอินฟราเรด (Fourier transform infrared spectroscopy (FTIR)) กล้องจุลทรรศ์อิเล็กตรอนแบบส่องกราดร่วมด้วยเครื่องวิเคราะห์ธาตุ (Scanning electron microscopy with energy-dispersive x-ray (SEM-EDX)) กล้องจุลทรรศ์อิเล็กตรอนแบบส่องผ่าน (Transmission electron microscope (TEM)) และเครื่องวิเคราะห์การเลี้ยวเบนรังสีเอกซ์ (X-ray diffraction (XRD)) จากการทำการทดลองพบว่าเมื่อใช้สารไดเมทิลฟอร์มาไมด์เป็นตัวทะละลายในสาร ละลายเปลือก จะไม่มีบริเวณรอยต่อระหว่างส่วนของแกนและเปลือกที่ชัดเจน เนื่องจากส่วนของเปลือกสามารถหลอมรวมเข้ากับส่วนของแกนได้ แต่เมื่อใช้เอทานอลเป็นตัวทำละลายในสารละลายเปลือกพบว่า เอทานอลจะทำปฏิกิริยากับสารพอลิอะคริโลไนไตรล์ ทำให้บริเวณรอยต่อของแกนและเปลือกแยกกันอย่างชัดเจน

ภาควิชา วิศวกรรมเคมี ลายมือชื่อนิสิต .....

สาขาวิชา วิศวกรรมเคมี ลายมือชื่อ อ.ที่ปรึกษาหลัก .....

ปีการศึกษา 2557

5670390121 : MAJOR CHEMICAL ENGINEERING

KEYWORDS: TITANIUM DIOXIDE / COAXIAL NANOFIBER / CORE/SHEATH INTERFACE

VERONICA WINOTO: Effect of solvent on interface of TiO_2-PVP/PAN flexible nanofibers. ADVISOR: ASSOC. PROF. VARONG PAVARAJARN, Ph.D., 186 pp.

Flexible TiO_2-PVP/PAN photocatalyst in form of core/sheath nanofibers were fabricated from combining sol-gel method and coaxial electrospinning technique. Polyacrylonitrile (PAN) was selected as core polymer, while polyvinylpyrrolidone (PVP) was selected as polymer for sheath solution to occur sol-gel process of titania. There are two solvents that commonly used in sol-gel process of titania, which are DMF and ethanol. PAN has limited solubility, therefore, the effect of solvent that occur at core/sheath interface is greatly affected properties of the final products. This research would mainly focus on investigating the effect of solvent at core/sheath interface in flexible nanofibers. The various conditions such as polymer concentration (PVP), titania-precusor (TTIP) amount, aging time of titania-precusor solution and electrical potential used in electrospinning process were investigated their effects. The resultant fibers were characterized by Fourier transform infrared spectroscopy (FTIR), Scanning electron microscopy with energy-dispersive x-ray (SEM-EDX), Transmission electron microscope (TEM), and X-ray diffraction (XRD). The result shows that there is no core/sheath interface when using DMF as solvent in sheath solution and the components from sheath section diffused into core section. After changing the solvent to ethanol, ethanol interact with PAN at core/sheath interface and this prevent fusion of sheath section into core section.

Department: Chemical Engineering Student's Signature .....

Field of Study: Chemical Engineering Advisor's Signature .....

Academic Year: 2014

ACKNOWLEDGEMENTS

First and foremost I would like to express my sincerest gratitude to my advisor, Associate Professor Dr. Varong Pavarajarn, Ph.D. who has supported me thoughout my thesis, excellent guidance, valuable encouragement, knowledge and patience. Without him this thesis would not have been written and completed. I am greatful to Associate Professor Dr. Tawatchai Charinpanitkul, Ph.D., Assistant Professor Dr. Apinan Soottitantawat Ph.D., and Associate Professor Dr. Panu Danwanichakul Ph.D. for serving as chairman and thesis committees respectively.

I would like to thank Miss Kamonwan Ananthaprayoon, all my friends and all members at Center of Excellence in Particle Technology (CEPT).

Finally, I would like to dedicate this thesis thoughtfully to my beloved parents, my grandparents and my families all who have always been supporting me, encouraging me with their best wishes and standing by my side through the good times and bad.

CONTENTS

Page

THAI ABSTRACT iv

ENGLISH ABSTRACT v

ACKNOWLEDGEMENTS vi

CONTENTS vii

LIST OF FIGURES xi

LIST OF TABLES xvii

CHAPTER I INTRODUCTION 1

CHAPTER II THEORY AND LITERATURE REVIEWS 4

2.1. Physical Properties of Materials Used 4

2.1.1. Titanium (IV) oxide 4

2.1.2. Polyacrylonitrile 7

2.1.3. Polyvinylpyrrolidone 8

2.1.4. Solvent for sheath solution 8

2.1.5. Methylene blue dye 9

2.2. Fabrication of TiO_2-PVP/PAN flexible nanofibers 9

2.2.1. Sol-gel process 9

2.2.2. Electrospinning process 10

2.2.3. Coaxial electrospinning process 12

2.3. Photocatalytic process 14

2.4. The effect of solvent at the interface investigation by spin coating technique 17

CHAPTER III EXPERIMENT 19

3.1. Chemicals 19

Page

3.2. Materials and equipments 19
3.3. Preparation of electrospinning solutions 20
3.3.1. Preparation of core solution 20
3.3.2. Preparation of sheath solution 20
3.4. Fabrication of core/sheath nanofibers 21
3.5. Calcination of as spun TiO_2-PVP/PAN core/sheath nanofibers 21
3.6. Producing thin films from spin coating technique 22
3.7. Photocatalytic process 22
3.8. Characterizations 22
3.8.1. Fourier transform infrared spectroscopy (FTIR) 22
3.8.2. X-ray diffraction (XRD) 23
3.8.3. Scanning electron microscopy with energy-dispersive x-ray (SEM-EDX). .. 23
3.8.4. Transmission electron microscope (TEM) 23
CHAPTER IV RESULTS AND DISCUSSION 24
4.1. Interaction among components in each solution 24
4.1.1. PAN and DMF 24
4.1.2. PVP and DMF 29
4.1.3. PVP and ethanol 32
4.1.4. TTIP, DMF and acetic acid 35
4.1.5. TTIP, ethanol and acetic acid 39
4.1.6. PVP solution and titania-precursor solution (both DMF solvent) 42
4.1.7. PVP solution and titania-precursor solution (both ethanol solvent) 44
4.1.8. Core solution and ethanol 47

Page

4.1.9. Core solution and sheath solution (DMF in sheath) 51
4.1.10. Core solution and sheath solution (ethanol solvent) 55
4.2. Core/Sheath structure confirmation 60
4.2.1. Core/Sheath structure (DMF in sheath) 60
4.2.2. Core/Sheath structure (ethanol in sheath) 62
4.2.3. Flexibility of resultant nanofibers 64
4.3. Morphology of resultant nanofibers 65
4.3.1. Effect of PVP concentration (DMF in sheath) 65
4.3.2. Effect of PVP concentration (ethanol in sheath) 67
4.3.3. Effect of TTIP amount (DMF in sheath) 69
4.3.4. Effect of TTIP amount (ethanol in sheath) 71
4.3.5. Effect of aging time of titania-precursor (DMF in sheath) 73
4.3.6. Effect of aging time of titania-precursor (ethanol in sheath) 75
4.3.7. Effect of electrical potential used (DMF in sheath) 77
4.3.8. Effect of electrical potential used (ethanol in sheath) 79
4.4. Core/Sheath interface studied by spin coating 82
4.4.1. For DMF in sheath 83
4.4.2. For ethanol in sheath 89
4.4.3. Core/Sheath interface when spins in another form 95
4.5. Photocatalytic activity 98
CHAPTER V CONCLUSIONS 105
5.1. Summary of the results 105
5.2. Conclusions 107

Page

REFERENCES 108

APPENDIX 118

APPENDIX A FTIR transmittance spectra 119

APPENDIX B FTIR spectra and table of peak which used to compare the structure of electrospinning nanofibers and spin coating films. 125

APPENDIX C SEM-EDX mapping of resultant core/sheath films. 165

APPENDIX D EDX patterns and atomic percentage of both films and calcined films. 173

APPENDIX E List of publication 181

VITA 186

LIST OF FIGURES

Page

Figure 2.1. Planar Ti_3O building-block representation (top) and TiO_6 polyhedra (bottom) for the TiO_2 phases rutile (a), anatase (b) and brookite (c) (Ti = white; O = red) [21]. 5

Figure 2.2. The overview of sol-gel process (https://str.llnl.gov/str/May05/gifs/Satcher 1.jpg). 10

Figure 2.3. Schematic diagram of the electrospinning apparatus [39]..... 11

Figure 2.4. Schematic of coaxial electrospinning process [43]..... 12

Figure 2.5. The alternative setup for coaxial electrospinning. A: capillary contains sheath solution, B: Taylor cone from sheath solution, C: smaller capillary contains core solution, D: Taylor cone from core solution, form core-shell structure and E: coaxial jet [43]. 13

Figure 2.6. Illustration of compound Taylor cone formation. A: charges on surface of sheath solution, B: viscous drag exerted on the core and C: sheath- core compound Taylor cone formed due to continuous viscous drag [43]..... 14

Figure 2.7. Schematic diagram illustrating photocatalytic principle of TiO_2 [47]..... 16

Figure 2.8. MB photocatalytic degradation pathway and its intermediates [5]. 17

Figure 4.1. FTIR transmittance spectra of (a) PAN, (b) core solution and (c) DMF. 25

Figure 4.2. FTIR transmittance spectra of (a) PVP, (b) PVP solution and (c) DMF. 29

Figure 4.3. FTIR transmittance spectra of (a) PVP, (b) PVP solution and (c) ethanol... 32

Figure 4.4. FTIR transmittance spectra of (a) TTIP, (b) acetic acid, (c) titania-precursor solution and (d) DMF. 36

LIST OF FIGURES

Page

Figure 4.5. FTIR transmittance spectra of (a) TTIP, (b) acetic acid, (c) titania-precursor solution and (d) ethanol. 41

Figure 4.6. FTIR transmittance spectra of (a) PVP solution, (b) sheath solution and (c) titania-precursor solution – DMF solvent. 43

Figure 4.7. FTIR transmittance spectra of (a) PVP solution, (b) sheath solution and (c) titania-precursor solution – ethanol solvent. 45

Figure 4.8. Picture of the obtained solution. 47

Figure 4.9. Schematic picture of the composition of the surface layer [75]. 48

Figure 4.10. FTIR transmittance spectra of (a) core solution, (b) solid phase of mixed solution, (c) liquid phase of mixed solution and (d) ethanol. 49

Figure 4.11. FTIR transmittance spectra of (a) core solution, (b) gel of core/sheath solution, (c) liquid phase of core/sheath solution and (d) sheath solution – DMF in sheath. 52

Figure 4.12. Picture of the obtained solution. 56

Figure 4.13. FTIR transmittance spectra of (a) core solution, (b) solid phase of core/sheath solution, (c) liquid phase of core/sheath solution and (d) sheath solution – ethanol in sheath. 57

Figure 4.14. TEM images of resultant core/sheath nanofibers (a) as spun and (b) calcined. 61

Figure 4.15. TEM images of (a) microtome of calcined nanofibers and (b) SAED pattern. 61

Figure 4.16. TEM images of resultant core/sheath nanofibers (a) as spun and (b) calcined. 62

LIST OF FIGURES

Page

Figure 4.17. TEM images of (a) microtome - 1 of calcined nanofibers, (b) SAED pattern of (a), (c) microtome - 2 of calcined nanofibers, and (d) SAED pattern of (c). 63

Figure 4.18. EDX patterns of microtome - 2 of calcined nanofibers. 63

Figure 4.19. (a) core/sheath calcined nanofibers – DMF in sheath, (b) curved to 3.4 mm and (c) 1.3 mm radius of curvature..... 64

Figure 4.20. (a) core/sheath calcined nanofibers – ethanol in sheath, (b) curved to 3.4 mm and (c) 1.3 mm radius of curvature. 64

Figure 4.21. SEM micrographs of resultant core/sheath nanofibers; PAN was fixed at 8wt% (a) PVP 10wt%, (b) PVP 11.5wt%, (c) PVP 13wt%, (d) calcined PVP 10wt%, (e) calcined PVP 11.5wt% and (f) calcined PVP 13wt% – DMF in sheath..... 66

Figure 4.22. The size distribution of resultant core/sheath nanofibers; PAN was fixed at 8wt% (a) PVP 10wt%, (b) PVP 11.5wt%, (c) PVP 13wt%, (d) calcined PVP 10wt%, (e) calcined PVP 11.5wt% and (f) calcined PVP 13wt% – DMF in sheath..... 67

Figure 4.23. SEM micrographs of resultant core/sheath nanofibers; PAN was fixed at 8wt% (a) PVP 10wt%, (b) PVP 11.5wt%, (c) PVP 13wt%, (d) calcined PVP 10wt%, (e) calcined PVP 11.5wt% and (f) calcined PVP 13wt% – ethanol in sheath..... 68

Figure 4.24. The size distribution of resultant core/sheath nanofibers; PAN was fixed at 8wt% (a) PVP 10wt%, (b) PVP 11.5wt%, (c) PVP 13wt%, (d) calcined PVP 10wt%, (e) calcined PVP 11.5wt% and (f) calcined PVP 13wt% – ethanol in sheath..... 69

Figure 4.25. SEM micrographs of resultant core/sheath nanofibers (a) TTIP 11vol%, (b) TTIP 15.5vol%, (c) TTIP 20vol%, (d) calcined TTIP 11vol%, (e) calcined TTIP 15.5vol% and (f) calcined TTIP 20vol% –DMF in sheath..... 70

Figure 4.26. The size distribution of resultant core/sheath nanofibers (a) TTIP 11vol%, (b) TTIP 15.5vol%, (c) TTIP 20vol%, (d) calcined TTIP 11vol%, (e) calcined TTIP 15.5vol% and (f) calcined TTIP 20vol% –DMF in sheath..... 71

LIST OF FIGURES

Page

Figure 4.27. SEM micrographs of resultant core/sheath nanofibers (a) TTIP 11vol%, (b) TTIP 15.5vol%, (c) TTIP 20vol%, (d) calcined TTIP 11vol%, (e) calcined TTIP 15.5vol% and (f) calcined TTIP 20vol% –ethanol in sheath..... 72

Figure 4.28. The size distribution of resultant core/sheath nanofibers (a) TTIP 11vol%, (b) TTIP 15.5vol%, (c) TTIP 20vol%, (d) calcined TTIP 11vol%, (e) calcined TTIP 15.5vol% and (f) calcined TTIP 20vol% –ethanol in sheath..... 73

Figure 4.29. SEM micrographs of resultant core/sheath nanofibers (a) age 0 min, (b) age 15 min, (c) age 30 min, (d) calcined age 0 min, (e) calcined age 15 min and (f) calcined age 30 min –DMF in sheath. 74

Figure 4.30. The size distribution of resultant core/sheath nanofibers (a) age 0 min, (b) age 15 min, (c) age 30 min, (d) calcined age 0 min, (e) calcined age 15 min and (f) calcined age 30 min –DMF in sheath. 75

Figure 4.31. SEM micrographs of resultant core/sheath nanofibers (a) age 0 min, (b) age 15 min, (c) age 30 min, (d) calcined age 0 min, (e) calcined age 15 min and (f) calcined age 30 min –ethanol in sheath. 76

Figure 4.32. The size distribution of resultant core/sheath nanofibers (a) age 0 min, (b) age 15 min, (c) age 30 min, (d) calcined age 0 min, (e) calcined age 15 min and (f) calcined age 30 min –ethanol in sheath. 77

Figure 4.33. SEM micrographs of resultant core/sheath nanofibers (a) 22 kV, (b) 24 kV, (c) 26 kV, (d) calcined 22 kV, (e) calcined 24 kV and (f) calcined 26 kV – DMF in sheath. 78

Figure 4.34. The size distribution of resultant core/sheath nanofibers (a) 22 kV, (b) 24 kV, (c) 26 kV, (d) calcined 22 kV, (e) calcined 24 kV and (f) calcined 26 kV – DMF in sheath. 79

LIST OF FIGURES

Page

Figure 4.35. SEM micrographs of resultant core/sheath nanofibers (a) 22 kV, (b) 24 kV, (c) 26 kV, (d) calcined 22 kV, (e) calcined 24 kV and (f) calcined 26 kV – ethanol in sheath. 80

Figure 4.36. The size distribution of resultant core/sheath nanofibers (a) 22 kV, (b) 24 kV, (c) 26 kV, (d) calcined 22 kV, (e) calcined 24 kV and (f) calcined 26 kV – ethanol in sheath. 81

Figure 4.37. SEM micrographs of resultant core/sheath (a) rough and (b) smooth nanofibers..... 82

Figure 4.38. Schematic of multilayer spin coating film..... 83

Figure 4.39. FTIR transmittance spectra of (a) fiber, (b) film, (c) calcined fiber and (d) calcined film – DMF in sheath. 84

Figure 4.40. SEM-EDX mapping of resultant core/sheath films (a) as spun and (b) calcined – DMF in sheath. 89

Figure 4.41. EDX patterns and atomic percentage of resultant core/sheath films (a) as spun and (b) calcined – DMF in sheath. 89

Figure 4.42. FTIR transmittance spectra of (a) fiber, (b) film, (c) calcined fiber and (d) calcined film – ethanol in sheath. 90

Figure 4.43. SEM-EDX mapping of resultant core/sheath films (a) as spun and (b) calcined – ethanol in sheath. 95

Figure 4.44. EDX patterns and atomic percentage of resultant core/sheath films (a) as spun and (b) calcined – ethanol in sheath. 95

Figure 4.45. SEM-EDX mapping of resultant core/sheath films when spin sheath first (a) DMF and (b) ethanol in sheath. 96

Figure 4.46. EDX patterns and atomic percentage of resultant core/sheath films when spin sheath first (a) DMF and (b) ethanol in sheath..... 96

LIST OF FIGURES

Page

Figure 4.47. SEM-EDX mapping of resultant core/sheath films when core section dried before spin sheath (a) DMF and (b) ethanol in sheath. 97

Figure 4.48. EDX patterns and atomic percentage of resultant core/sheath films when core section dried before spin sheath (a) DMF and (b) ethanol in sheath. 97

Figure 4.49. XRD patterns of coaxial nanofibers. 101

Figure 4.50. XRD patterns of sheath nanofibers. 102

Figure 4.51. XRD patterns of P25 commercial powder. 103

Figure 4.52. XRD patterns of sheath solution's powder. 104

LIST OF TABLES

Page

Table 4.1. FTIR peak assignment for PAN. 26

Table 4.2. FTIR peak assignment for core solution. 27

Table 4.3. FTIR peak assignment for DMF. 28

Table 4.4. FTIR peak assignment for PVP. 30

Table 4.5. FTIR peak assignment for PVP solution. 31

Table 4.6. FTIR peak assignment for PVP solution. 33

Table 4.7. FTIR peak assignment for ethanol. 34

Table 4.8. FTIR peak assignment for TTIP. 36

Table 4.9. FTIR peak assignment for acetic acid. 37

Table 4.10. FTIR peak assignment for titania-precursor solution. 38

Table 4.11. FTIR peak assignment for titania-precursor solution. 41

Table 4.12. FTIR peak assignment for sheath solution. 43

Table 4.13. FTIR peak assignment for sheath solution. 45

Table 4.14. FTIR peak assignment for solid phase of mixed solution. 49

Table 4.15. FTIR peak assignment for liquid phase of mixed solution. 50

Table 4.16. FTIR peak assignment for gel of core/sheath solution. 53

Table 4.17. FTIR peak assignment for liquid phase of core/sheath solution. 54

Table 4.18. FTIR peak assignment for solid phase of core/sheath solution. 57

Table 4.19. FTIR peak assignment for liquid phase of core/sheath solution. 59

Table 4.20. Size and standard deviation of resultant core/sheath nanofibers – vary PVP concentration and DMF in sheath. 66

LIST OF TABLES

Page

Table 4.21. Size and standard deviation of resultant core/sheath nanofibers – vary PVP concentration and ethanol in sheath. 68

Table 4.22. Size and standard deviation of resultant core/sheath nanofibers – vary TTIP amount and DMF in sheath. 70

Table 4.23. Size and standard deviation of resultant core/sheath nanofibers – vary TTIP amount and ethanol in sheath. 72

Table 4.24. Size and standard deviation of resultant core/sheath nanofibers – vary aging time and DMF in sheath. 74

Table 4.25. Size and standard deviation of resultant core/sheath nanofibers – vary aging time and ethanol in sheath. 76

Table 4.26. Size and standard deviation of resultant core/sheath nanofibers – vary electrical potential and DMF in sheath. 78

Table 4.27. Size and standard deviation of resultant core/sheath nanofibers – vary electrical potential and ethanol in sheath. 80

Table 4.28. FTIR peak assignment for resultant nanofibers. 84

Table 4.29. FTIR peak assignment for resultant film. 85

Table 4.30. FTIR peak assignment for resultant calcined nanofibers. 86

Table 4.31. FTIR peak assignment for resultant calcined film. 87

Table 4.32. FTIR peak assignment for resultant nanofibers. 90

Table 4.33. FTIR peak assignment for resultant film. 92

Table 4.34. FTIR peak assignment for resultant calcined nanofibers. 93

Table 4.35. FTIR peak assignment for resultant calcined film. 94

Table 4.36. Degradation percentage of various condition of both coaxial nanofibers and sheath solution's powder (using the UV-A lamp). 99

LIST OF TABLES

Page

Table 4.37. Degradation percentage of PVP 11.5wt%/TTIP 15.5wt%/Age 15 min/24 kV in various photocatalyst type with both UV-A and UV-B lamp. 100

CHAPTER I

INTRODUCTION

Nowadays, people are concerned about environmental problems and one of the main problems is water pollution. Water pollution caused by the contamination of unwanted materials in the water resource, such as organic chemicals from agricultural, automotive factory, chemical industry, computer and electronics manufacturing industry, paper dyeing factory, textile dyeing industry and other plants. Most of the contaminants are carcinogens and some leading cause of disabilities, reproductive problems, diseases and deaths. Thus, the removal of the contaminants is necessary. Methylene blue (MB) dye, one of enormous water contaminant, is the common basic dye that found most in paper or printing dyeing factory and textile dyeing industries. At present, there are many researches develop physical, chemical and biological methods to treat colored wastewater [1, 2]. Semiconductor photocatalytic degradation, one of the most effective water treatment process, decomposed the contaminants due to reductive and oxidative reaction occur after the generation of electron-hole pairs and light absorption [3]. Titanium (IV) oxide or titania is used as a photocatalyst in this process.

Titanium (IV) oxide or titania is one of high efficient photocatalyst that has been widely investigated and used because of its high chemical stability, strong oxidizing power of its photogenerated hole [2], nontoxicity, relatively inexpensive and long durability. Besides photocatalyst, the prominent applications of titania are dye-sensitized, solar cells, gas sensor, nanomedicine, skin care product and antimicrobial applications [4]. Titania has a significant degradation effect of both organic and inorganic pollutants. The photocatalytic activity of titania mostly influenced by its properties such as crystal structure, particle size, porosity and specific surface area [5]. Titania photocatalyst can be prepared by various method and also in various

form such as titania nanowires, nanocomposites, nanoparticles, spheres, hollow spheres, nanotubes, nanorods and nanofibers. Titania nanofibers are more suitable form to deal with wastewater compared to the other form because nanofibers can easily been removed and handled after the treatment is complete. Many researches produce titania nanofibers by combining sol-gel method and electrospinning process [6, 7].

Electrospinning first appeared in 1934 as a new method for small diameter fibers fabrication and 35 years later Taylor developed a jet forming and this is the first time that melts polymer could be fabricated into fibers. The research of experimental parameters, fiber morphologies and properties were few and unconcerned until in 1990s electrospinning nanofibers were successfully fabricated. After that, many polymers have been used to fabricate membranes and fiber mats [8]. In present, electrospinning has been considered as nanotechnology for nanofiber production due to its simplicity, inexpensive operation, high efficiency and enable to produce various properties and applications of nanofibers [9]. New technologies have been introduced to improve product from electrospinning process, coaxial electrospinning can accommodate two different fluids and become an extraordinary booming technique [10, 11].

Polyacrylonitrile (PAN) is a polymer with good stability and mechanical properties. There is a wide range of applications using PAN nanofibers because of its temperature resistance and flexibility. The outstanding application of PAN nanofiber is it used as precursors for producing carbon nanofibers, but also used in multiple fields including tissue engineering, sensing, composites and battery separators [12]. It is known PAN has excellent tensile strength because the nitrile groups with a large dipole which provide high cohesive energy density and chain stiffness [13]. Polyvinylpyrrolidone (PVP), functional polymer, has been widely used together with titania in electrospinning process. The properties of PVP that attract attention are a

good environmental stability, easy process ability, moderate electrical conductivity and rich information in charge transport mechanism [14].

Spin coating method was used to produce thin films. Thin films can be used to determine the effect of solvent that occur at interface of materials. The interface phenomena that occur in all materials affected the formation of material properties and structures significantly. Therefore, it is necessary to determine, classify and control material properties. By controlling material properties would lead to the appropriate development process of the product [15, 16].

In this research, flexible TiO_2-PVP/PAN photocatalyst in form of core/sheath nanofibers was fabricated from combining sol-gel method and coaxial electrospinning technique. Polyvinylpyrrolidone (PVP) was selected as polymer for sheath solution to occur sol-gel process of titania. There are two solvents that commonly used in sol-gel process of titania, which are DMF and ethanol. PVP is compatible with both solvent. Polyacrylonitrile (PAN) was selected as core polymer because of its temperature resistance, high flexibility and tensile strength. PAN has limited solubility, it is soluble in polar solvents like N,N'-dimethylformamide (DMF). Hence, the effect of solvent that occur at core/sheath interface has greatly affected properties of the final products. This work would mainly focus on investigating the effect of solvent at core/sheath interface in flexible nanofibers, which the core section is made from polyacrylonitrile (PAN) and the sheath section is made from titanium (IV) oxide (TiO_2)-polyvinylpyrrolidone (PVP). The solvent of the sheath solution was varied to be N,N'-dimethylformamide (DMF) and ethanol.

CHAPTER II

THEORY AND LITERATURE REVIEWS

2.1. Physical Properties of Materials Used

2.1.1. Titanium (IV) oxide

Titanium (Ti) is a gray metal element with molecular weight of 47.9 and oxidation number of +4, +3 and +2. In general, titanium is corrosion resistance and flammable. Normally titanium was found in the form of titanium (IV) dioxide or known as titania (with oxidation number of +4). TiO_2 is also known as titania, titanic oxide, titanium white, titanic anhydride or titanic acid anhydride [17]. Titania, a white semiconductor material with molecular weight of 79.9, has been recognized as one of the major heterogeneous photocatalyst and has three different crystalline forms, which are brookite, anatase and rutile. Crytalline titania was used as photocatalyst degradation of both organic and inorganic pollutants in wastewater treatment.

Brookite is orthorhombic (a = 5.4558 Å, b = 9.1819 Å and c = 5.1429 Å), while anatase and rutile are orthogonal (a = 3.7845 Å, c = 9.5143 Å for anatase and a = 4.5937 Å, c = 2.9587 Å for rutile) [18]. Anatase with band gap ~3.2 eV and rutile with band gap ~3.0 eV, have received the most attention, due to their excellent electronic, chemical and optical properties [19]. Among the three crystal forms of TiO_2, anatase is generally considered to have the highest photocatalytic activity because of its comparatively high density of surface oxygen and low recombination of photogenerated electron-hole pair [20]. The crystalline structures of titania is shown in Figure 2.1.

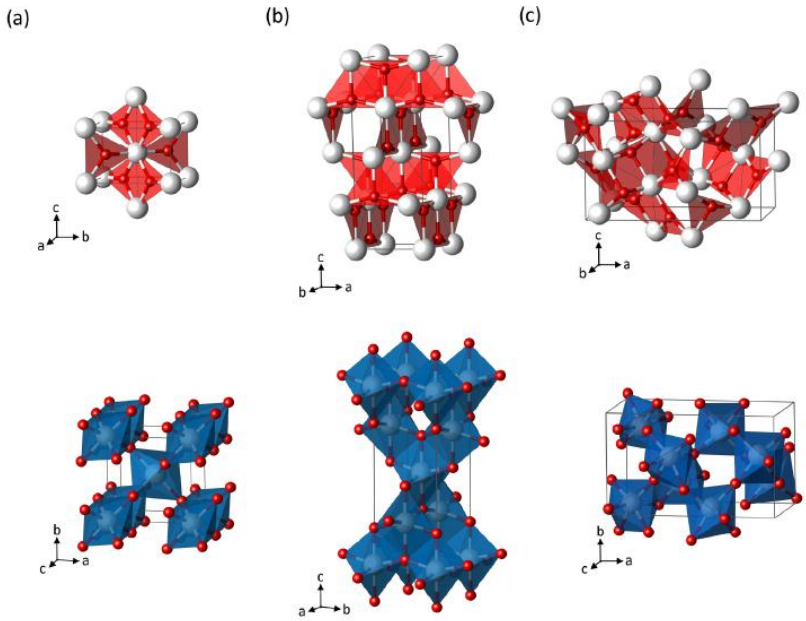

Figure 2.1. Planar Ti_3O building-block representation (top) and TiO_6 polyhedra (bottom) for the TiO_2 phases rutile (a), anatase (b) and brookite (c) (Ti = white; O = red) [21].

The electrospinning technique in photocatalyst research of C.-J. Li and G.-R. Xu (2011) confirmed that TiO_2 composed of anatase phase with a trace percentage of rutile phase had better photocatalytic activity and also report that calcination temperature exhibits different photocatalytic activity due to the increase of temperature TiO_2 transfers from anatase to rutile, the Ti-O bond breaks in the anatase phase and rearranges in octahedral conformation to form the rutile phase [22]. The studied of anatase and rutile ratio that is optimal for photocatalytic activity of electrospun TiO_2/ZnO nanofibers by C.C. Pei and W.W.-F. Leung (2013) shows that the optimal combination of semiconductors can reduce the band gap energy when compared with TiO_2 nanofibers alone and enhance charge separation on photo-

excitation, there reduce electron-hole recombination of increased photocatalytic activity [20].

TiO_2 photocatalysis is widely used in a variety of applications and products in environmental and energy fields. In the review of K. Nakata and A. Fujishima (2012), reported that titania has strong oxidizing abilities for the decomposition of organic pollutants, superhydrophilicity, chemical stability, long durability, nontoxicity, relatively inexpensive, transparency to visible light and compatibility with modern technology. The results show that the photocatalytic activity of TiO_2 depends on structures and the dimensionality, nanofibers were classified as one-dimensional structure that has lower levels of recombination in photocatalytic process and can be obtained in accordance with electrospinning process [23]. In the same year, K.-J. Hwang et al. (2012) successfully prepared titania powders by using TiO_2 colloidal sol prepared from titaniumtetraisopropoxide (TTIP), used as a starting material by applying the sol-gel method and continuously calcined synthesized TiO_2 powder at 500°C. The effect of aging times and temperatures on physical and chemical properties of TiO_2 sol particles was investigated. In addition, photocatalytic activity was studied by degrading 10 ppm of MB dye, the results show that the photocatalytic activity of TiO_2 is greatly dependent on crystallite size and mixing ratio of anatse and rutile rather than the adsorption amount of MB dye [2].

The photocatalytic activity of TiO_2 have been continuously studied, V. Rives (2013) reported that one of the main drawback of titania as photocatalyst was the large value of its band gap 3.2 eV for anatase and 3.0 eV for rutile, as a consequence numerous effort has been made to extend the activity of TiO_2 into the visible region to improve the efficiency of TiO_2, such as dye sensitization, doping with non-metal atoms or transition metals. The photocatalytic activity of titania begins after titania is activated by a UV photon, which results in the excitation of an electron from the valence band (VB) to the conduction band (CB). The efficiency of titania is limited by

recombination of photogenerated electrons and holes, but the efficiency can be increased by the presence of metals. The loaded metal is trapping and subsequently transferring of photoexcited electrons onto the photocatalyst surface and decreasing the recombination of electron-hole pairs [18].

2.1.2. Polyacrylonitrile

Polyacrylonitrile (PAN) is a semicrystalline organic polymer resin with good stability, mechanical properties, temperature resistance and flexibility. Normally, PAN nanofiber was used as precursors for producing carbon nanofibers [13]. From a review paper of S.K. Nataraj et al. (2012) reporting that PAN and copolymers of PAN have been widely studied for commercial or technical exploitations. PAN may be crosslinked, but also exist depending on solvents and its physical properties at that environment. Crosslink of PAN impart some important physical properties, such as insolubility and resistance to swelling in common organic solvents. The limited solubility of PAN affected in dissolving it for spinning, PAN only soluble in polar solvents like DMF, DMSO, DMAc, dimethylsulfone, tetramethylsulfide and aqueous solutions of ethylene carbonate, also some mineral salts [24].

J.S. Im et al. (2008) successfully prepared PAN nanofibers containing TiO_2 catalyst, polymer solution was prepared with weight ratio of PAN : TiO_2 : DMF equals 1 : 1 : 9. The resultant nanofibers were used to degrade rhodamine B dye [25]. Moreover, the morphology of PAN nanofibers was investigated by S.R. Dhakate et al. (2011), PAN/DMF solution is enabled to electrospun into ultra-thin nanofibers. The diameter of nanofibers was influenced by solution and process control properties. Polymer content of 5% with tip to collector distance 20 cm, collector speed of 2000 rpm and flow rate of 0.25 ml/hr were conditions that can produce ~100 nm nanofibers [26].

2.1.3. Polyvinylpyrrolidone

Polyvinylpyrrolidone (PVP) also known as polyvidone or povidone, it is a water soluble polymer but also soluble in other polar solvents. C. Cheng et al. (2011) reported that PVP is introduced to low temperature preparation of a good quality TiO_2 film used in flexible dye-sensitized solar cells (DSSCs) and it is found that by characteristics and measurements, the dispersion of TiO_2 particles can be improved by PVP [14].

The effects of polymer media on electrospun TiO_2 nanofibers have been studied by J.-Y. Chen et al. (2008). TTIP sol-gel solution was prepared by a mixture of 3 ml of acetic acid and 3 ml of ethanol, followed by an addition of TTIP precursors. The polymer based sol-gel solution was prepared by adding 0.42 g of PVP and 8 ml of ethanol. The mixture was yellow and transparent after 1 hr. Then, the as spun nanofibers were calcined at 450-550°C, varied temperature, for 2 hr. The result shows that more PVP loading in electrospinning solutions caused the formation of undesired beads, which had been associated with the conflict between the surface tension and the charge density [27]. Acetic acid was used for the sol-gel process of TiO_2 electrospinning solutions [19, 20, 28] and for stabilization [29].

2.1.4. Solvent for sheath solution

Typical electrospinnable precursor solution should contain a salt precursor, a polymer and a relatively volatile solvent such as ethanol, water, isopropanol, chloroform or N,N'-dimethylformamide [30]. Due to the limited solubility of PAN, therefore DMF was selected as solvent for both core and sheath solution in this research. It is confirmed that DMF is a good solvent for both TTIP/PVP solution [28] and PAN [25, 26].

In addition, the solvent used to dissolve polymer affected spinnability of electrospinning solution and nanofibers morphology significantly. Moreover, selected solvent must be completely evaporated without leaving any residue on nanofibers. Ethanol was selected as solvent because it is easy to evaporate and commonly used as solvent for TTIP/PVP solution in many researches [19, 20, 22, 27, 29, 31-33] and for TTIP/PMMA solution [34, 35].

2.1.5. Methylene blue dye

Methylene blue (MB) dye is a cationic dye which is commonly used in dyeing industries. The existence of this dye in wastewater might cause the burning effect of eye, nausea, vomiting and diarrhea [36]. The removal of MB dye from textile simulated sample was studied by M. H. Ehrampoush et al. (2011) with effect of pH, TiO_2 concentration on MB and COD removal, MB concentration and rotation and aeration rate. The result shows that by the increase of MB concentration, the efficiency of catalyst for degrading dye decreased and the optimum concentration range for photocatalytic degradation of dyes in the range of 0.055 to 12.5 g/l [1].

2.2. Fabrication of TiO_2-PVP/PAN flexible nanofibers

2.2.1. Sol-gel process

The sol-gel synthesis of titanium dioxide related with three reactions, which are hydrolysis (a) and condensation by oxolation (b) and alcoxolation reactions (c).

$$Ti(OR)_4 + H_2O \leftrightarrow Ti(OR)_3OH + ROH \quad (a)$$

$$(OR)_3Ti\text{-}OH + HO\text{-}Ti(OR)_3 \leftrightarrow (OR)_3Ti\text{-}O\text{-}Ti(OR)_3 + H_2O \quad (b)$$

$$(OR)_3Ti\text{-}OH + RO\text{-}Ti(OR)_3 \leftrightarrow (OR)_3Ti\text{-}O\text{-}Ti(OR)_3 + ROH \quad (c)$$

Sol-gel process has been widely studied to investigate the optimized synthesis conditions. By optimizing synthesis conditions, the morphological properties

obtained would be improved [37]. The overview of the sol-gel process is shown in Figure 2.2.

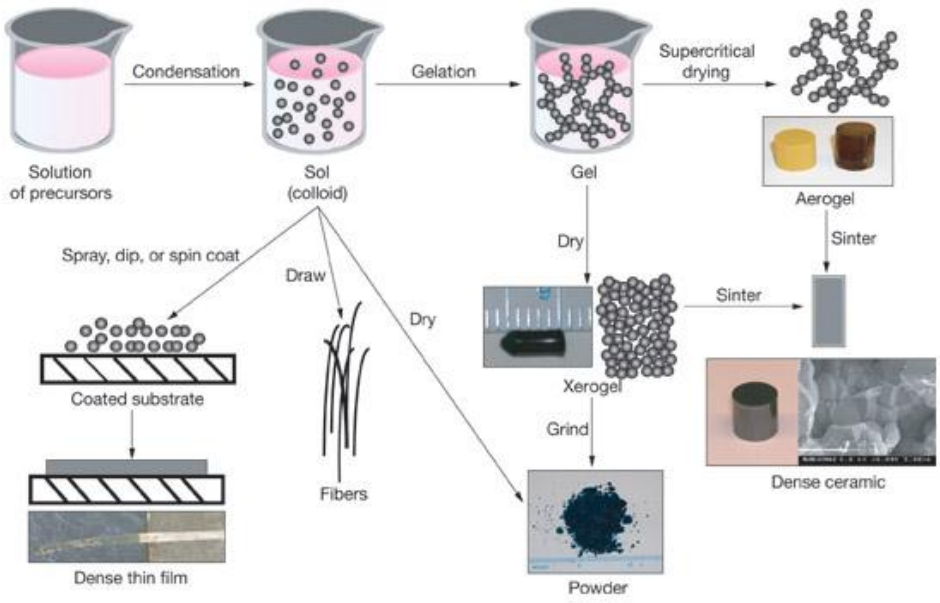

Figure 2.2. The overview of sol-gel process (https://str.llnl.gov/str/May05/gifs/Satcher 1.jpg).

A review paper of U.G. Akpan and B.H. Hameed (2010) reported that various sol-gel and sol-gel related system of doping TiO_2, such as codoping with transition metal ions, rare earth metal ions, alkaline earth metal ions, other metal and non-metal ions, it can be concluded that codoping of TiO_2 generally enhance the photocatalytic efficiency of catalyst and TiO_2 doped with alkaline earth metals by co-precipitation for the better results [38].

2.2.2. Electrospinning process

Electrospinning is the process which a high voltage is applied to a polymer fluid such that charges are induced within the fluid. When charges within the fluid reached a critical amount, a fluid jet will erupt from the droplet at the tip of the

needle resulting in the formation of a Taylor cone. The electrospinning jet will move from the high potential region to low potential region, which refer as grounded collector. The electrospinning process is shown in Figure 2.3.

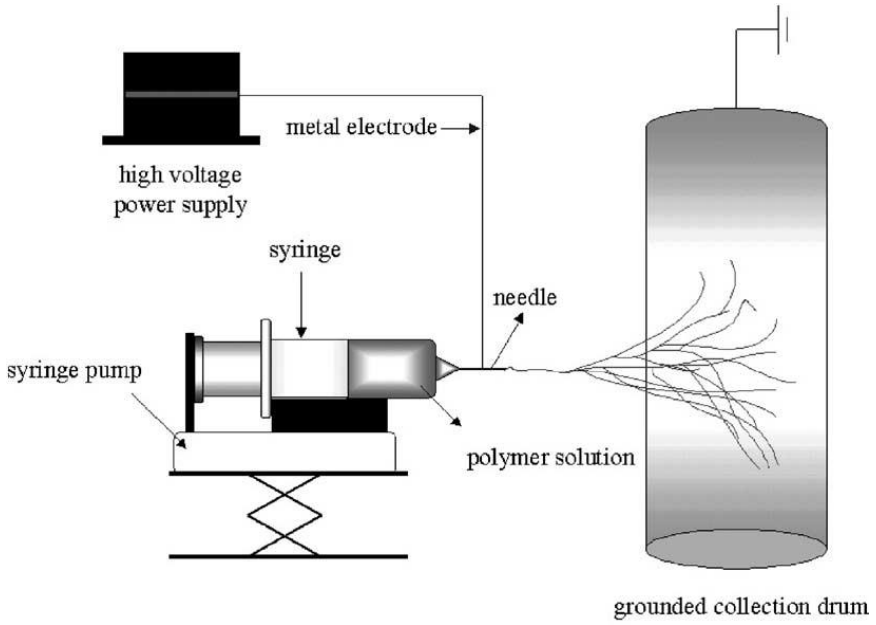

Figure 2.3. Schematic diagram of the electrospinning apparatus [39].

The morphologies of resultant nanofibers dependent on many parameters such as polymer solution parameters, processing conditions and ambient parameters. The parameters that influence the nanofibers most is polymer solution parameters [40]. Miao et al. (2010) reported that the formation of nanofibers is determined by many operating parameters such as concentration, surface tension, viscosity, conductivity and flow rate of polymer solution also applied voltage [8].

In this research, electrospinning process was mostly used to fabricated titania nanofibers. Previously, PAN with DMF solvent were selected as core solution composition because of its temperature resistance and flexibility. N.A. Garcia-Gomez et al. (2014) investigated the concentration of PAN in DMF, 8wt% PAN was completely dissolved in DMF solvent [41]. For sheath solution, A.W. Tan et al. (2013) reported that in a typical procedure PVP/ethanol solution was prepared in a ratio of

PVP : ethanol equals 0.45 g : 7.5 ml. Also, the precursor solution was prepared by mixing TTIP : acetic acid : ethanol in a ratio of 1.5 g : 3 ml : 3 ml. The sheath solution was continuously stirred for 1 hr [42].

2.2.3. Coaxial electrospinning process

Core-shell fibers from coaxial electrospinning process has similar way to set up in many researches, the principal of coaxial electrospinning is based on basic electrospinning techinique. The difference between coaxial and basic electrospinning is coaxial electrospinning needs more modification, especially for coaxial nozzle part, because the outer needle or nozzle which used to feed sheath solution must be suitable with the inner needle that feed core solution. The coaxial electrospinning setup is shown in Figure 2.4.

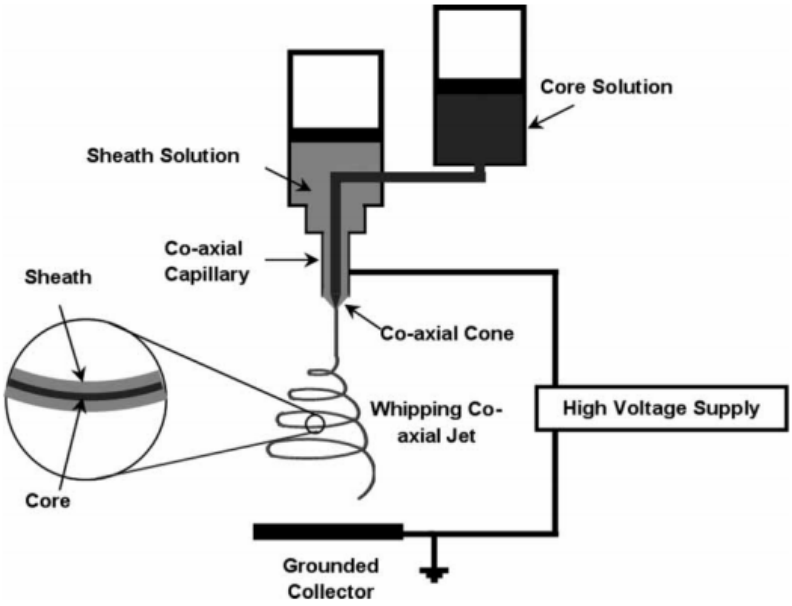

Figure 2.4. Schematic of coaxial electrospinning process [43].

Syringe pumps were used to control the feeding rates of both core and sheath electrospinning solutions. The design consists of two separate syringes with different sized capillaries, a smaller capillary is inserted from outside into the Taylor

cone formed at the exit of the bigger capillary. The alternative setup is shown in Figure 2.5.

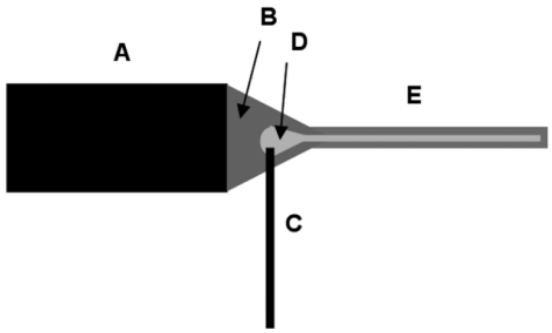

Figure 2.5. The alternative setup for coaxial electrospinning. A: capillary contains sheath solution, B: Taylor cone from sheath solution, C: smaller capillary contains core solution, D: Taylor cone from core solution, form core-shell structure and E: coaxial jet [43].

The process of coaxial electrospinning begins with the polymer solutions which are charged using high voltage, the charge accumulation mostly occurs on the surface of the sheath liquid coming out of the outer coaxial capillary. Then, pendant droplet of the sheath solution elongates and stretches due to the charge-charge repulsion to form a conical shape. After reaching critical point due to the increased applied potential, the charge accumulates, then a fine jet extends from the cone. The viscous dragging and contact friction generated in core and sheath solution until the stresses occur will cause a compound co-axial jet develops at the tip of the cones. The illustration is shown in Figure 2.6.

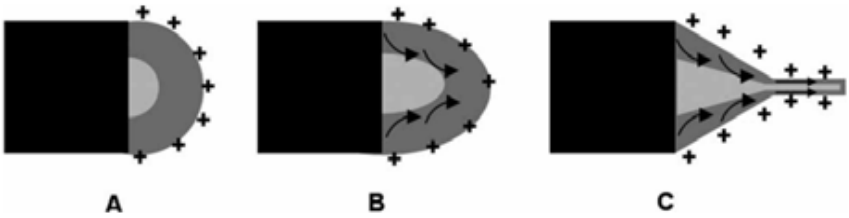

Figure 2.6. Illustration of compound Taylor cone formation. A: charges on surface of sheath solution, B: viscous drag exerted on the core and C: sheath- core compound Taylor cone formed due to continuous viscous drag [43].

Coaxial electrospinning process is the new technology that fabricated core/sheath nanofibers by simple loading procedures with more applications and benefits, which require less post modification [44]. The demand of coaxial nanofibers and core/sheath types of nanostructures increased, due to the various applications of a combined nanofiber from both organic and inorganic compounds. T. Lan et al. (2014) have successfully prepared core/sheath of CTA-Hap nanofiber adsorbents by using coaxial electrospinning process CTA (core) and-Hap (sheath) nanofibers morphologies were homogeneous and no bead formation. The average diameter size was ~220 nm [45]. Besides that, calcination temperature plays an important role due to its profound effect on morphology, surface area, pore volume and crystalline phase composition of the prepared nanofibers. All those previous factors affect the photocatalytic activity [46].

2.3. Photocatalytic process

The mechanism of activation with UV light and photosensitized oxidation for MB and its intermediate product was investigated by R. Zuo et al. (2014). At first, electron and hole are generated in a conduction band and valence band of TiO_2 by UV irradiation, respectively, as shown in (1). Then, the positive hole can oxidize hydroxide ions adsorbed on TiO_2 particles surface to produce hydroxyl radical, as

shown in (2) and (3). Superoxide radical anions are produced by the reaction of the electrons of conduction band and oxygen (4). The superoxide radical anion reacts with proton and formed hydroperoxyl radical (5).

$TiO_2 + h\nu\ (UV) \longrightarrow TiO_2\ (e^-_{CB} + h^+_{VB})$ (1)

$TiO_2\ (h^+_{VB}) + H_2O \longrightarrow TiO_2 + H^+ + OH^*$ (2)

$TiO_2\ (h^+_{VB}) + OH^- \longrightarrow TiO_2 + OH^*$ (3)

$TiO_2\ (e^-_{CB}) + O_2 \longrightarrow TiO_2 + O_2^{*-}$ (4)

$O_2^{*-} + H^+ \longrightarrow HO_2$ (5)

The mechanism of photosensitized oxidation, in the presence of catalyst the excited state of MB injects electron into conduction band (6). According to (7) to (10), MB dye is converted to cation dye radical and undergoes degradation to yield products.

$MB^* + TiO_2 \longrightarrow MB^{*+}\ e^-_{CB}\ (TiO_2)$ (6)

$O_2 + e^- \longrightarrow O_2^{*-}$ (7)

$MB^{*+} + OH^- \longrightarrow MB + OH^*$ (8)

$MB^{*+} + OH^* \longrightarrow$ products (9)

$MB^{*+} + O_2^{*-} \longrightarrow$ products (10)

The hydroxyl radical existing on the surface of diatomite accelerated the degradation of MB (3) [5]. Photocatalytic principle of TiO_2 and photocatalytic degradation pathway of MB are shown in Figure 2.7 and Figure 2.8, respectively.

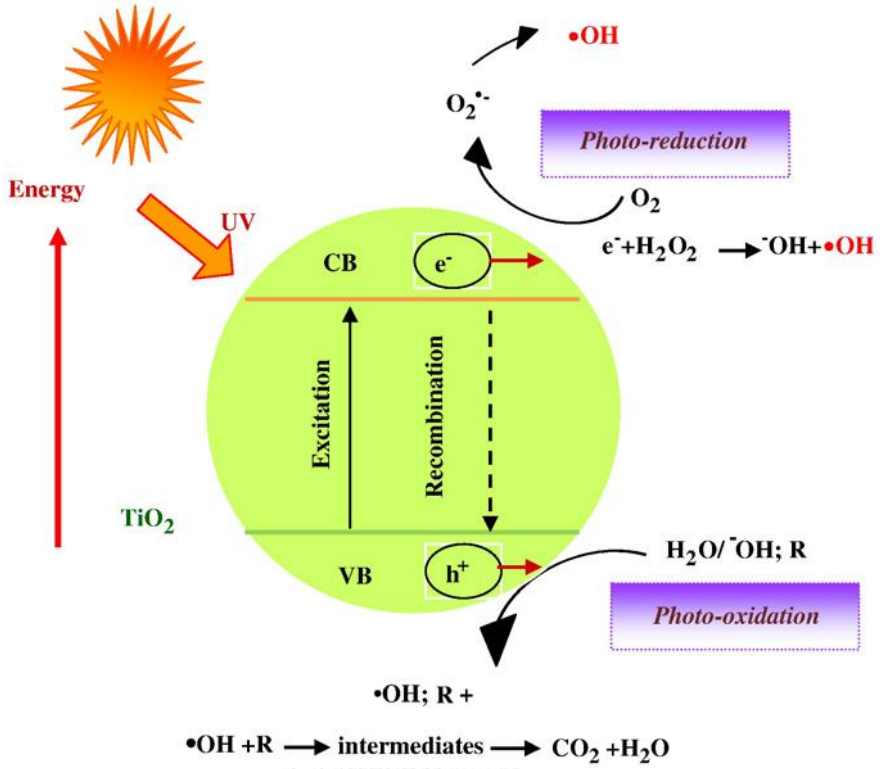

Figure 2.7. Schematic diagram illustrating photocatalytic principle of TiO_2 [47].

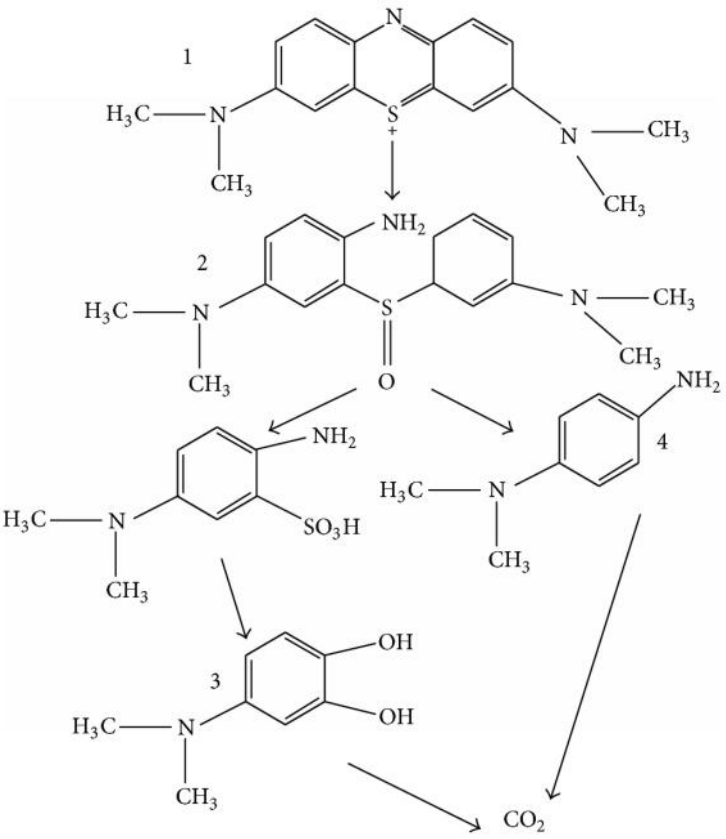

Figure 2.8. MB photocatalytic degradation pathway and its intermediates [5].

2.4. The effect of solvent at the interface investigation by spin coating technique

The interfacial phenomena that occur in all materials affected the formation of material properties and structures significantly. Interface study is necessary in order to determine, classify and control material properties. By controlling material properties would lead to the appropriate development process of the product. In this research, the effect of solvent at core/sheath interface of TiO_2-PVP/PAN flexible nanofibers was investigated by spin coating technique and fourier transform infrared spectroscopy (FTIR). The benefit of spin coating technique is this procedure can be repeated to form multi-layers. X. Wang et al. (2013) reported that spin coating

method is a versatile technique that produce smaller and more uniform TiO_2 grains on the film, which attributed to a greater photocatalytic activity [16].

CHAPTER III

EXPERIMENT

3.1. Chemicals

3.1.1. Titanium (IV) isopropoxide (TTIP) was purchased from Sigma-Aldrich.

3.1.2. Polyvinylpyrrolidone (PVP) with average Mw ~ 1,300,000 was purchased from Sigma-Aldrich.

3.1.3. Polyacrylonitrile (PAN) with average Mw ~ 150,000 was purchased from Sigma-Aldrich.

3.1.4. N,N'-dimethylformamide (DMF) was purchased from QRëC Chemical Co.,Ltd.

3.1.5. Ethanol 99.9% (Absolute Denatured) was purchased from QRëC Chemical Co.,Ltd.

3.1.6. Acetic acid (Glacial) was purchased from QRëC Chemical Co.,Ltd.

3.1.7. Methylene blue (MB) dye was purchased from Ajax Finechem Pty Ltd.

3.1.8. Ethanol 95.5% was purchased from CT Chemical Co.,Ltd.

3.1.9. Acetone was purchased from CT Chemical Co.,Ltd.

3.2. Materials and equipments

3.2.1. High voltage power supply (ES50P-20W Serial No. 29-0211-003, Gamma High Voltage Research, Ormond Beach,FL 32174) was used to generate positive DC voltage.

3.2.2. Syringe pump A (KDS-100-A Serial No. 115269, kdScientific) was equipped in order to control the steady flow rate of core solution.

3.2.3. Syringe pump B (KDS-100-B Serial No. 115269, kdScientific) was equipped in order to control the steady flow rate of sheath solution.

3.2.4. The 22G x 1½" (0.7 x 40 mm) stainless needle (NIPRO) was used to feed core solution.

3.2.5. Coaxial copper nozzle of which core diameter equals 0.7 mm and sheath diameter equals 1.5 mm.

3.2.6. Two plastic 10 ml syringes (NIPRO) were used to fill electrospinning solutions.

3.2.7. Aluminum foil was used to be ground collector.

3.2.8. Voltage power supply (Protek, DF1730SB3A) was used to generate DC power supply for a rotating plane.

3.2.9. Rotating plane was used to hold a microscope slide in spin coating process.

3.2.10. Microscope slide with the dimension of 25.4 x 76.2 mm and 1 mm thick was used to collect thin film.

3.3. Preparation of electrospinning solutions

In the coaxial electrospinning process, core and sheath solutions were separately supplied into the electrospinning nozzle.

3.3.1. Preparation of core solution

Core solution or PAN/DMF solution was prepared by mixing polyacrylonitrile in N,N'-dimethylformamide and stirred at 60°C until the solution was homogeneous.

3.3.2. Preparation of sheath solution

The sheath solution was prepared by mixing PVP solution and titania-precursor solution. First, polyvinylpyrrolidone was dissolved in a solvent for 30 min to gain PVP solution. In another vial, titania-precursor solution was prepared by mixing titanium (IV) isopropoxide (TTIP) with solvent and acetic acid. The aging time

of titania-precursor solution was varied from 0 - 30 min. Then, titania-precursor solution was slowly poured into PVP solution. The solution at this stage must remain transparent. The mixing solution was stirred for 70 min to gain sheath solution. The solvent of the sheath solution was varied to be either N,N'-dimethylformamide or ethanol.

3.4. Fabrication of core/sheath nanofibers

Both core and sheath solutions were separately supplied into 2 syringes. The first syringe contains 10 ml of PAN/DMF solution. PAN/DMF solution was fed to syringe pump A. The second syringe contains 10 ml of sheath solution. The sheath solution was fed to syringe pump B. Next, the flow rate for both core and sheath solutions were set to be 0.8 ml/hr for syringe pump A and 1.2 ml/hr for syringe pump B, respectively. Both syringes were then connected to coaxial nozzle. The distance between coaxial nozzle and collector was fixed to be 25 cm. The high voltage power supply with electrical potential of 22-26 kV was connected to coaxial nozzle. Grounding electrode was connected to a rotating collector which was covered with aluminum foil. The speed of the rotating collector was 400 rpm.

3.5. Calcination of as spun TiO_2-PVP/PAN core/sheath nanofibers

The resultant core/sheath nanofibers were calcined in a box furnace. The initial temperature inside furnace box was room temperature and would be slowly increased to the target temperature after applying heat. The calcination temperature, heating rate and duration time were fixed to be 500°C, 10°C/min and 2 hr, respectively.

3.6. Producing thin films from spin coating technique

Before the spin coating started, the microscope slide must be sonicated and cleaned with deionized water, ethanol 95.5% and acetone for 1 hr for each solvent. Next, the voltage power supply with electrical potential of 5 V was connected to a rotating plane. A clean microscope slide was placed on a rotating plane and set the electrical potential at 5 V. The solution was filled inside the dropper. The solution was slowly dropped on the microscope slide at the rate of approximately 1 ml/min. Then, the microscope slide with the thin film was placed in oven and dry for 12 hr.

3.7. Photocatalytic process

Photocatalytic degradation activity of resultant flexible nanofibers was evaluated by degrading methylene blue (MB) dye under the UV light. The MB dye solution was prepared at concentration of 10 ppm. The ratio between synthesized photocatalyst and MB dye was fixed at 1 mg : 10 ml. The intensity was measured by UV-vis spectrophotometer at 664 nm.

3.8. Characterizations

3.8.1. Fourier transform infrared spectroscopy (FTIR)

Functional groups of resultant nanofibers and thin film solutions were identified by using fourier transform infrared spectroscopy (FTIR) model Nicolet 6700, Thermo Scientific at Center of Excellence in Particle Technology Chemical Engineering laboratory, Chulalongkorn University. Sample preparation was done before measurement by mixing sample with potassium bromide (KBr) in a ratio of 1 : 100 and compressed into thin pellet.

3.8.2. X-ray diffraction (XRD)

The crystalline phases of resultant photocatalyst were analyzed by using x-ray diffraction (XRD) model AXS Diffraktometer D8, Erz. Nr. : 7KP2025-1LA14-1-Z P02, Serial-Nr. : 202328, 230 V 50 Hz 6,5 kVA, 76181 Karisruhe (Germany), Bruker at Department of Materials Science, Faculty of Science, Chulalongkorn University. The CuKα radiation was used to scan samples in the 2 theta range of 5-80 degree at scanning step of 0.02 degree and step time 0.5 s.

3.8.3. Scanning electron microscopy with energy-dispersive x-ray (SEM-EDX).

Morphology of both obtained nanofibers and thin films were characterized by using scanning electron microscopy (SEM) model JSM-6610LV, JEOL at Scientific and Technological Research Equipment Center (STREC), Chulalongkorn University. The size of nanofibers was measured using Image Pro Plus 4.5 program. In additional, the composition of nanofibers and thin films were investigated by energy-dispersive x-ray (EDX) that accompanied with SEM at Scientific and Technological Research Equipment Center (STREC), Chulalongkorn University.

3.8.4. Transmission electron microscope (TEM)

The core/sheath structure of both as spun and calcined nanofibers were observed by using transmission electron microscope (TEM) model JEM-1400, 120 kV, JEOL at Scientific and Technological Research Equipment Center (STREC), Chulalongkorn University.

CHAPTER IV

RESULTS AND DISCUSSION

The effects of solvent on interface of TiO_2-PVP/PAN flexible nanofibers were investigated in this chapter. Fourier transform infrared spectroscopy (FTIR) was used mainly to analyze resultant fibers and films. The various conditions such as polymer concentration (PVP), amount of titania-precursor (TTIP), aging time of titania-precursor solution and electrical potential used in electrospinning process were investigated for their effects. The last part of this chapter will explain the photocatalytic activity of TiO_2-PVP/PAN nanofibers.

4.1. Interaction among components in each solution

The interaction among components must be investigated to determine the resultant nanofibers structure and the effect of solvent on the interaction that occurring at core/sheath interface. This research mainly focuses on the new peaks that appeared in FTIR transmittance spectra and the limited solubility of polyacrylonitrile (PAN), therefore other interaction that occur e.g., polymer soluble in solvent will be neglected.

4.1.1. PAN and DMF

To investigate the effect of solvent on the interaction at the interface of resultant nanofibers, the interaction between PAN and N,N'-dimethylformamide (DMF) must be studied for the first step. The mixed solution between PAN/DMF was core solution. The concentration of PAN in core solution was fixed at 8wt%. The FTIR transmittance spectra of PAN, core solution and DMF are shown in Figure 4.1.

In Figure 4.1., all peaks that appeared from core solution (b) was compared with peaks from PAN (a) and DMF (c). The green line shows the peaks that resemble between core solution and DMF, the black line shows the resemblance peaks of

both PAN, DMF with core solution and the red line shows the peaks that resemble between core solution and PAN.

FTIR spectra of PAN showed prominent peaks at 2940 cm^{-1}, 2243 cm^{-1} and 1454 cm^{-1} corresponding to stretching vibration of methylene (-CH_2) [48], stretching vibration of nitrile unit C≡N in the polymer chain [49], and C-H bond [50], respectively. The main characteristic bands of DMF showed at 1666 cm^{-1}, 1388 cm^{-1} and 1257 cm^{-1} corresponding to C=O stretching [51], N-C-H bending mode [52] and C-N asymmetric stretching [52]. Since all peaks of core solution resemble to either PAN or DMF, hence, there is no interaction occurred between PAN and DMF it was just polymer (PAN) soluble in solvent (DMF).

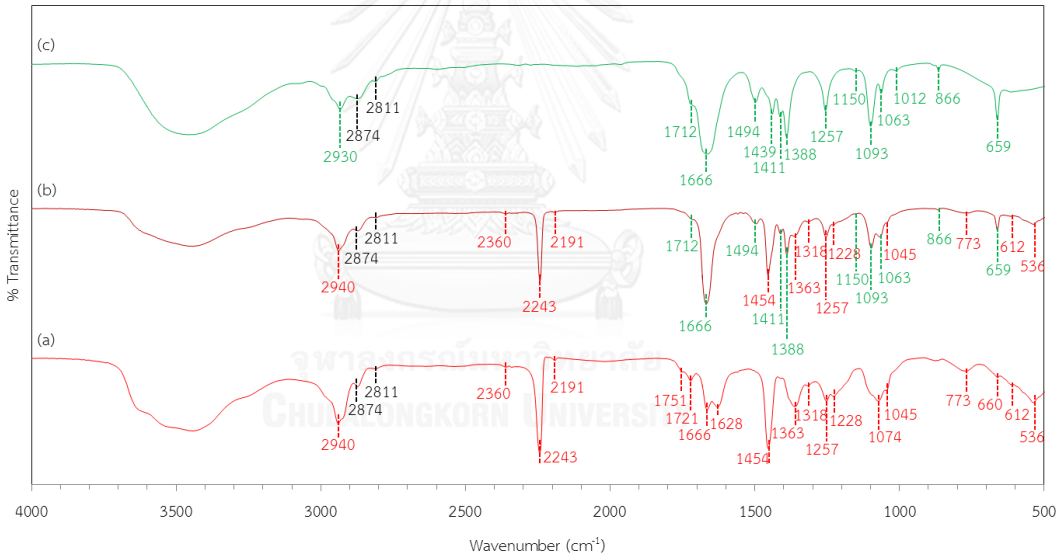

Figure 4.1. FTIR transmittance spectra of (a) PAN, (b) core solution and (c) DMF.

The details of FTIR peaks are listed in Table 4.1Table 4.2. and Table **4.3**.

Table 4.1. FTIR peak assignment for PAN.

PAN		
Wavenumber (cm^{-1})	Functional groups	References
2940	CH_2, stretching vibration	[48]
2874	CH, CH_2, CH_3, symmetric	[53]
2811	aliphatic group	[54]
2360	C=O, stretching vibration	[51]
2243	C≡N, stretching vibration	[49]
2191	no data	
1751	C=O	[55]
1721	C=O	[55]
1666	C=O, stretching	[51]
1628	C=N	[56]
1454	C-H	[50]
1363	CH_3, bending vibration	[53]
1318	CH in plane	[57]
1257	C-N, asymmetric stretching	[52]
1228	no data	
1074	C-N, bending vibration	[53]
1045	CH in plane	[57]
773	no data	
660	O=C-N, stretching	[57]
612	no data	
536	C=O, twisting	[53]

Table 4.2. FTIR peak assignment for core solution.

PAN/DMF		
Wavenumber (cm^{-1})	Functional groups	References
2940	CH_2, stretching vibration	[48]
2874	CH, CH_2, CH_3, symmetric	[53]
2811	aliphatic group	[54]
2360	C=O, stretching vibration	[51]
2243	C≡N, stretching vibration	[49]
2191	no data	
1712	C=O	[48]
1666	C=O, stretching	[51]
1494	no data	
1454	C-H	[50]
1411	CH_3, asymmetric	[52]
1388	N-C-H, bending	[52]
1363	CH_3, bending vibration	[53]
1318	CH in plane	[57]
1257	C-N, asymmetric stretching	[52]
1228	no data	
1150	no data	
1093	CH_3, rocking	[52]
1063	CH_3, rocking	[52]
1045	CH in plane	[57]
866	C-N, stretching	[52]
773	no data	

659	O=C-N, stretching	[52]
612	no data	
536	C=O, twisting	[53]

Table 4.3. FTIR peak assignment for DMF.

DMF		
Wavenumber (cm^{-1})	Functional groups	References
2930	CH_3, symmetric stretching mode	[52]
2874	CH, CH_2, CH_3, symmetric	[53]
2811	aliphatic group	[54]
1712	C=O	[48]
1666	C=O, stretching	[51]
1494	no data	
1439	CH_3, asymmetric	[52]
1411	CH_3, asymmetric	[52]
1388	N-C-H, bending	[52]
1257	C-N, asymmetric stretching	[52]
1150	no data	
1093	CH_3, rocking	[52]
1063	CH_3, rocking	[52]
1012	C-N, stretching	[52]
866	C-N, stretching	[52]
659	O=C-N, stretching	[52]

4.1.2. PVP and DMF

Next, PVP solution was investigated. The PVP solution is a polymer solution which was prepared to mix with titania-precursor solution to obtain sheath solution. Core solution from section 4.1.1. and sheath solution in section 4.1.2. and 4.1.3. were prepared for the coaxial electrospinning process. The solvent of sheath solution was varied to be DMF and ethanol. Thus, the solvent of PVP solution and titania-precursor solution was varied in accordance with sheath solution. PVP solution with ethanol solvent will be further studies in section 4.1.3. In this section DMF solvent was used in PVP solution. The concentration of PVP that used as FTIR solution sample was 11.5wt%. The FTIR transmittance spectra of PVP, PVP solution and DMF are shown in Figure 4.2.

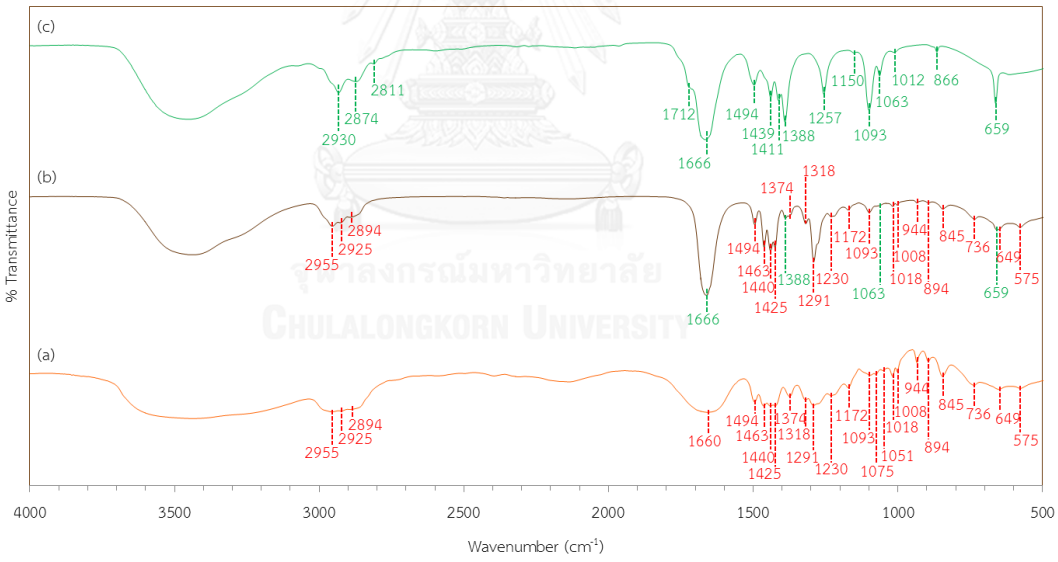

Figure 4.2. FTIR transmittance spectra of (a) PVP, (b) PVP solution and (c) DMF.

The details of FTIR peaks are listed in Table 4.4. and Table **4.5**.

Table 4.4. FTIR peak assignment for PVP.

PVP		
Wavenumber (cm^{-1})	Functional groups	References
2955	C-H, stretching vibration	[58]
2925	C-H, asymmetric stretching vibration	[59]
2894	C-H, stretching	[60]
1660	C=O, stretching	[61]
1494	C-N, characteristic adsorption bonds of PVP	[62]
1463	C-N, characteristic adsorption bonds of PVP	[62]
1440	CH_3	[63]
1425	CH_2, bending vibration	[64]
1374	heterocyclic in PVP	[63]
1318	heterocyclic in PVP	[63]
1291	C-N, stretching vibration	[58]
1230	no data	
1172	C-N, stretching vibration	[58]
1093	CH_3, rocking	[52]
1075	CN, stretching	[65]
1051	no data	
1018	C-N, stretching in pyrrolidine ring	[66]
1008	no data	
944	no data	
894	no data	
845	C-H, out of plane bending	[63]
736	no data	

649	no data	
575	N-C=O, vibration	[67]

Table 4.5. FTIR peak assignment for PVP solution.

PVP/DMF		
Wavenumber (cm^{-1})	Functional groups	References
2955	C-H, stretching vibration	[58]
2925	C-H, asymmetric stretching vibration	[59]
2894	C-H, stretching	[60]
1666	C=O, stretching	[51]
1494	C-N, characteristic adsorption bonds of PVP	[62]
1463	C-N, characteristic adsorption bonds of PVP	[62]
1440	CH_3	[63]
1425	CH_2, bending vibration	[64]
1388	N-C-H, bending	[52]
1374	heterocyclic in PVP	[63]
1318	heterocyclic in PVP	[63]
1291	C-N, stretching vibration	[58]
1230	no data	
1172	C-N, stretching vibration	[58]
1093	CH_3, rocking	[52]
1063	CH_3, rocking	[52]
1018	C-N, stretching in pyrrolidine ring	[66]
1008	no data	

944	no data	
894	no data	
845	C-H, out of plane bending	[63]
736	no data	
659	O=C-N, stretching	[52]
649	no data	
575	N-C=O, vibration	[67]

4.1.3. PVP and ethanol

The interaction of PVP solution (ethanol solvent) was investigated in this section. The concentration of PVP that used as FTIR solution sample was 11.5wt%. The FTIR transmittance spectra of PVP, PVP solution and ethanol are shown in Figure 4.3. The blue line shows the peaks that resemble between PVP solution and ethanol.

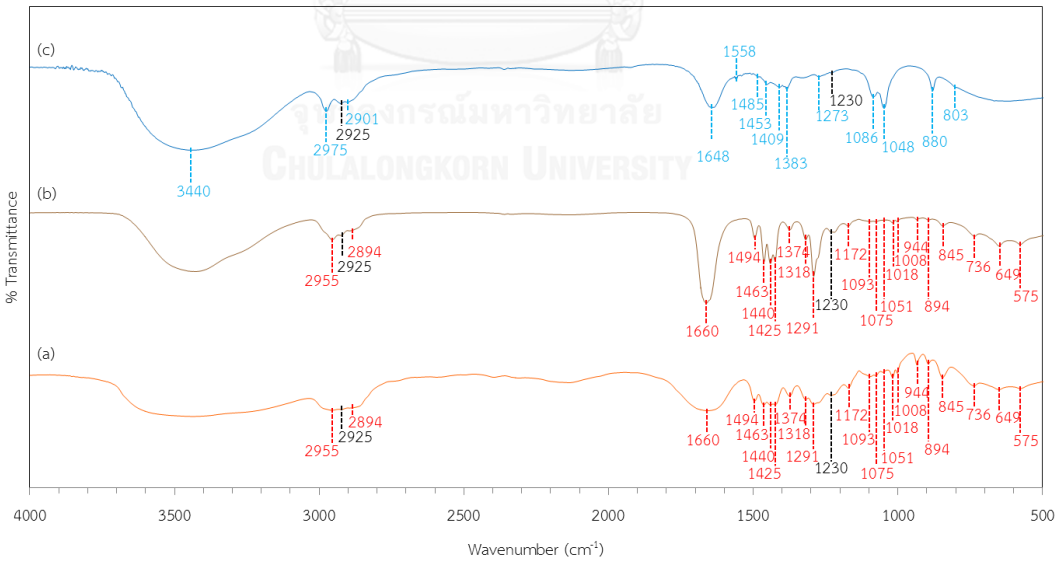

Figure 4.3. FTIR transmittance spectra of (a) PVP, (b) PVP solution and (c) ethanol.

The details of FTIR peaks are listed in Table 4.6. and Table **4.7**.

Table 4.6. FTIR peak assignment for PVP solution.

PVP/Ethanol		
Wavenumber (cm^{-1})	Functional groups	References
2955	C-H, stretching vibration	[58]
2925	C-H, asymmetric stretching vibration	[59]
2894	C-H, stretching	[60]
1660	C=O, stretching	[61]
1494	C-N, characteristic adsorption bonds of PVP	[62]
1463	C-N, characteristic adsorption bonds of PVP	[62]
1440	CH_3	[63]
1425	CH_2, bending vibration	[64]
1374	heterocyclic in PVP	[63]
1318	heterocyclic in PVP	[63]
1291	C-N, stretching vibration	[58]
1230	no data	
1172	C-N, stretching vibration	[58]
1093	CH_3, rocking	[52]
1075	CN, stretching	[65]
1051	no data	
1018	C-N, stretching in pyrrolidine ring	[66]
1008	no data	
944	no data	
894	no data	
845	C-H, out of plane bending	[63]
736	no data	

649	no data	
575	N-C=O, vibration	[67]

Table 4.7. FTIR peak assignment for ethanol.

Ethanol		
Wavenumber (cm^{-1})	Functional groups	References
3440	O-H, stretching vibration	[55]
2975	CH, stretching	[60]
2925	C-H, asymmetric stretching vibration	[59]
2901	O-H	[68]
1648	no data	
1558	no data	
1485	no data	
1453	C-H, bending	[57]
1409	COH, plane bending	[55]
1383	CH_3, symmetric umbrella	[55]
1273	no data	
1230	no data	
1086	no data	
1048	C-H, in plane	[57]
880	no data	
803	no data	

After comparing all peaks of PVP solution for both DMF and ethanol solvents with pure components, using the results from section 4.1.2. and 4.1.3., it was found

that there are no interaction occurred in both solutions. The things that happened due to the mixing process was PVP dissolved in both solvents.

4.1.4. TTIP, DMF and acetic acid

Titania-precursor solution is the source of TiO_2 in flexible nanofibers. It was mixed together with PVP solution to obtain a sheath solution for the coaxial electrospinning process as explained in section 4.1.2. The interaction between titanium (IV) isopropoxide (TTIP), DMF and acetic acid in titania-precursor solution was studied on this section. The FTIR solution sample was prepared by mixing TTIP 15.5vol%, DMF 6 ml and acetic acid 6 ml for 15 min, then the titania-precursor solution was age for 15 min. The FTIR transmittance spectra of TTIP, acetic acid, titania-precursor solution and DMF are shown in Figure 4.4.

The purple line shows the peaks that resemble between titania-precursor solution and TTIP, while the pink line shows the resemblance peaks between titania-precursor and acetic acid. After comparing all peaks of titania-precursor solution with other pure components, it was found that there is no interaction between TTIP, DMF and acetic acid. Sol-gel process does not occur in titania-precursor solution with DMF solvent (15 min aging time).

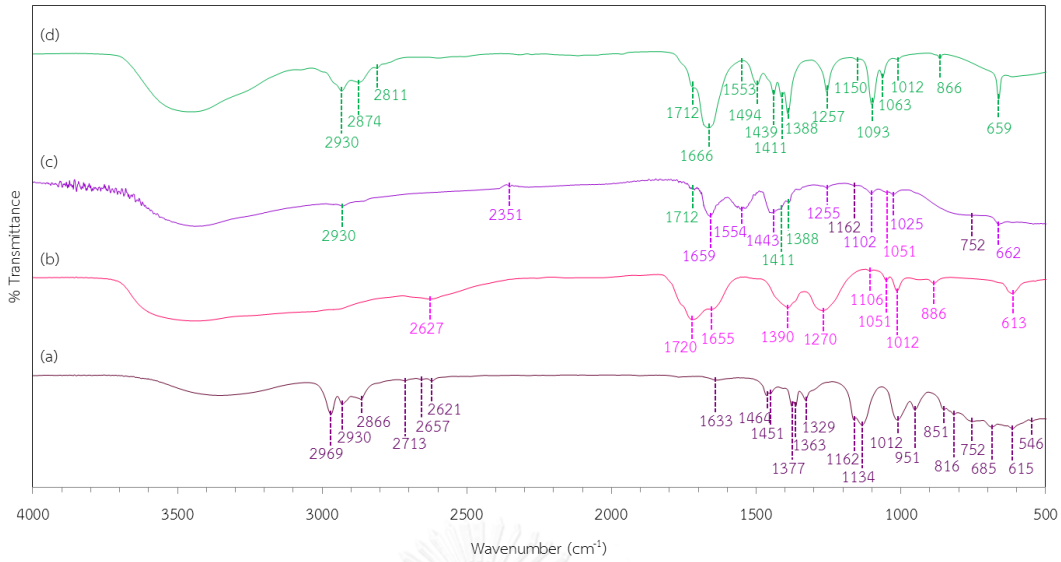

Figure 4.4. FTIR transmittance spectra of (a) TTIP, (b) acetic acid, (c) titania-precursor solution and (d) DMF.

The details of FTIR peaks are listed in Table 4.8., Table **4.9**. and Table **4.10**.

Table 4.8. FTIR peak assignment for TTIP.

TTIP		
Wavenumber (cm^{-1})	Functional groups	References
2969	no data	
2930	CH_3, symmetric stretching mode	[52]
2866	C-H	[69]
2713	no data	
2657	no data	
2621	no data	
1633	carbonyl group	[66]
1464	no data	
1451	C-H, stretching vibration	[56]

1377	CH_3, symmetric bending mode	[60]
1363	CH_3, symmetric bending mode	[60]
1329	CH_3, symmetric bending mode	[60]
1162	no data	
1134	C-C, stretching	[60]
1012	C-O, stretching	[60]
951	C-O, stretching in isopropanol	[60]
851	CH_3, rocking	[60]
816	Ti-O-Ti	[70]
752	Ti-O-Ti	[70]
685	no data	
615	Ti-O, stretching	[70]
546	no data	

Table 4.9. FTIR peak assignment for acetic acid.

Acetic acid		
Wavenumber (cm^{-1})	Functional groups	References
2627	no data	
1720	carbonyl group	[71]
1655	C=O	[59]
1390	no data	
1270	no data	
1106	no data	
1051	OH, vibration	[55]
1012	C=O	[60]

886	no data	
613	C-C	[72]

Table 4.10. FTIR peak assignment for titania-precursor solution.

TTIP/DMF/Acetic acid		
Wavenumber (cm^{-1})	Functional groups	References
2930	CH_3, symmetric stretching mode	[52]
2351	C=O	[51]
1712	C=O	[48]
1659	C=O, stretching	[51]
1554	C-N	[73]
1443	CH_3, asymmetric	[52]
1411	CH_3, asymmetric	[52]
1388	N-C-H, bending	[52]
1255	C-N, asymmetric stretching	[52]
1162	no data	
1102	no data	
1051	OH, vibration	[55]
1025	C=O, stretching	[55]
752	no data	
662	no data	

4.1.5. TTIP, ethanol and acetic acid

Besides DMF, ethanol was selected as another solvent which used to prepare titania-precursor solution. The interaction between TTIP, ethanol and acetic acid in titania-precursor solution was studied in this section. The FTIR solution sample was prepared by mixing TTIP 15.5vol%, ethanol 6 ml and acetic acid 6 ml for 15 min, then the titania-precursor solution was aged for 15 min. The FTIR transmittance spectra of TTIP, acetic acid, titania-precursor solution and ethanol are shown in Figure 4.5.

According to the FTIR spectra of titania-precursor solution in Figure 4.5. (c), there were 4 new peaks occurred from titania-precursor solution at 1540 cm^{-1}, 1443 cm^{-1}, 1344 cm^{-1} and 1021 cm^{-1} corresponding to C-C stretching [57], bending vibration of CH_3 [74], O-H in plane blending vibration [74], and C=O stretching [55], respectively. The new peaks confirmed that there was an interaction occurring between TTIP, ethanol and acetic acid in the titania-precursor solution.

According to the research of M. Hatat-Fraile et al. (2013) and M.E. Simonsen and E.G. Søgaard (2010), the interaction that occurred was sol-gel process related to 3 reactions, which are hydrolysis (a1 and a2) and condensation by oxolation (b) [37, 74]. First, ethanol in titania-precursor solution will react according to (a1). Then the product from (a1) was produced and condensation by oxolation will take place according to (b). Water was produced as by product from (b) and it continue to interact according to (a2). The sol-gel process that occurred was a chain reaction.

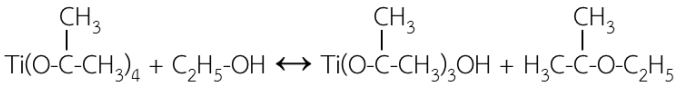

(a1)

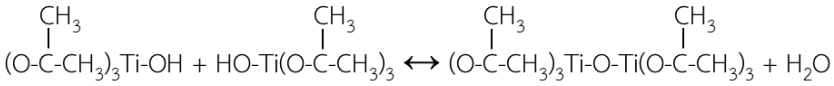

(b)

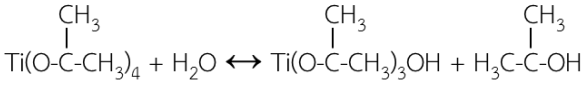

(a2)

All new peaks are matched to the structure of  , by product from (c). Besides that, the peaks at 752 cm^{-1} for Ti-O-Ti [70] and 615 cm^{-1} for Ti-O stretching [70] also confirmed the structure of other product that produced by this sol-gel process. Therefore, the interaction that occurred between TTIP, DMF and acetic acid in the titania-precursor solution (ethanol solvent) was sol-gel process.

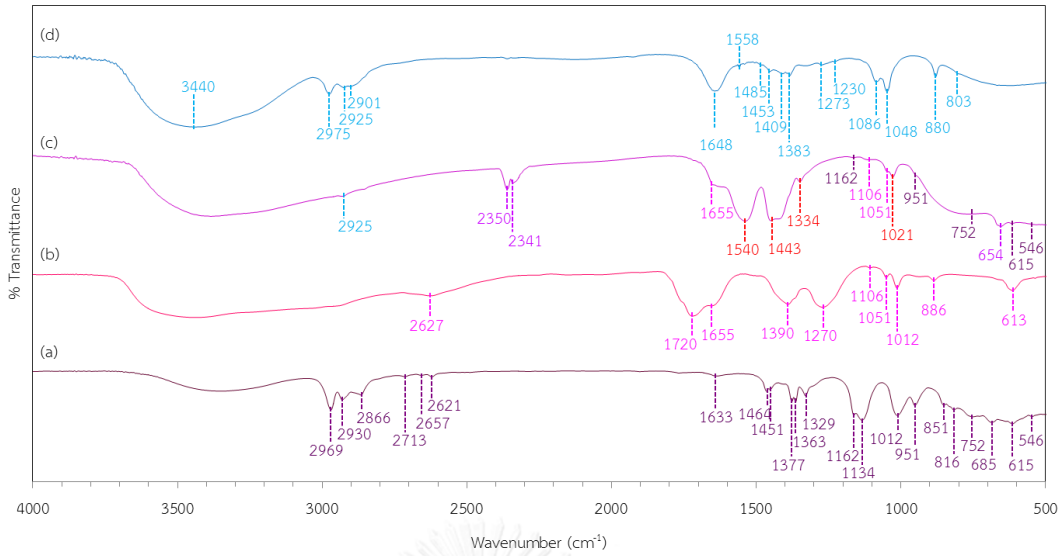

Figure 4.5. FTIR transmittance spectra of (a) TTIP, (b) acetic acid, (c) titania-precursor solution and (d) ethanol.

The details of FTIR peaks are listed in Table 4.11.

Table 4.11. FTIR peak assignment for titania-precursor solution.

TTIP/Ethanol/Acetic acid		
Wavenumber (cm^{-1})	Functional groups	References
2925	C-H, asymmetric stretching vibration	[59]
2350	no data	
2341	no data	
1655	C=O	[59]
1540	C-C, stretching	[57]
1443	CH_3, bending vibration	[74]
1334	O-H, in plane bending	[74]
1162	no data	
1106	no data	

1051	OH, vibration	[55]
1021	C=O, stretching	[55]
951	C-O, stretching in isopropanol	[60]
752	Ti-O-Ti	[70]
654	no data	
615	Ti-O, stretching	[70]
546	no data	

4.1.6. PVP solution and titania-precursor solution (both DMF solvent)

From the result in section 4.1.2. and 4.1.4., it was found that there is no interaction occurred in both PVP solution and titania-precursore solution. In this section, PVP solution and titania-precursor solution will be mixed to obtain sheath solution and the interaction of it will be investigated. PVP solution and titania-precursor solution for the FTIR solution sample were prepared the same with the solutions in section 4.1.2. and 4.1.4., respectively. FTIR transmittance spectra of PVP solution, sheath solution and titania-precursor solution are shown in Figure 4.6.

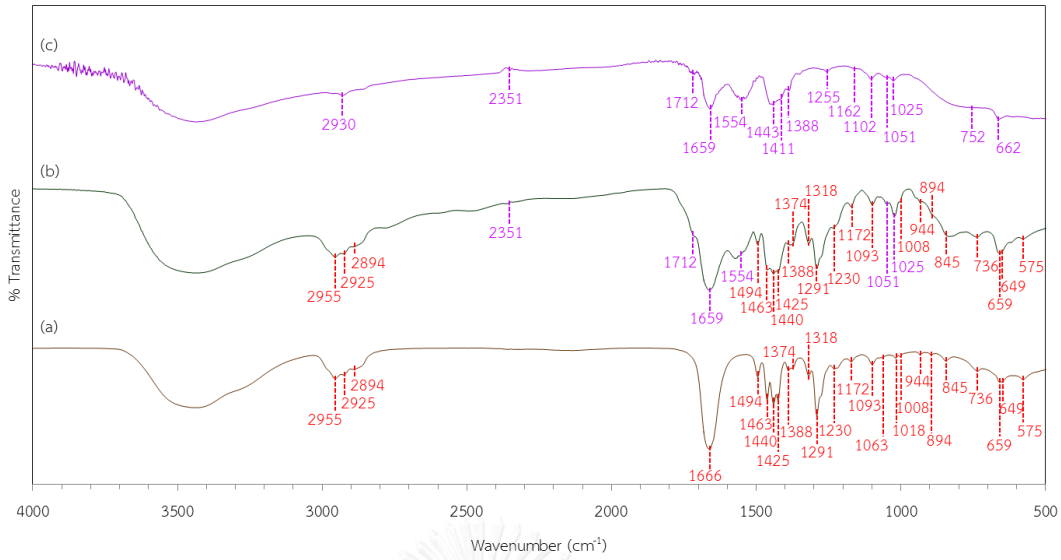

Figure 4.6. FTIR transmittance spectra of (a) PVP solution, (b) sheath solution and (c) titania-precursor solution – DMF solvent.

The details of FTIR peaks are listed in Table 4.12.

Table 4.12. FTIR peak assignment for sheath solution.

PVP/TTIP/DMF/Acetic acid		
Wavenumber (cm^{-1})	Functional groups	References
2955	C-H, stretching vibration	[58]
2925	C-H, asymmetric stretching vibration	[59]
2894	C-H, stretching	[60]
2351	C=O	[51]
1712	C=O	[48]
1659	C=O, stretching	[51]
1554	C-N	[73]
1494	C-N, characteristic adsorption bonds of PVP	[62]
1463	C-N, characteristic adsorption bonds of PVP	[62]

1440	CH_3	[63]
1425	CH_2, bending vibration	[64]
1388	N-C-H, bending	[52]
1374	heterocyclic in PVP	[63]
1318	heterocyclic in PVP	[63]
1291	C-N, stretching vibration	[58]
1230	no data	
1172	C-N, stretching vibration	[58]
1093	CH_3, rocking	[52]
1051	OH, vibration	[55]
1025	C=O, stretching	[55]
1008	no data	
944	no data	
894	no data	
845	C-H, out of plane bending	[63]
736	no data	
659	O=C-N, stretching	[52]
649	no data	
575	N-C=O, vibration	[67]

4.1.7. PVP solution and titania-precursor solution (both ethanol solvent)

In this section, the interaction of PVP solution and titania-precursor solution will be investigated. PVP solution and titania-precursor solution for the FTIR solution sample were prepared the same with the solutions in section 4.1.3. and 4.1.5., respectively. FTIR transmittance spectra of PVP solution, sheath solution and titania-precursor solution are shown in Figure 4.7.

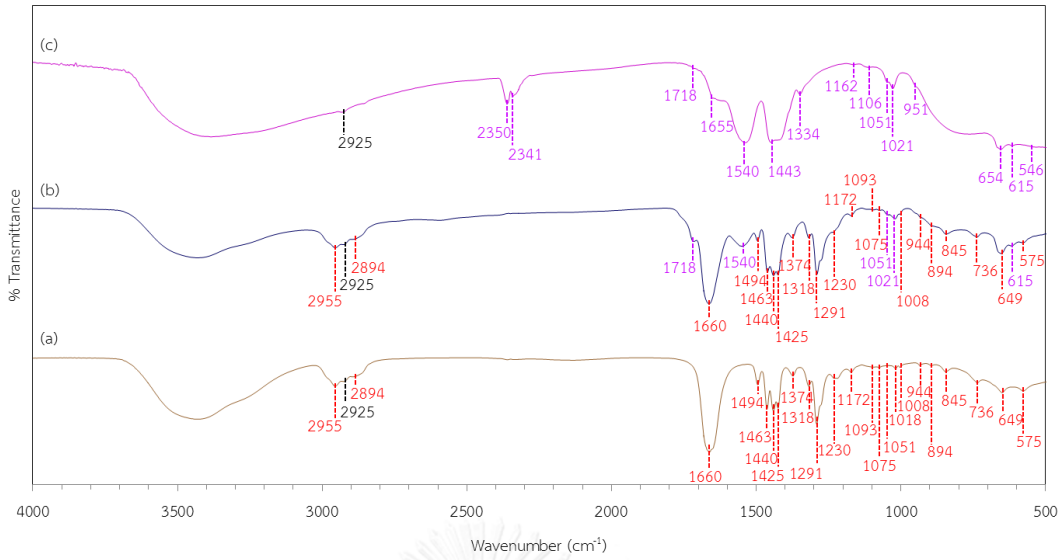

Figure 4.7. FTIR transmittance spectra of (a) PVP solution, (b) sheath solution and (c) titania-precursor solution – ethanol solvent.

The details of FTIR peaks are listed in Table 4.13.

Table 4.13. FTIR peak assignment for sheath solution.

PVP/TTIP/Ethanol/Acetic acid		
Wavenumber (cm^{-1})	Functional groups	References
2955	C-H, stretching vibration	[58]
2925	C-H, asymmetric stretching vibration	[59]
2894	C-H, stretching	[60]
1718	C=O, stretching	[50]
1660	C=O, stretching	[61]
1540	C-C, stretching	[57]
1494	C-N, characteristic adsorption bonds of PVP	[62]
1463	C-N, characteristic adsorption bonds of PVP	[62]
1440	CH_3	[63]

1425	CH_2, bending vibration	[64]
1374	heterocyclic in PVP	[63]
1318	heterocyclic in PVP	[63]
1291	C-N, stretching vibration	[58]
1230	no data	
1172	C-N, stretching vibration	[58]
1093	CH_3, rocking	[52]
1075	CN, stretching	[65]
1051	OH, vibration	[55]
1021	C=O, stretching	[55]
1008	no data	
944	no data	
894	no data	
845	C-H, out of plane bending	[63]
736	no data	
649	no data	
615	Ti-O, stretching	[70]
575	N-C=O, vibration	[67]

After comparing all peaks of sheath solution for both DMF and ethanol solvents with PVP and titania-precursor solutions, using the results from section 4.1.6. and 4.1.7., it was found that there are no interaction occurred in both solutions. For sheath solution in section 4.1.6., the things that happened was PVP solution mixed with titania-precursor solution and obtained sheath solution. On the other hand, after changing the solvent from DMF to ethanol, in the sheath solution in section 4.1.7., the things that happened was totally different. Referring to the results section

4.1.5., the sol-gel process occurred in titania-precursor solution only when ethanol solvent was used. From section 4.1.7., there no interaction occurred. This has shown that the sol-gel process in titania-precursor solution was completely occurred in 15 min of aging time and there is no significant change after it was mixed with PVP solution to obtained sheath solution.

4.1.8. Core solution and ethanol

Since ethanol was selected as another solvent for sheath solution, the interaction between core solution and ethanol must be investigated due to the limitation of PAN solubility. After core solution and ethanol were mixed, the mixed solution is separated into 2 phases, solid phase and liquid phase, immediately as shown in Figure 4.8. Then, the functional groups of both mixed solid and liquid phases were investigated in this topic.

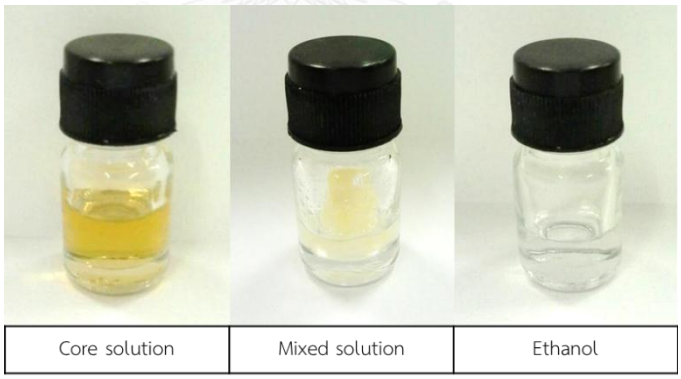

Figure 4.8. Picture of the obtained solution.

The immediate separation into 2 phases of the mixed solution happened due to the dissolution of PAN. According to a review paper of B.A. Miller-Chou and J.L. Koenig (2003), the structure of the surface layers of polymer during dissolvation could be explained by using the schematic in Figure 4.9. At first, after a pure polymer is contacting with pure solvent, the solvent will try to diffuse into a pure polymer,

but a polymer will resist it and some dissolve parts will form into infiltration layers. When infiltration layers were formed, a polymer containing free volume and the solvent molecules fill the empty spaces and start to diffuse. Then, the solid swollen layers were formed. Afterwards, the mixed solution will turn to gel layers which consist of swollen polymer, rubber-like state, and liquid layer [75]. This theory fits the behavior of the mixed solution. The mixed solution in Figure 4.8. is in the gel layers state and consist of solid swollen polymer and liquid layer.

Figure 4.9. Schematic picture of the composition of the surface layer [75].

The FTIR transmittance spectra of core solution, solid and liquid phases of mixed solution and ethanol are shown in Figure 4.10. The peaks of the solid phase in mixed solution were totally matched with core solution ones, thus the solid swollen polymer was confirmed to be PAN.

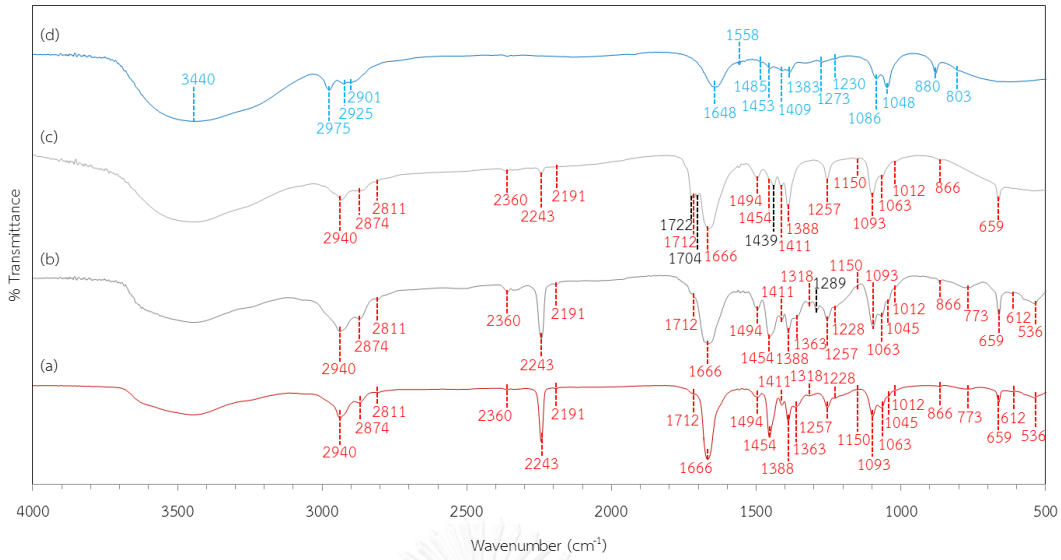

Figure 4.10. FTIR transmittance spectra of (a) core solution, (b) solid phase of mixed solution, (c) liquid phase of mixed solution and (d) ethanol.

The details of FTIR peaks are listed in Table 4.14. and Table **4.15**.

Table 4.14. FTIR peak assignment for solid phase of mixed solution.

Mixed (s)		
Wavenumber (cm^{-1})	Functional groups	References
2940	CH_2, stretching vibration	[48]
2874	CH, CH_2, CH_3, symmetric	[53]
2811	aliphatic group	[54]
2360	C=O, stretching vibration	[51]
2243	C≡N, stretching vibration	[49]
2191	no data	
1712	C=O	[48]
1666	C=O, stretching	[51]
1494	no data	

1454	C-H	[50]
1411	CH_3, asymmetric	[52]
1388	N-C-H, bending	[52]
1363	CH_3, bending vibration	[53]
1318	CH in plane	[57]
1289	C-N stretching vibration	[58]
1257	C-N, asymmetric stretching	[52]
1228	no data	
1150	no data	
1093	CH_3, rocking	[52]
1063	CH_3, rocking	[52]
1045	CH in plane	[57]
1012	no data	
866	C-N, stretching	[52]
773	no data	
659	O=C-N, stretching	[52]
612	no data	
536	C=O, twisting	[53]

Table 4.15. FTIR peak assignment for liquid phase of mixed solution.

Mixed (l)		
Wavenumber (cm^{-1})	Functional groups	References
2940	CH_2, stretching vibration	[48]
2874	CH, CH_2, CH_3, symmetric	[53]
2811	aliphatic group	[54]

2360	C=O, stretching vibration	[51]
2243	C≡N, stretching vibration	[49]
2191	no data	
1722	C=O	[55]
1712	C=O	[48]
1704	no data	
1666	C=O, stretching	[51]
1494	no data	
1454	C-H	[50]
1439	C-H, bending	[51]
1411	CH_3, asymmetric	[52]
1388	N-C-H, bending	[52]
1257	C-N, asymmetric stretching	[52]
1150	no data	
1093	CH_3, rocking	[52]
1063	CH_3, rocking	[52]
1012	no data	
866	C-N, stretching	[52]
659	O=C-N, stretching	[52]

4.1.9. Core solution and sheath solution (DMF in sheath)

This topic will study the interaction between core solution and sheath solution. In electrospinning process, core and sheath solutions must be compatible. After core and sheath solutions were mixed, at first the mixed seems to be homogenous, but after 12 hours, some parts of the mixed solution become gel and

they separated into 2 phases, gel form and liquid phase. This gel was formed because of the nature behavior of sheath solution, confirmed by the data listed in Table 4.16. and Table **4.17**. The FTIR transmittance spectra of core solution, gel and liquid phase of mixed solution and sheath solution are shown in Figure 4.11.

According to Figure 4.11., the FTIR spectra of mixed solution for both gel and liquid phase similar to the spectra of either core or sheath solution. Therefore, it was found that there is no interaction occurred in the mixed solution.

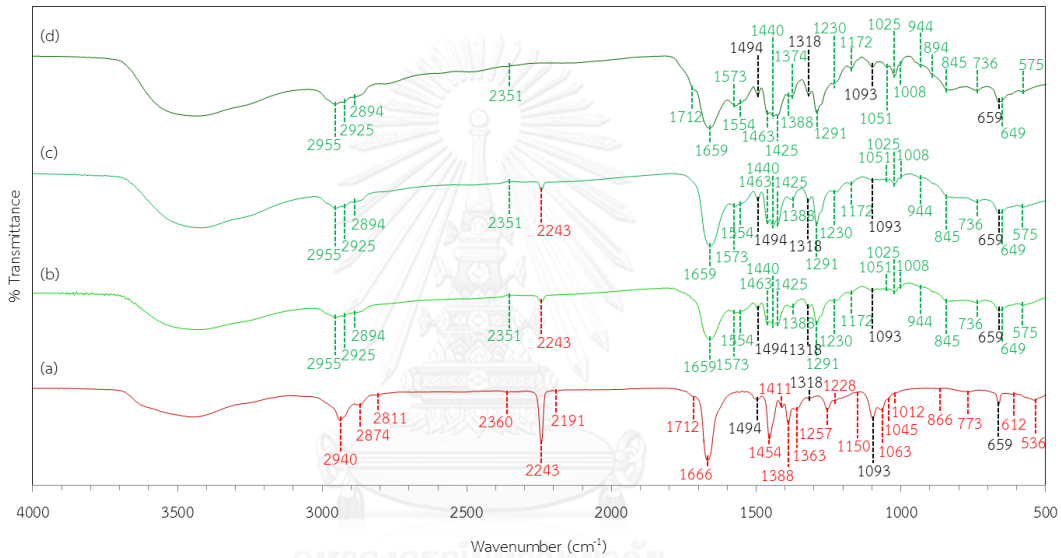

Figure 4.11. FTIR transmittance spectra of (a) core solution, (b) gel of core/sheath solution, (c) liquid phase of core/sheath solution and (d) sheath solution – DMF in sheath.

The details of FTIR peaks are listed in Table 4.16. and Table **4.17**.

Table 4.16. FTIR peak assignment for gel of core/sheath solution.

Mixed (gel)		
Wavenumber (cm^{-1})	Functional groups	References
2955	C-H, stretching vibration	[58]
2925	C-H, asymmetric stretching vibration	[59]
2894	C-H, stretching	[60]
2351	C=O	[51]
2243	C≡N, stretching vibration	[49]
1659	C=O, stretching	[51]
1573	C=N, stretching	[76]
1554	C-N	[73]
1494	C-N, characteristic adsorption bonds of PVP	[62]
1463	C-N, characteristic adsorption bonds of PVP	[62]
1440	CH_3	[63]
1425	CH_2, bending vibration	[64]
1388	N-C-H, bending	[52]
1318	heterocyclic in PVP	[63]
1291	C-N, stretching vibration	[58]
1230	no data	
1172	C-N, stretching vibration	[58]
1093	CH_3, rocking	[52]
1051	OH, vibration	[55]
1025	C=O, stretching	[55]
1008	no data	
944	no data	

845	C-H, out of plane bending	[63]
736	no data	
659	O=C-N, stretching	[52]
649	no data	
575	N-C=O, vibration	[67]

Table 4.17. FTIR peak assignment for liquid phase of core/sheath solution.

Mixed (I)		
Wavenumber (cm^{-1})	Functional groups	References
2955	C-H, stretching vibration	[58]
2925	C-H, asymmetric stretching vibration	[59]
2894	C-H, stretching	[60]
2351	C=O	[51]
2243	C≡N, stretching vibration	[49]
1659	C=O, stretching	[51]
1573	C=N, stretching	[76]
1554	C-N	[73]
1494	C-N, characteristic adsorption bonds of PVP	[62]
1463	C-N, characteristic adsorption bonds of PVP	[62]
1440	CH_3	[63]
1425	CH_2, bending vibration	[64]
1388	N-C-H, bending	[52]
1318	heterocyclic in PVP	[63]
1291	C-N, stretching vibration	[58]

1230	no data	
1172	C-N, stretching vibration	[58]
1093	CH_3, rocking	[52]
1051	OH, vibration	[55]
1025	C=O, stretching	[55]
1008	no data	
944	no data	
845	C-H, out of plane bending	[63]
736	no data	
659	O=C-N, stretching	[52]
649	no data	
575	N-C=O, vibration	[67]

4.1.10. Core solution and sheath solution (ethanol solvent)

Similar to the results from section 4.1.8., after core and sheath solutions were mixed, the mixed solution is separated into 2 phases, solid phase and liquid phase, immediately as shown in Figure 4.12.

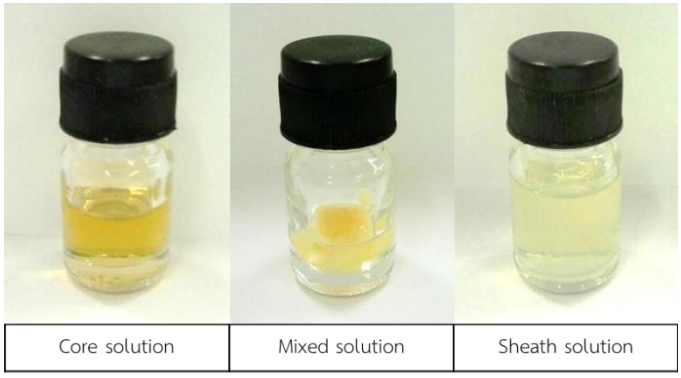

Figure 4.12. Picture of the obtained solution.

The interaction that occurred in this section was similar and explained in section 4.1.8. according to a review paper of B.A. Miller-Chou and J.L. Koenig (2003). The mixed solution in Figure 4.12. is in the gel layers state and consist of solid swollen polymer and liquid layer.

The FTIR transmittance spectra of core solution, solid and liquid phases of mixed solution and sheath solution are shown in Figure 4.13. The spectra of the solid phase of mixed solution are mostly similar to the spectra of core solution. The black lines which represent the resemblance peaks of sheath solution with both solid and liquid phases of mixed solution show that sheath solution is minority remain in solid phase of mixed solution, but the solid swollen polymer is still confirmed as PAN.

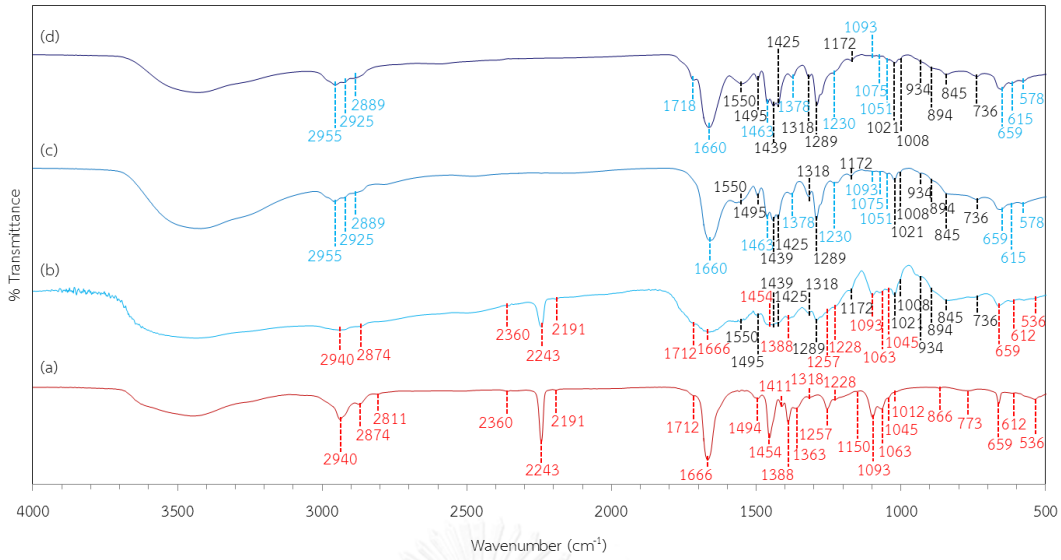

Figure 4.13. FTIR transmittance spectra of (a) core solution, (b) solid phase of core/sheath solution, (c) liquid phase of core/sheath solution and (d) sheath solution – ethanol in sheath.

The details of FTIR peaks are listed in Table 4.18. and Table **4.19**.

Table 4.18. FTIR peak assignment for solid phase of core/sheath solution.

Mixed (s)		
Wavenumber (cm^{-1})	Functional groups	References
2940	CH_2, stretching vibration	[48]
2874	CH, CH_2, CH_3, symmetric	[53]
2360	C=O, stretching vibration	[51]
2243	C≡N, stretching vibration	[49]
2191	no data	
1712	C=O	[48]
1666	C=O, stretching	[51]
1550	C-C, stretching	[57]

1495	C-N, characteristic adsorption bonds of PVP	[62]
1454	C-H	[50]
1439	CH_3	[63]
1425	CH_2, bending vibration	[64]
1388	N-C-H, bending	[52]
1318	heterocyclic in PVP	[63]
1289	C-N, stretching vibration	[58]
1257	C-N, asymmetric stretching	[52]
1228	no data	
1172	C-N, stretching vibration	[58]
1093	CH_3, rocking	[52]
1063	CH_3, rocking	[52]
1045	CH in plane	[57]
1021	C=O, stretching	[55]
1008	no data	
934	no data	
894	no data	
845	C-H, out of plane bending	[63]
736	no data	
659	O=C-N, stretching	[52]
612	no data	
536	C=O, twisting	[53]

Table 4.19. FTIR peak assignment for liquid phase of core/sheath solution.

Mixed (I)		
Wavenumber (cm^{-1})	Functional groups	References
2955	C-H, stretching vibration	[58]
2925	C-H, asymmetric stretching vibration	[59]
2889	C-H, stretching	[60]
1660	C=O, stretching	[61]
1550	C-C, stretching	[57]
1495	C-N, characteristic adsorption bonds of PVP	[62]
1463	C-N, characteristic adsorption bonds of PVP	[62]
1439	CH_3	[63]
1425	CH_2, bending vibration	[64]
1378	heterocyclic in PVP	[63]
1318	heterocyclic in PVP	[63]
1289	C-N, stretching vibration	[58]
1230	no data	
1172	C-N, stretching vibration	[58]
1093	CH_3, rocking	[52]
1075	CN, stretching	[65]
1051	OH, vibration	[55]
1021	C=O, stretching	[55]
1008	no data	
934	no data	
894	no data	

845	C-H, out of plane bending	[63]
736	no data	
659	no data	
615	Ti-O, stretching	[70]
578	N-C=O, vibration	[67]

4.2. Core/Sheath structure confirmation

This section confirmed that core/sheath structure nanofibers were successfully fabricated from coaxial electrospinning process. The core/sheath structure of both as spun and calcined nanofibers were confirmed by TEM images. Furthermore, TEM microtome and SAED were used to describe calcined nanofibers structure and titania crystalline.

4.2.1. Core/Sheath structure (DMF in sheath)

The concentration of PAN in core solution was fixed to be 8wt% in DMF. The compositions of sheath solution was PVP 11.5wt%/TTIP 15.5wt%/DMF/acetic acid. According to Figure 4.14. both as spun and calcined were confirmed to be core/sheath structure.

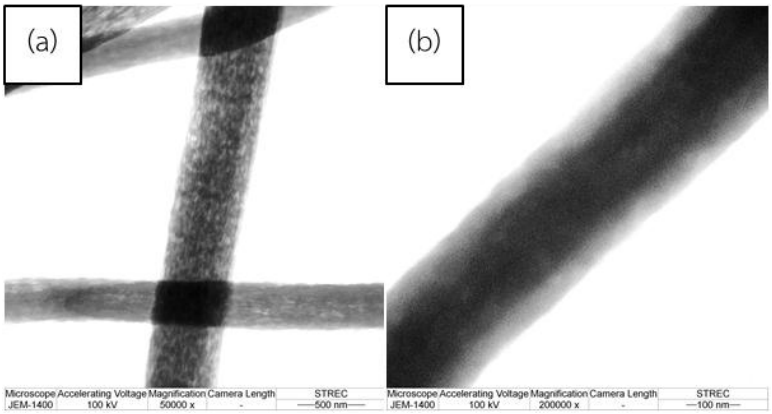

Figure 4.14. TEM images of resultant core/sheath nanofibers (a) as spun and (b) calcined.

The resultant calcined nanofibers in Figure 4.14. (b) were further investigated by using TEM microtome and SAED as shown in Figure 4.15. Referring to the results from section 0., sheath solution can mix with core solution, the structure shown in Figure 4.15. (a) also confirmed that titania from sheath solution, the darker color, diffused into core section. The diffusion of sheath section into core section resulting titania was trapped inside and decrease of titania amount on the surface. The weak signals from selected area electron diffraction (SAED) also confirmed this structure.

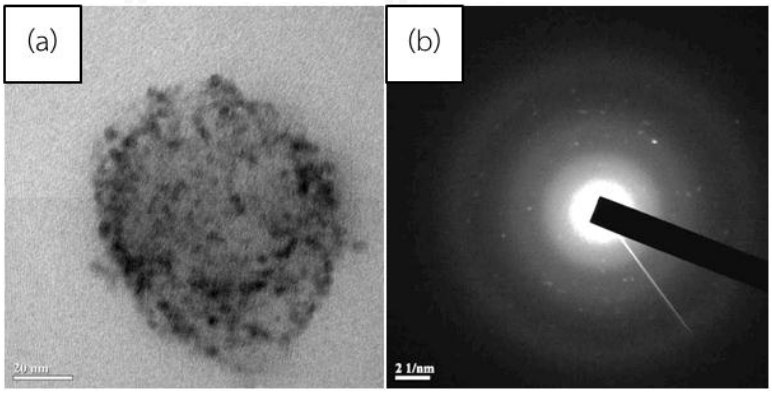

Figure 4.15. TEM images of (a) microtome of calcined nanofibers and (b) SAED pattern.

4.2.2. Core/Sheath structure (ethanol in sheath)

The concentration of PAN in core solution was fixed to be 8wt% in DMF. The compositions of sheath solution was PVP 11.5wt%/TTIP 15.5wt%/ethanol/acetic acid. Similar to the result in section 4.2.1., Figure 4.16. confirmed that core/sheath structure nanofibers were successfully fabricated from coaxial electrospinning technique.

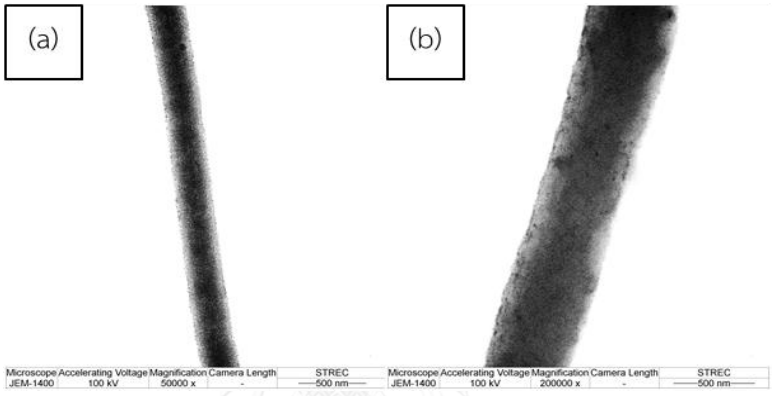

Figure 4.16. TEM images of resultant core/sheath nanofibers (a) as spun and (b) calcined.

The resultant nanofibers was not uniform, there are 2 different structures occurred when use ethanol as solvent in sheath solution. The first and the second structures were shown in Figure 4.17.(a) and (c), respectively. It is shown that some inner parts of the sheath section were diffused into core section for the first structure. The diffusion of sheath section into core section resulting titania was partly trapped inside and decrease of titania amount on the surface. The weak signals from selected area electron diffraction (SAED) in Figure 4.17. (b) show that titania in sheath section was mostly amorphous. According to Figure 4.17. (c), titania was separated and a little part of it remained on the surface of the resultant fibers. The signals from selected area electron diffraction (SAED) in Figure 4.54. (d) shows the crystalline of

titania on the surface of nanofibers. The EDX patterns in Figure 4.18. confirmed the second structure of resultant nanofibers.

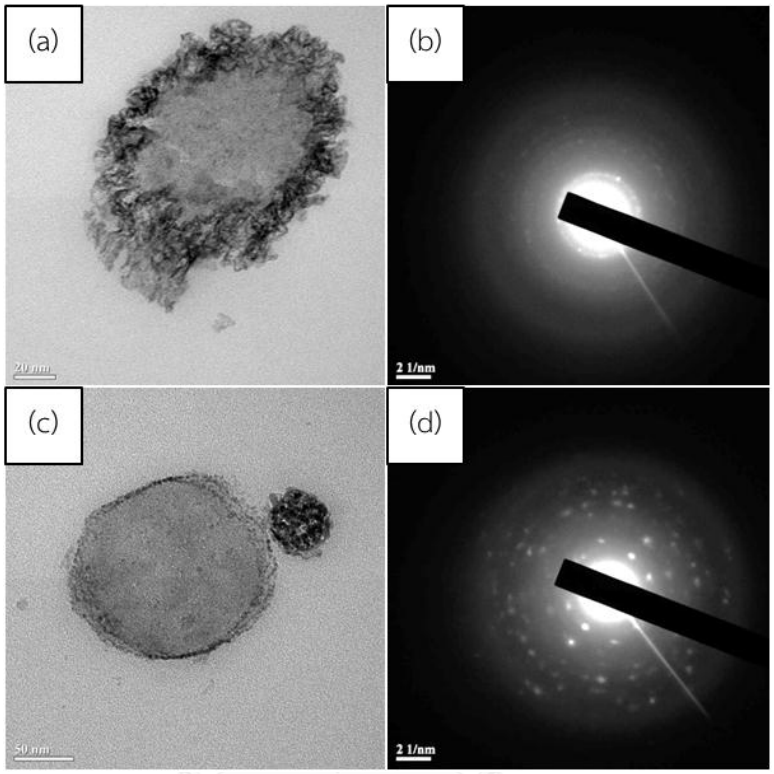

Figure 4.17. TEM images of (a) microtome - 1 of calcined nanofibers, (b) SAED pattern of (a), (c) microtome - 2 of calcined nanofibers, and (d) SAED pattern of (c).

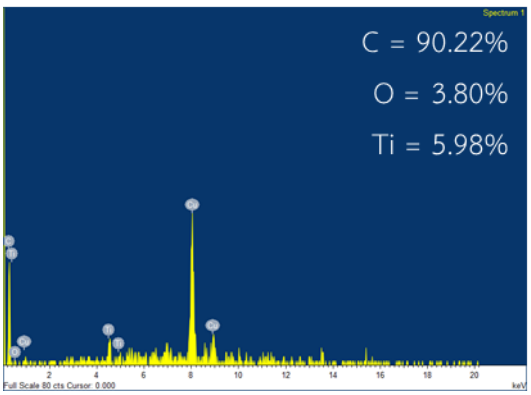

Figure 4.18. EDX patterns of microtome - 2 of calcined nanofibers.

4.2.3. Flexibility of resultant nanofibers

The flexibility of nanofibers would improve the properties and wider their applications. According to the research of A. Biswas et al. (2012), the flexible nanofibers can be easily bent to radius of curvature of 3.4 mm and can be bent to an even smaller radius of curvature of 1.3 mm [6].

From Figure 4.19. and Figure **4.20**., it is shown that the resultant calcined nanofibers, both DMF and ethanol in sheath, can be easily bent to radius of curvature of 3.4 and 1.3 mm. Therefore, flexible nanofibers were successfully fabricated by coaxial electrospinning technique in this work.

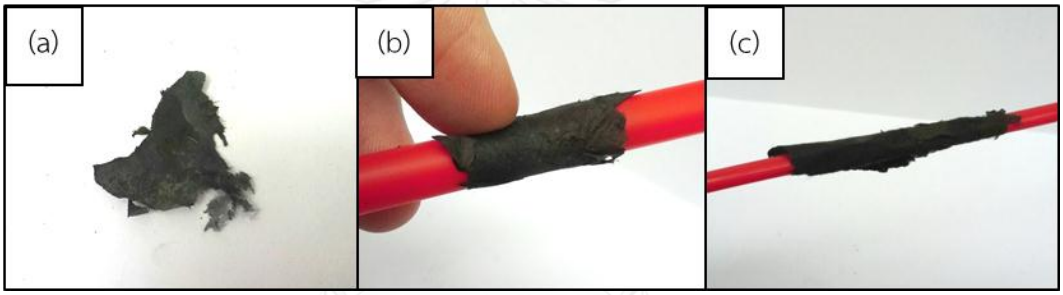

Figure 4.19. (a) core/sheath calcined nanofibers – DMF in sheath, (b) curved to 3.4 mm and (c) 1.3 mm radius of curvature.

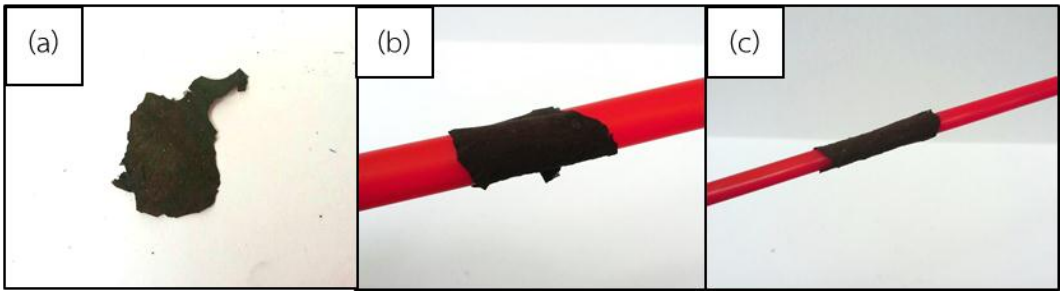

Figure 4.20. (a) core/sheath calcined nanofibers – ethanol in sheath, (b) curved to 3.4 mm and (c) 1.3 mm radius of curvature.

4.3. Morphology of resultant nanofibers

In this section, the morphology of resultant nanofibers both as spun and calcined was investigated by SEM micrographs.

4.3.1. Effect of PVP concentration (DMF in sheath)

The polymer concentration affected the size of the resultant nanofibers due to its viscosity changes. In this work, the concentration of PVP was varied to be 10wt%, 11.5wt% and 13wt% corresponding to the viscosity of 0.3303 Pa.s, 0.5417 Pa.s and 0.7486 Pa.s, respectively. SEM micrographs of the resultant nanofibers are shown in Figure 4.21. The size and standard deviation of resultant nanofibers are listed in Table 4.20. The size distribution of resultant nanofibers are shown in Figure 4.22.

It shows that by increasing PVP concentration, the viscosity was increased and the difference between size of nanofibers before and after calcined are significant. The difference of size of nanofibers before and after calcined at PVP 13wt% shows that titania was trapped in core solution more. If titania were fabricated a lot then the size of nanofibers before and after calcined would not be much different.

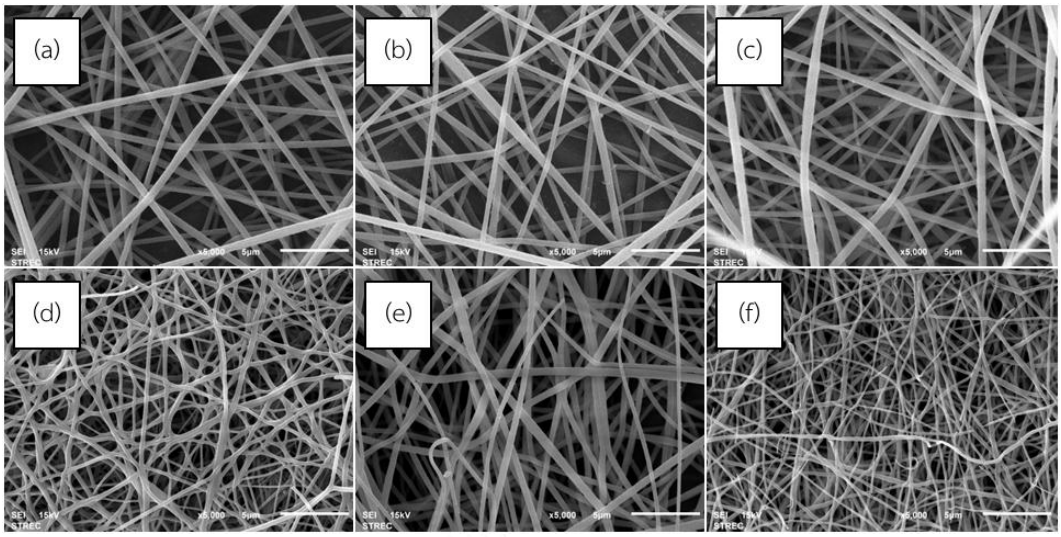

Figure 4.21. SEM micrographs of resultant core/sheath nanofibers; PAN was fixed at 8wt% (a) PVP 10wt%, (b) PVP 11.5wt%, (c) PVP 13wt%, (d) calcined PVP 10wt%, (e) calcined PVP 11.5wt% and (f) calcined PVP 13wt% – DMF in sheath.

Table 4.20. Size and standard deviation of resultant core/sheath nanofibers – vary PVP concentration and DMF in sheath.

Condition	As spun			Calcined		
	Size	S.D.	Bead	Size	S.D.	Bead
PVP 10wt%	334 nm	107.21	x	223 nm	56.21	x
PVP 11.5wt%	377 nm	60.79	x	249 nm	114.93	x
PVP 13wt%	346 nm	96.00	x	186 nm	58.42	x

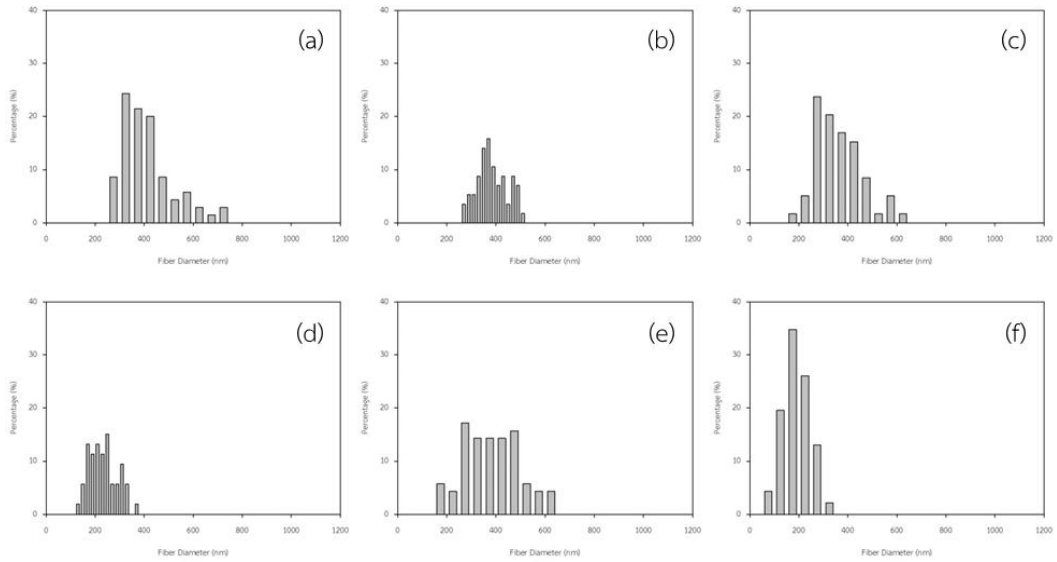

Figure 4.22. The size distribution of resultant core/sheath nanofibers; PAN was fixed at 8wt% (a) PVP 10wt%, (b) PVP 11.5wt%, (c) PVP 13wt%, (d) calcined PVP 10wt%, (e) calcined PVP 11.5wt% and (f) calcined PVP 13wt% – DMF in sheath.

4.3.2. Effect of PVP concentration (ethanol in sheath)

For ethanol in sheath, the concentration of PVP was varied to be 10wt%, 11.5wt% and 13wt% corresponding to the viscosity of 0.4936 Pa.s, 0.6066 Pa.s and 0.7986 Pa.s, respectively. SEM micrographs of the resultant nanofibers are shown in Figure 4.23. The size and standard deviation of resultant nanofibers are listed in Table 4.21. The size distribution of resultant nanofibers are shown in Figure 4.24

It shows that by increasing PVP concentration, the viscosity was increased and the size of nanofibers before and after calcined are decreased. At PVP 13wt%, high viscosity will drag sheath solution more, thus the more amount of titania occurred in resultant nanofibers.

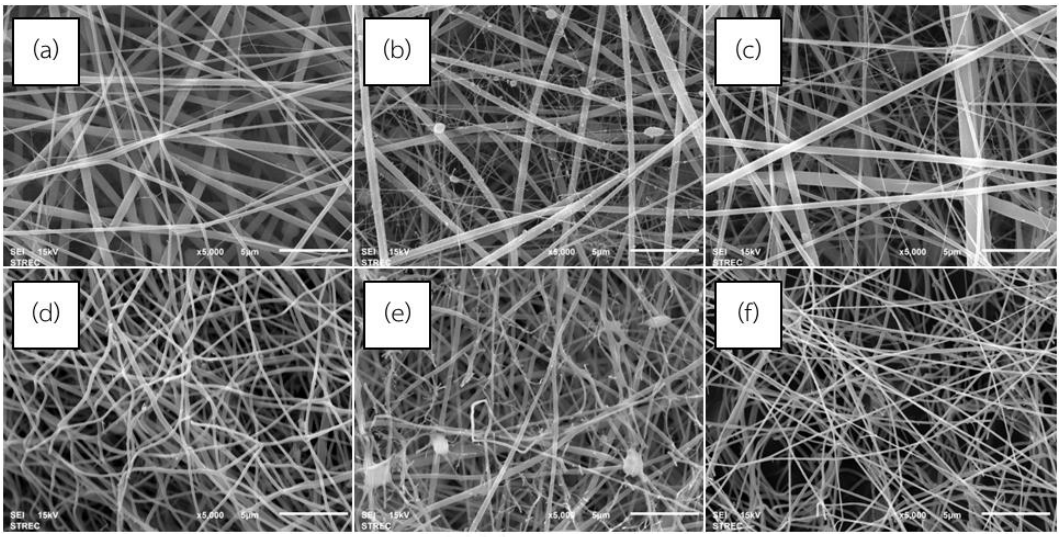

Figure 4.23. SEM micrographs of resultant core/sheath nanofibers; PAN was fixed at 8wt% (a) PVP 10wt%, (b) PVP 11.5wt%, (c) PVP 13wt%, (d) calcined PVP 10wt%, (e) calcined PVP 11.5wt% and (f) calcined PVP 13wt% – ethanol in sheath.

Table 4.21. Size and standard deviation of resultant core/sheath nanofibers – vary PVP concentration and ethanol in sheath.

Condition	As spun			Calcined		
	Size	S.D.	Bead	Size	S.D.	Bead
PVP 10wt%	311 nm	194.87	x	209 nm	70.87	x
PVP 11.5wt%	227 nm	159.23	√	160 nm	90.69	√
PVP 13wt%	206 nm	116.39	x	154 nm	45.02	x

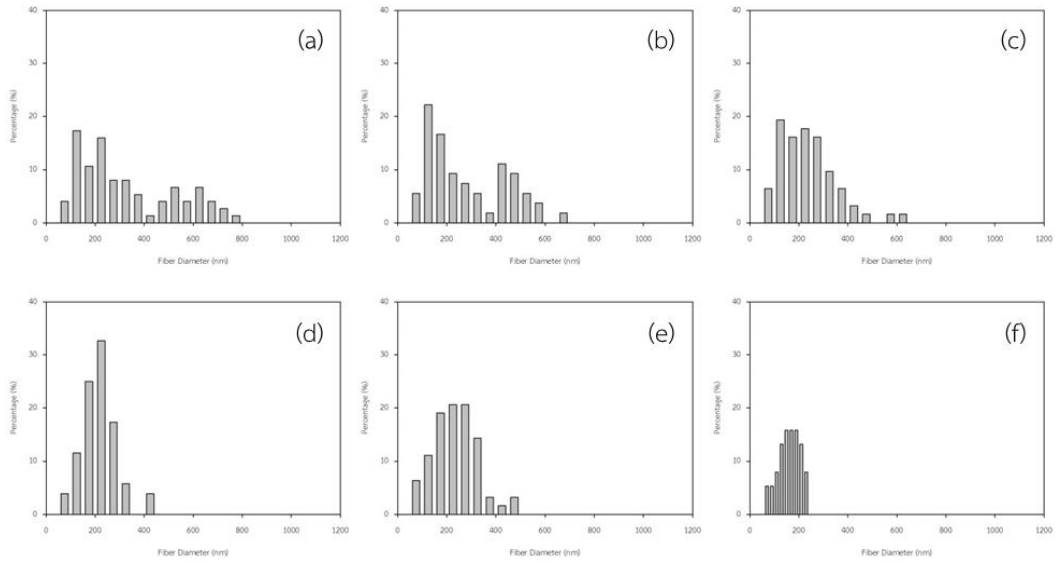

Figure 4.24. The size distribution of resultant core/sheath nanofibers; PAN was fixed at 8wt% (a) PVP 10wt%, (b) PVP 11.5wt%, (c) PVP 13wt%, (d) calcined PVP 10wt%, (e) calcined PVP 11.5wt% and (f) calcined PVP 13wt% – ethanol in sheath.

4.3.3. Effect of TTIP amount (DMF in sheath)

The amount of TTIP added in sheath solution is the titania load for photocatalyst, by adding more TTIP might improved photocatalytic effeciency. In this work, the amount of TTIP was varied to be 11vol%, 15.5vol% and 20vol%. SEM micrographs of the resultant nanofibers are shown in Figure 4.25. The size and standard deviation of resultant nanofibers are listed in Table 4.22. The size distribution of resultant nanofibers are shown in Figure 4.26.

It shows that by increasing the amount of TTIP, the difference between size of the resultant nanofibers before and after calcined are significant. Similar to the results in section 4.3.1., at TTIP 20vol% the difference between the size of nanofibers before and after calcined was not much, thus, titania were fabricated more.

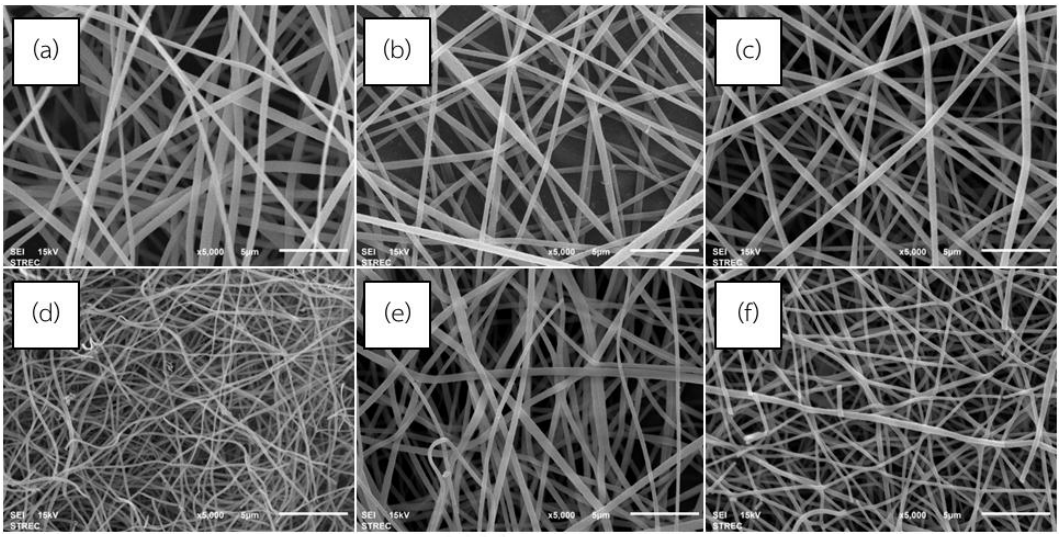

Figure 4.25. SEM micrographs of resultant core/sheath nanofibers (a) TTIP 11vol%, (b) TTIP 15.5vol%, (c) TTIP 20vol%, (d) calcined TTIP 11vol%, (e) calcined TTIP 15.5vol% and (f) calcined TTIP 20vol% –DMF in sheath.

Table 4.22. Size and standard deviation of resultant core/sheath nanofibers – vary TTIP amount and DMF in sheath.

Condition	As spun			Calcined		
	Size	S.D.	Bead	Size	S.D.	Bead
TTIP 11vol%	406 nm	113.64	x	182 nm	52.65	x
TTIP 15.5vol%	377 nm	60.79	x	294 nm	114.93	x
TTIP 20vol%	312 nm	102.83	x	223 nm	72.93	x

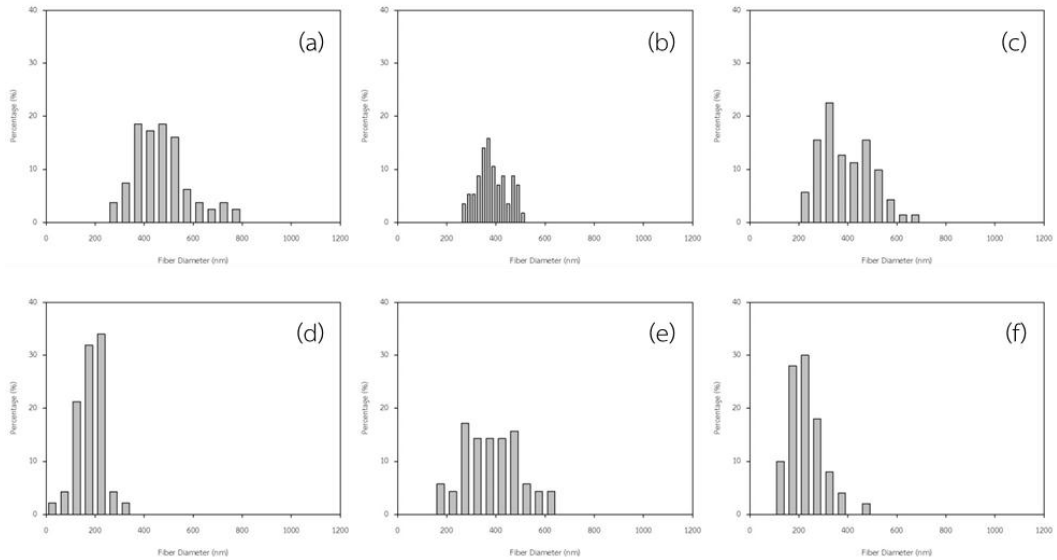

Figure 4.26. The size distribution of resultant core/sheath nanofibers (a) TTIP 11vol%, (b) TTIP 15.5vol%, (c) TTIP 20vol%, (d) calcined TTIP 11vol%, (e) calcined TTIP 15.5vol% and (f) calcined TTIP 20vol% –DMF in sheath.

4.3.4. Effect of TTIP amount (ethanol in sheath)

According to the interaction that occurred in section 4.1.5., the amount of TTIP will affected the sol-gel process. In this work, the amount of TTIP was varied to be 11vol%, 15.5vol% and 20vol%. SEM micrographs of the resultant nanofibers are shown in Figure 4.27. The size and standard deviation of resultant nanofibers are listed in Table 4.23. The size distribution of resultant nanofibers are shown in Figure 4.28. The increase of TTIP amount makes the nanofibers size smaller. The structure of the nanofibers could not be discussed more by these data.

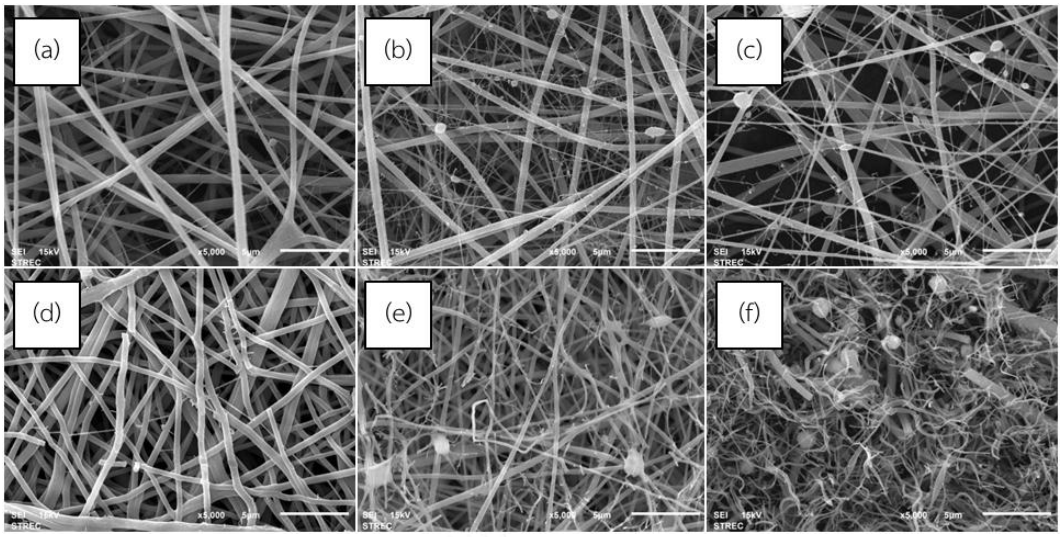

Figure 4.27. SEM micrographs of resultant core/sheath nanofibers (a) TTIP 11vol%, (b) TTIP 15.5vol%, (c) TTIP 20vol%, (d) calcined TTIP 11vol%, (e) calcined TTIP 15.5vol% and (f) calcined TTIP 20vol% –ethanol in sheath.

Table 4.23. Size and standard deviation of resultant core/sheath nanofibers – vary TTIP amount and ethanol in sheath.

Condition	As spun			Calcined		
	Size	S.D.	Bead	Size	S.D.	Bead
TTIP 11vol%	344 nm	107.21	x	338 nm	143.01	x
TTIP 15.5vol%	227 nm	159.23	√	160 nm	90.69	√
TTIP 20vol%	254 nm	204.36	√	172 nm	123.27	√

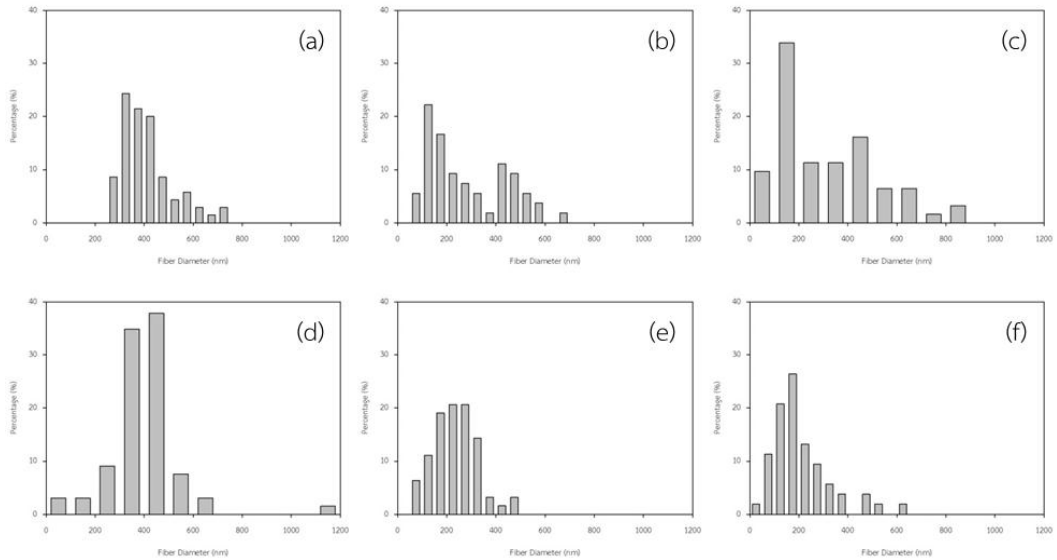

Figure 4.28. The size distribution of resultant core/sheath nanofibers (a) TTIP 11vol%, (b) TTIP 15.5vol%, (c) TTIP 20vol%, (d) calcined TTIP 11vol%, (e) calcined TTIP 15.5vol% and (f) calcined TTIP 20vol% –ethanol in sheath.

4.3.5. Effect of aging time of titania-precursor (DMF in sheath)

The aging time of titania-precursor solution for DMF solvent in sheath is not supposed to affect any of the resultant nanofibers properties because the sol-gel process does not take place in accordance with the results in section 4.1.4. In this work, the aging time of titania-precursor was varied to be 0 min, 15 min and 30 min. SEM micrographs of the resultant nanofibers are shown in Figure 4.29. The size and standard deviation of resultant nanofibers are listed in Table 4.24. The size distribution of resultant nanofibers are shown in Figure 4.30. The increase of aging time makes the nanofibers size smaller. The structure of the nanofibers could not be discussed more by these data.

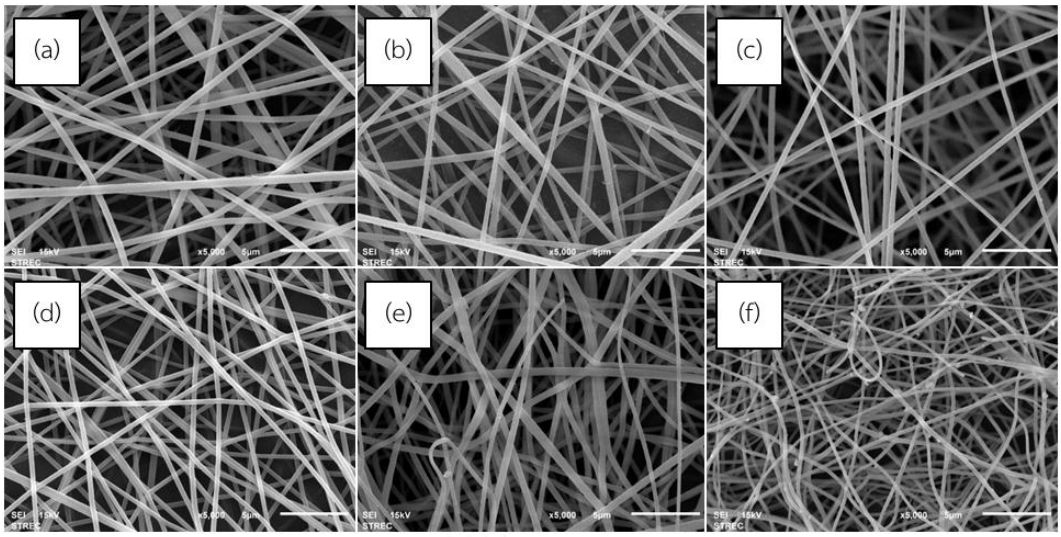

Figure 4.29. SEM micrographs of resultant core/sheath nanofibers (a) age 0 min, (b) age 15 min, (c) age 30 min, (d) calcined age 0 min, (e) calcined age 15 min and (f) calcined age 30 min –DMF in sheath.

Table 4.24. Size and standard deviation of resultant core/sheath nanofibers – vary aging time and DMF in sheath.

Condition	As spun			Calcined		
	Size	S.D.	Bead	Size	S.D.	Bead
Age 0 min	444 nm	94.00	x	313 nm	69.51	x
Age 15 min	377 nm	60.79	x	294 nm	114.93	x
Age 30 min	362 nm	77.90	x	245 nm	89.28	x

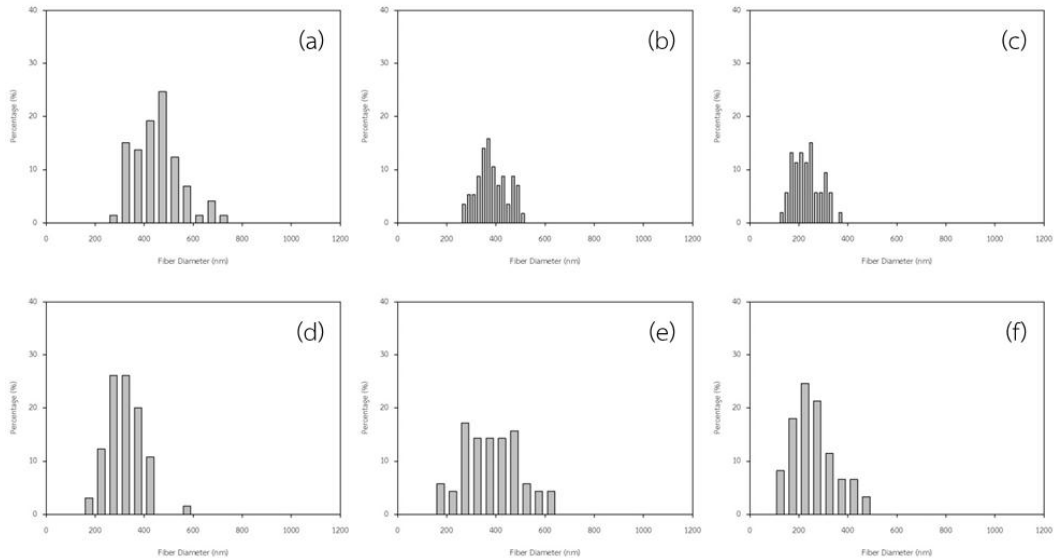

Figure 4.30. The size distribution of resultant core/sheath nanofibers (a) age 0 min, (b) age 15 min, (c) age 30 min, (d) calcined age 0 min, (e) calcined age 15 min and (f) calcined age 30 min –DMF in sheath.

4.3.6. Effect of aging time of titania-precursor (ethanol in sheath)

According to the interaction that occurred in section 4.1.5., the aging time of Titania-precursor solution will affect the sol-gel process. Similar to the previous section, in this work, the aging time of titania-precursor was varied to be 0 min to 30 min. SEM micrographs of the resultant nanofibers are shown in Figure 4.31. The size and standard deviation of resultant nanofibers are listed in Table 4.25. The size distribution of resultant nanofibers are shown in Figure 4.32. The increase of titania-precursor aging time makes the nanofibers size smaller. It shows that at aging time 15 min and 30 min the size of the nanofibers were not significantly different, it confirmed the results from section 4.1.7.

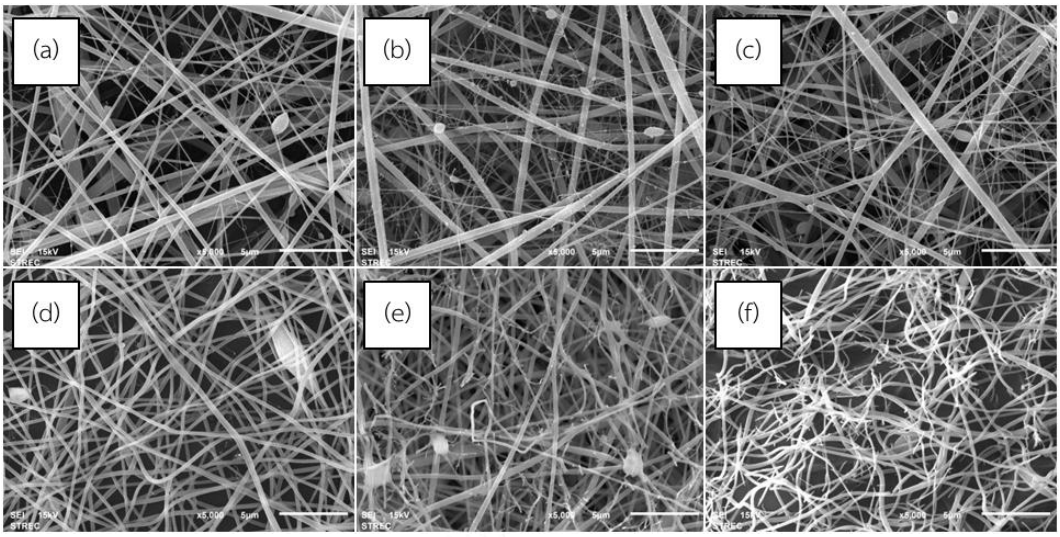

Figure 4.31. SEM micrographs of resultant core/sheath nanofibers (a) age 0 min, (b) age 15 min, (c) age 30 min, (d) calcined age 0 min, (e) calcined age 15 min and (f) calcined age 30 min –ethanol in sheath.

Table 4.25. Size and standard deviation of resultant core/sheath nanofibers – vary aging time and ethanol in sheath.

Condition	As spun			Calcined		
	Size	S.D.	Bead	Size	S.D.	Bead
Age 0 min	252 nm	124.58	x	239 nm	59.31	x
Age 15 min	227 nm	159.23	√	160 nm	90.69	√
Age 30 min	215 nm	138.07	√	141 nm	65.71	x

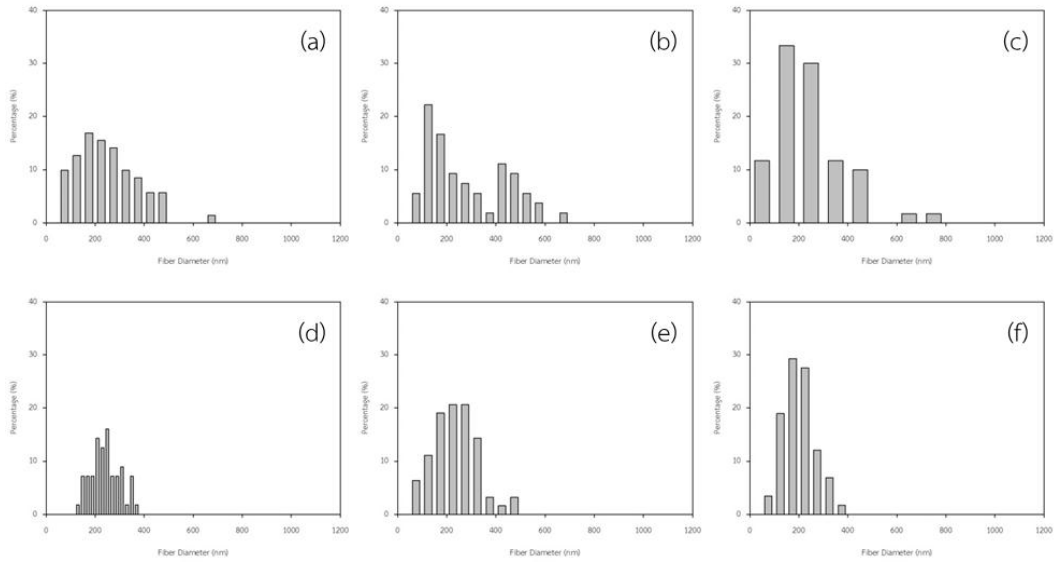

Figure 4.32. The size distribution of resultant core/sheath nanofibers (a) age 0 min, (b) age 15 min, (c) age 30 min, (d) calcined age 0 min, (e) calcined age 15 min and (f) calcined age 30 min –ethanol in sheath.

4.3.7. Effect of electrical potential used (DMF in sheath)

In this work, the electrical potential used was varied to be 22 kV, 24 kV and 26 kV. SEM micrographs of the resultant nanofibers are shown in Figure 4.33. The size and standard deviation of resultant nanofibers are listed in Table 4.26. The size distribution of resultant nanofibers are shown in Figure 4.34. The structure of the nanofibers could not be discussed more by these data, but it shows that 22 kV and 26 kV are not the proper electrical potential for this system.

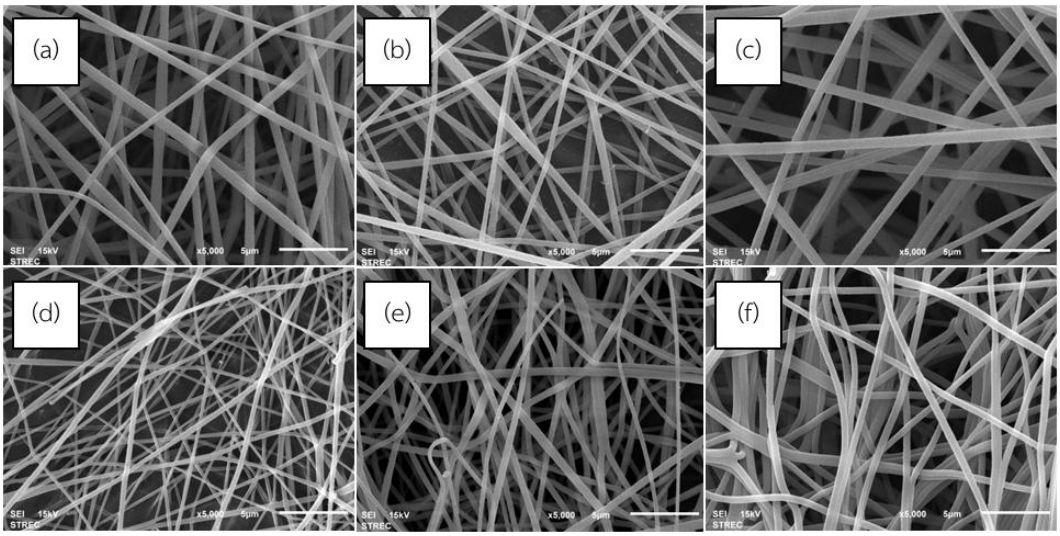

Figure 4.33. SEM micrographs of resultant core/sheath nanofibers (a) 22 kV, (b) 24 kV, (c) 26 kV, (d) calcined 22 kV, (e) calcined 24 kV and (f) calcined 26 kV – DMF in sheath.

Table 4.26. Size and standard deviation of resultant core/sheath nanofibers – vary electrical potential and DMF in sheath.

Condition	As spun			Calcined		
	Size	S.D.	Bead	Size	S.D.	Bead
22 kV	530 nm	115.70	x	211 nm	73.46	x
24 kV	377 nm	60.79	x	294 nm	114.93	x
26 kV	638 nm	148.59	x	429 nm	81.22	x

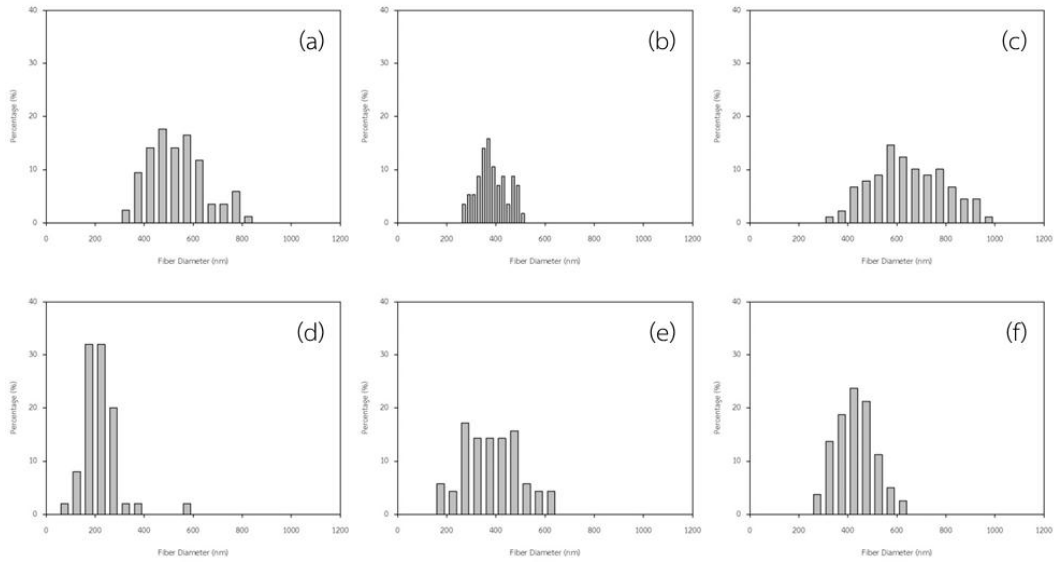

Figure 4.34. The size distribution of resultant core/sheath nanofibers (a) 22 kV, (b) 24 kV, (c) 26 kV, (d) calcined 22 kV, (e) calcined 24 kV and (f) calcined 26 kV – DMF in sheath.

4.3.8. Effect of electrical potential used (ethanol in sheath)

In this work, the electrical potential used was varied to be 22 kV, 24 kV and 26 kV. SEM micrographs of the resultant nanofibers are shown in Figure 4.35. The size and standard deviation of resultant nanofibers are listed in Table 4.27. The size distribution of resultant nanofibers are shown in Figure 4.36. Similar to the previous section, the structure of the nanofibers could not be discussed more by these data, but it shows that 22 kV and 26 kV are not the proper electrical potential for this system.

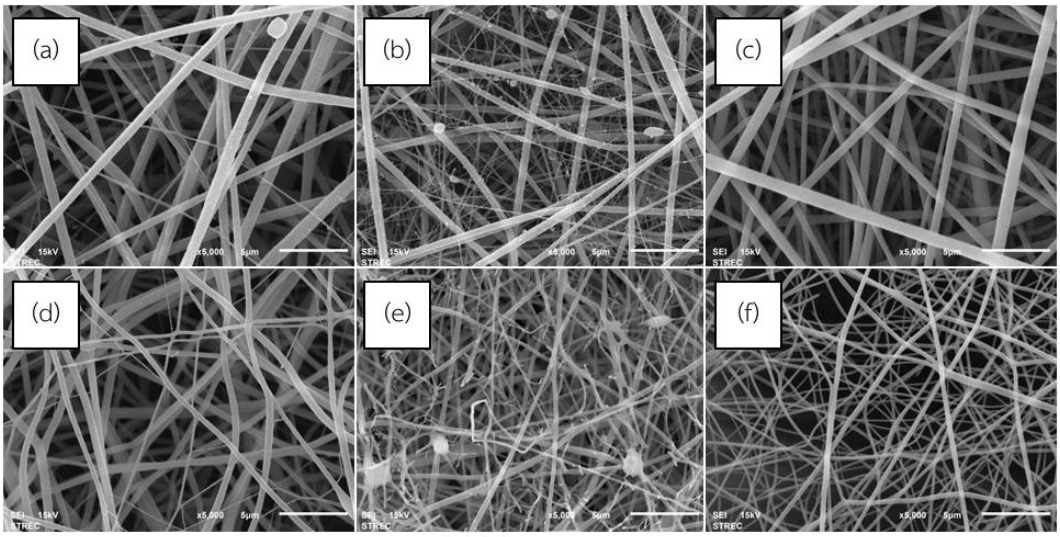

Figure 4.35. SEM micrographs of resultant core/sheath nanofibers (a) 22 kV, (b) 24 kV, (c) 26 kV, (d) calcined 22 kV, (e) calcined 24 kV and (f) calcined 26 kV – ethanol in sheath.

Table 4.27. Size and standard deviation of resultant core/sheath nanofibers – vary electrical potential and ethanol in sheath.

Condition	As spun			Calcined		
	Size	S.D.	Bead	Size	S.D.	Bead
22 kV	502 nm	236.04	x	368 nm	149.88	x
24 kV	227 nm	159.23	√	160 nm	90.69	√
26 kV	531 nm	163.88	x	191 nm	60.77	x

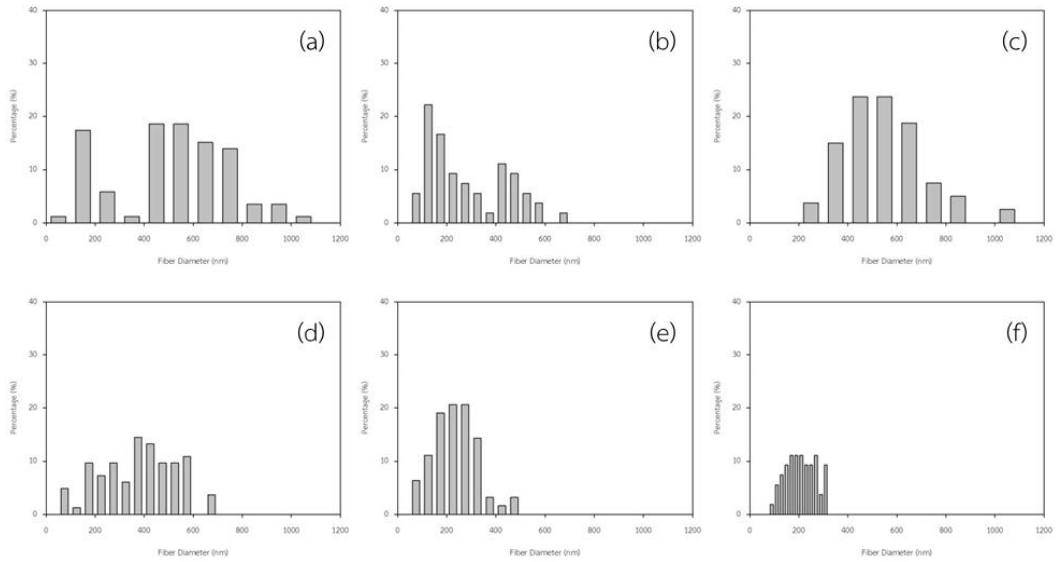

Figure 4.36. The size distribution of resultant core/sheath nanofibers (a) 22 kV, (b) 24 kV, (c) 26 kV, (d) calcined 22 kV, (e) calcined 24 kV and (f) calcined 26 kV – ethanol in sheath.

From all results in section 4.3., it shows that nanofibers with DMF in sheath are larger and more uniform in size and no beads. On the other hand, nanofibers with ethanol in sheath are smaller and non uniform in size and there are beads occurred in some condition.

The overall as spun nanofibers have the rough surface as shown in Figure 4.37. (a) and the calcined nanofibers have a smoother surface as shown in Figure 4.37. (b), this happened due to some parts of sheath section diffused into core section and titania was trapped or titania loss in coaxial electrospinning process.

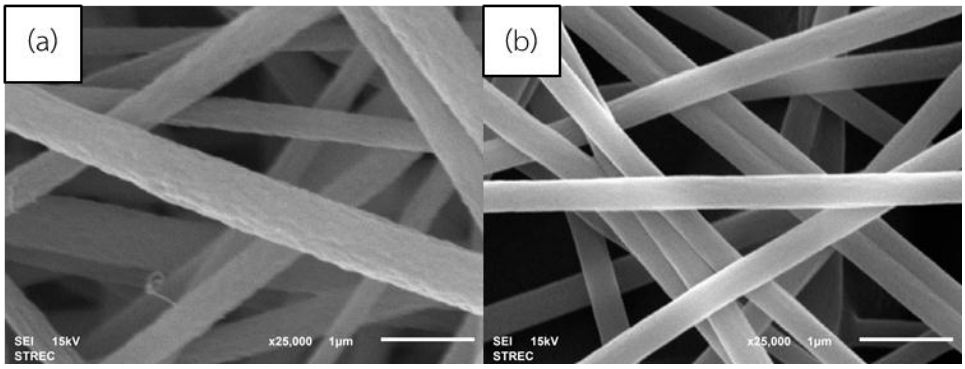

Figure 4.37. SEM micrographs of resultant core/sheath (a) rough and (b) smooth nanofibers.

4.4. Core/Sheath interface studied by spin coating

From section 4.1., the interaction among components in each solution were studied and all interactions were investigated. It is rather difficult to investigate the behavior of core and sheath solutions while electrospinning process occurs. Thus, in this work, spin coating multilayer films were used as the simulation model to investigate the solution behavior in electrospinning process. The FTIR spectra were used to compare the functional group of nanofibers from electrospinning and spin coating films, also the functional group of calcined nanofibers and calcined films. The behavior of nanofibers were studied by using the films, while the calcined nanofibers were studied by using the calcined films.

In spin coating process, core solution was spun as the first layer film while the second layer was sheath solution as shown in Figure 4.38.

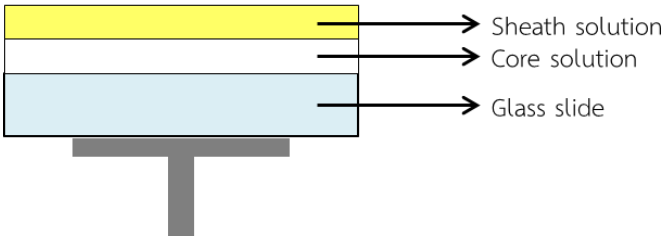

Figure 4.38. Schematic of multilayer spin coating film.

4.4.1. For DMF in sheath

The concentration of PAN in core solution was fixed to be 8wt% in DMF. The compositions of sheath solution was PVP 11.5wt%/TTIP 15.5wt%/DMF/acetic acid. The FTIR transmittance spectra of fiber, film, calcined fiber and calcined film are shown in Figure 4.39. According to Figure 4.39.(a) and (b), all spectra of fiber are similar to film, but some minority spectra in film does not appear in the spectra of fiber. Besides that, in Figure 4.39. (c) and (d) the majority spectra of calcined fiber are similar to calcined film, but some spectra of calcined fiber does not appear in calcined film. Thus, the spin coating films can investigate only the overall image of nanofibers core/sheath interface behavior.

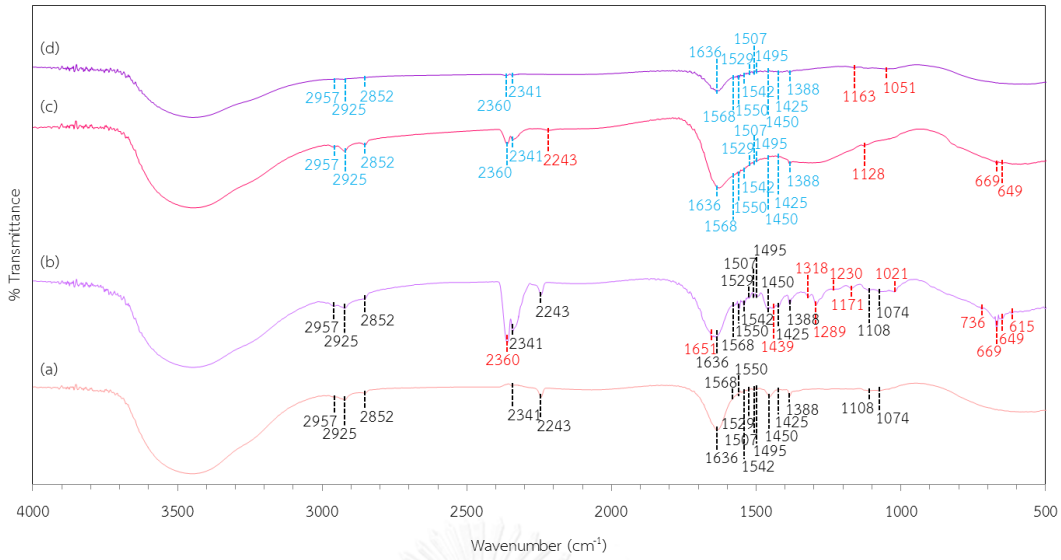

Figure 4.39. FTIR transmittance spectra of (a) fiber, (b) film, (c) calcined fiber and (d) calcined film – DMF in sheath.

The details of FTIR peaks are listed in Table 4.28., Table **4.29**., Table **4.30**. and Table **4.31**.

Table 4.28. FTIR peak assignment for resultant nanofibers.

Fiber		
Wavenumber (cm^{-1})	Functional groups	References
2957	C-H, stretching vibration	[58]
2925	C-H, asymmetric stretching vibration	[59]
2852	CH_2, symmetric stretching	[49]
2341	C=O	[51]
2243	C≡N, stretching vibration	[49]
1636	C=C	[50]
1568	N-H	[71]
1550	C-N	[73]

1542	C-C, stretching	[57]
1529	C=O, asymmetric stretching vibration	[77]
1507	C-N, stretching	[52]
1495	C-N, characteristic adsorption bonds of PVP	[62]
1450	C-N, stretching vibration	[57]
1425	CH_2, bending vibration	[64]
1388	N-C-H, bending	[52]
1108	no data	
1074	C-N, bending vibration	[53]

Table 4.29. FTIR peak assignment for resultant film.

Film		
Wavenumber (cm^{-1})	Functional groups	References
2957	C-H, stretching vibration	[58]
2925	C-H, asymmetric stretching vibration	[59]
2852	CH_2, symmetric stretching	[49]
2360	C=O, stretching vibration	[51]
2341	C=O	[51]
2243	C≡N, stretching vibration	[49]
1651	C=O, stretching vibration	[77]
1636	C=C	[50]
1568	N-H	[71]
1550	C-N	[73]
1542	C-C, stretching	[57]

1529	C=O, asymmetric stretching vibration	[77]
1507	C-N, stretching	[52]
1495	C-N, characteristic adsorption bonds of PVP	[62]
1450	C-N, stretching vibration	[57]
1439	CH_3	[63]
1425	CH_2, bending vibration	[64]
1388	N-C-H, bending	[52]
1318	heterocyclic in PVP	[63]
1289	C-N, stretching vibration	[58]
1230	no data	
1171	C-N, stretching vibration	[58]
1108	no data	
1074	C-N, bending vibration	[53]
1021	C=O, stretching	[55]
736	no data	
669	O=C-N, stretching	[52]
649	no data	
615	Ti-O, stretching	[70]

Table 4.30. FTIR peak assignment for resultant calcined nanofibers.

Calcined fiber		
Wavenumber (cm^{-1})	Functional groups	References
2957	C-H, stretching vibration	[58]
2925	C-H, asymmetric stretching vibration	[59]

2852	CH_2, symmetric stretching	[49]
2360	C=O, stretching vibration	[51]
2341	C=O	[51]
2243	C≡N, stretching vibration	[49]
1636	C=C	[50]
1568	N-H	[71]
1550	C-N	[73]
1542	C-C, stretching	[57]
1529	C=O, asymmetric stretching vibration	[77]
1507	C-N, stretching	[52]
1495	C-N, characteristic adsorption bonds of PVP	[62]
1450	C-N, stretching vibration	[57]
1425	CH_2, bending vibration	[64]
1388	N-C-H, bending	[52]
1128	no data	
669	O=C-N, stretching	[52]
649	no data	

Table 4.31. FTIR peak assignment for resultant calcined film.

Calcined film		
Wavenumber (cm^{-1})	Functional groups	References
2957	C-H, stretching vibration	[58]
2925	C-H, asymmetric stretching vibration	[59]
2852	CH_2, symmetric stretching	[49]

2360	C=O, stretching vibration	[51]
2341	C=O	[51]
1636	C=C	[50]
1568	N-H	[71]
1550	C-N	[73]
1542	C-C, stretching	[57]
1529	C=O, asymmetric stretching vibration	[77]
1507	C-N, stretching	[52]
1495	C-N, characteristic adsorption bonds of PVP	[62]
1450	C-N, stretching vibration	[57]
1425	CH_2, bending vibration	[64]
1388	N-C-H, bending	[52]
1163	no data	
1051	OH, vibration	[55]

SEM-EDX mapping of resultant core/sheath films are shown in Figure 4.40. and EDX patterns and atomic percentage of resultant core/sheath films in Figure 4.41. The results show that before calcination carbon percentage was high while titania percentage was low, but in contrast, after calcination, titania percentage was higher and carbon percentage was lower. This phenomena explained that after calcination polymer was gone and titania remained. From Figure 4.40., it shows that titania diffused from sheath section into core section which confirmed the structure of the resultant fiber in section 4.2.1.

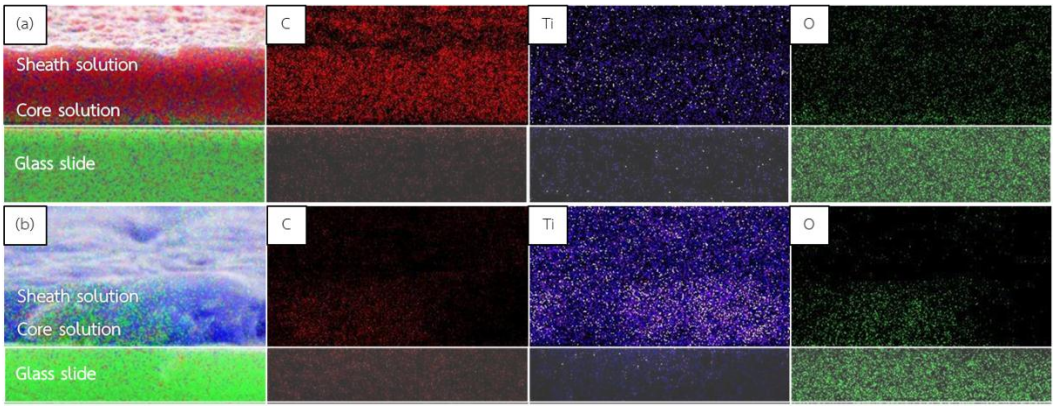

Figure 4.40. SEM-EDX mapping of resultant core/sheath films (a) as spun and (b) calcined – DMF in sheath.

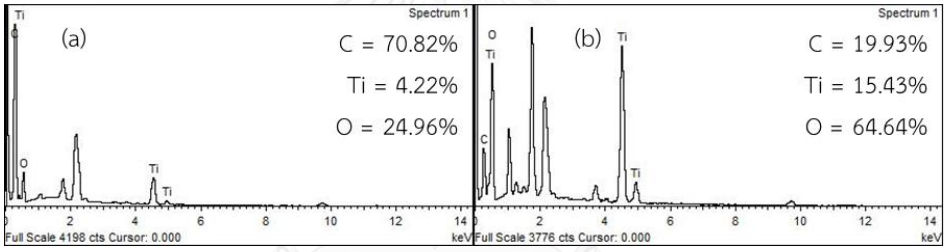

Figure 4.41. EDX patterns and atomic percentage of resultant core/sheath films (a) as spun and (b) calcined – DMF in sheath.

4.4.2. For ethanol in sheath

The concentration of PAN in core solution was fixed to be 8wt% in DMF. The compositions of sheath solution was PVP 11.5wt%/TTIP 15.5wt%/ethanol/acetic acid. The FTIR transmittance spectra of fiber, film, calcined fiber and calcined film are shown in Figure 4.42. According to Figure 4.42. (a) and (b), all spectra of fiber are similar to the spectra of film, only 2 peaks that are different. Besides that, in Figure 4.42. (c) and (d) the spectra of calcined fiber are similar to calcined film only about

half. Thus, the spin coating film can investigated overall of the core/sheath interface behavior of fiber, but the calcined film can only can investigate half.

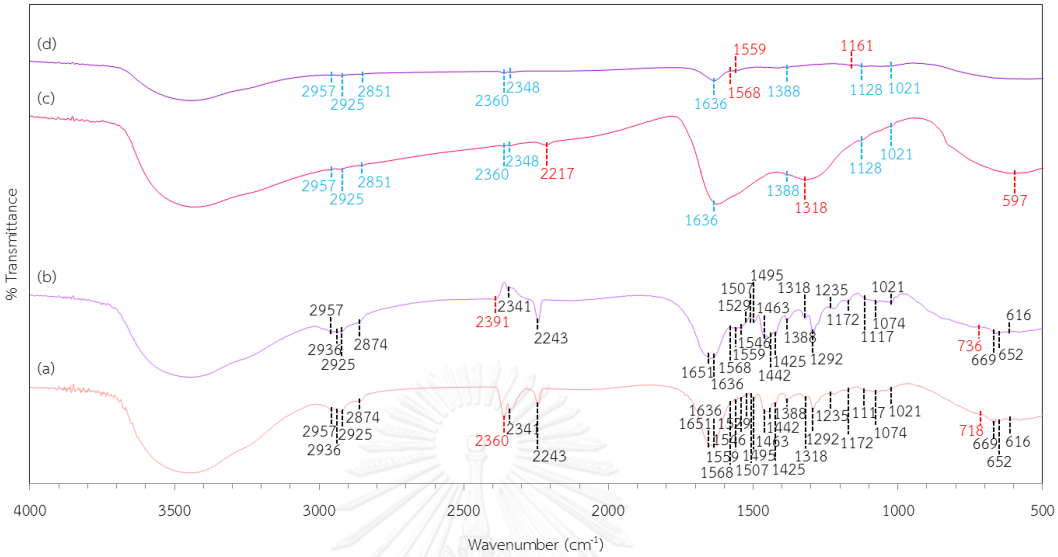

Figure 4.42. FTIR transmittance spectra of (a) fiber, (b) film, (c) calcined fiber and (d) calcined film – ethanol in sheath.

The details of FTIR peaks are listed in Table 4.32., **Table 4.33**., Table **4.34**. and Table **4.35**.

Table 4.32. FTIR peak assignment for resultant nanofibers.

Fiber		
Wavenumber (cm^{-1})	Functional groups	References
2957	C-H, stretching vibration	[58]
2936	C-H, stretching	[51]
2925	C-H, asymmetric stretching vibration	[59]
2874	CH, CH_2, CH_3, symmetric	[53]
2360	C=O, stretching vibration	[51]
2341	no data	

2243	C≡N, stretching vibration	[49]
1651	C=O, stretching vibration	[77]
1636	C=C	[50]
1568	N-H	[71]
1559	O-C-N, asymmetric stretching	[77]
1546	C-C, stretching	[57]
1529	C=O, asymmetric stretching vibration	[77]
1507	C-N, stretching	[52]
1495	C-N, characteristic adsorption bonds of PVP	[62]
1463	C-N, characteristic adsorption bonds of PVP	[62]
1442	CH_3	[63]
1425	CH_2, bending vibration	[64]
1388	N-C-H, bending	[52]
1318	CH in plane	[57]
1292	C-N, stretching vibration	[58]
1235	no data	
1172	C-N, stretching vibration	[58]
1117	C-O, stretching vibration	[58]
1074	C-N, bending vibration	[53]
1021	C=O, stretching	[55]
718	no data	
669	O=C-N, stretching	[52]
652	no data	
616	Ti-O, stretching	[70]

Table 4.33. FTIR peak assignment for resultant film.

Film		
Wavenumber (cm^{-1})	Functional groups	References
2957	C-H, stretching vibration	[58]
2936	C-H, stretching	[51]
2925	C-H, asymmetric stretching vibration	[59]
2874	CH, CH_2, CH_3, symmetric	[53]
2391	no data	
2341	no data	
2243	C≡N, stretching vibration	[49]
1651	C=O, stretching vibration	[77]
1636	C=C	[50]
1568	N-H	[71]
1559	O-C-N, asymmetric stretching	[77]
1546	C-C, stretching	[57]
1529	C=O, asymmetric stretching vibration	[77]
1507	C-N, stretching	[52]
1495	C-N, characteristic adsorption bonds of PVP	[62]
1463	C-N, characteristic adsorption bonds of PVP	[62]
1442	CH_3	[63]
1425	CH_2, bending vibration	[64]
1388	N-C-H, bending	[52]
1318	CH in plane	[57]
1292	C-N, stretching vibration	[58]

1235	no data	
1172	C-N, stretching vibration	[58]
1117	C-O, stretching vibration	[58]
1074	C-N, bending vibration	[53]
1021	C=O, stretching	[55]
736	no data	
669	O=C-N, stretching	[52]
652	no data	

Table 4.34. FTIR peak assignment for resultant calcined nanofibers.

Calcined fiber		
Wavenumber (cm^{-1})	Functional groups	References
2957	C-H, stretching vibration	[58]
2925	C-H, asymmetric stretching vibration	[59]
2851	C-H, symmetric stretching	[49]
2360	C=O, stretching vibration	[51]
2348	no data	
2217	no data	
1636	C=C	[50]
1388	N-C-H, bending	[52]
1318	CH in plane	[57]
1128	no data	
1021	C=O, stretching	[55]
597	C-H, bending vibration	[77]

Table 4.35. FTIR peak assignment for resultant calcined film.

Calcined film		
Wavenumber (cm^{-1})	Functional groups	References
2957	C-H, stretching vibration	[58]
2925	C-H, asymmetric stretching vibration	[59]
2851	C-H, symmetric stretching	[49]
2360	C=O, stretching vibration	[51]
2348	no data	
1636	C=C	[50]
1568	N-H	[71]
1559	O-C-N, asymmetric stretching	[77]
1388	N-C-H, bending	[52]
1161	no data	
1128	no data	
1021	C=O, stretching	[55]

SEM-EDX mapping of resultant core/sheath films are shown in Figure 4.43. and EDX patterns and atomic percentage of resultant core/sheath films in Figure 4.44. Similar to the previous section, the results show that before calcination carbon percentage was high while titania percentage was low, but in contrast, after calcination, titania percentage was higher and carbon percentage was lower. This phenomena explained that after calcination polymer was gone and titania remained. From Figure 4.43., it shows that titania partly diffused from sheath section into core section which confirmed the structure of the resultant fiber in section 4.2.2. It is clearly showed that titania mainly disperse in sheath section on the top.

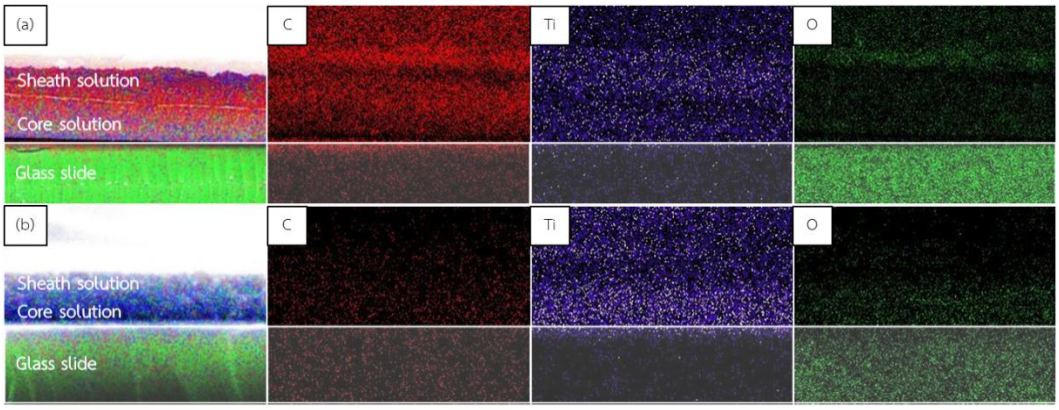

Figure 4.43. SEM-EDX mapping of resultant core/sheath films (a) as spun and (b) calcined – ethanol in sheath.

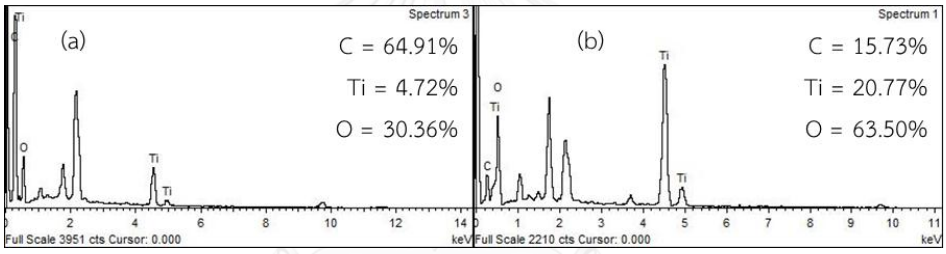

Figure 4.44. EDX patterns and atomic percentage of resultant core/sheath films (a) as spun and (b) calcined – ethanol in sheath.

4.4.3. Core/Sheath interface when spins in another form

To prove that gravity does not take effect in the spin coating process, thus, sheath solution was spun as the first layer film while the second layer was core solution. For both solvent, SEM-EDX mapping of resultant core/sheath films are shown in Figure 4.45. and EDX patterns and atomic percentage of resultant core/sheath films in Figure 4.44. According to Figure 4.45 (a) and (b), DMF and ethanol in sheath, the results are the same with ones in the previous section. For DMF in sheath, titania from sheath section could dispersed into core section. For ethanol in sheath, titania is partly diffused into core section, but it mainly disperse in

sheath section on the bottom. Therefore, the behavior of core/sheath interface still matched with ones in section 4.2.1., 4.2.2. 4.4.1. and 4.4.2.

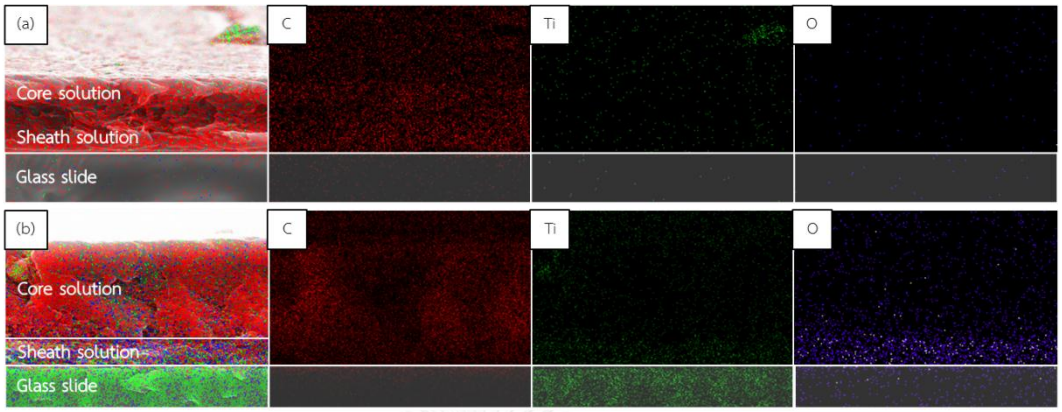

Figure 4.45. SEM-EDX mapping of resultant core/sheath films when spin sheath first (a) DMF and (b) ethanol in sheath.

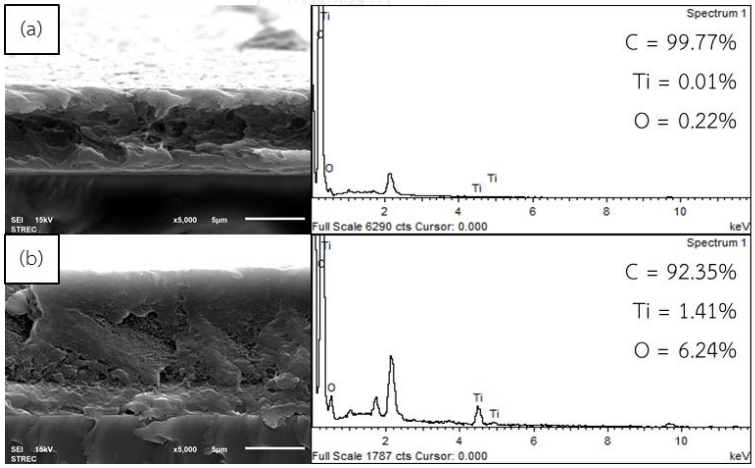

Figure 4.46. EDX patterns and atomic percentage of resultant core/sheath films when spin sheath first (a) DMF and (b) ethanol in sheath.

Next, in spin coating process, the core solution was spun as the first layer film. Then, dry the first layer for 12 hr in the oven. After the first layer dried, spun sheath solution as the second layer film. For both solvent, SEM-EDX mapping of resultant core/sheath films are shown in Figure 4.48. and EDX patterns and atomic

percentage of resultant core/sheath films in Figure 4.48. This confirmed that the interaction between core/sheath solution occur only in wet solution. After dry the first layer film, core and sheath section were clearly separated into 2 different layers and no interaction occur.

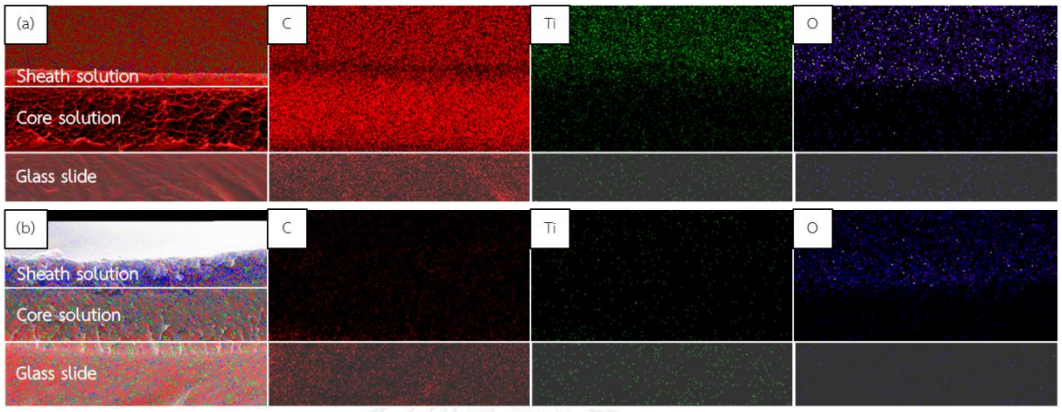

Figure 4.47. SEM-EDX mapping of resultant core/sheath films when core section dried before spin sheath (a) DMF and (b) ethanol in sheath.

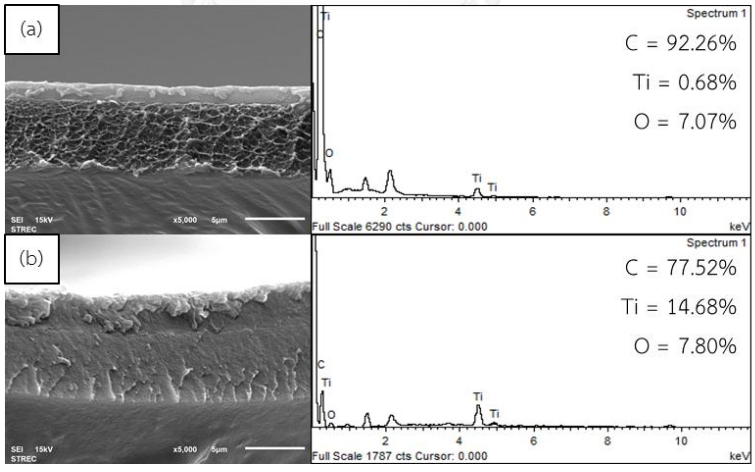

Figure 4.48. EDX patterns and atomic percentage of resultant core/sheath films when core section dried before spin sheath (a) DMF and (b) ethanol in sheath.

4.5. Photocatalytic activity

In this section, the photocatalytic activities of resultant nanofibers were investigated. The degradation percentage of various condition of resultant photocatalysts were shown in Table 4.36. All results confirmed the structure of nanofibers in section 4.2.1., 4.2.2., 4.3.1., 4.3.2., 4.3.3., 4.3.4., 4.3.5., 4.3.6., 4.3.7., 4.3.8., 4.4.1. and 4.4.2. (e.g. for DMF in sheath, after varying PVP concentration, it was found that by increasing PVP concentration titania was trapped in core solution more).

Table 4.36. Degradation percentage of various condition of both coaxial nanofibers and sheath solution's powder (using the UV-A lamp).

Solvent type	Variation type	Various condition	Fiber (%degradation)	Powder (%degradation)
DMF solvent	vary PVP	PVP 10 %wt	1.11	not degrade
		PVP 11.5 %wt	2.35	not degrade
		PVP 13 %wt	not degrade	not degrade
	vary TTIP	TTIP 11 %vol	not degrade	6.14
		TTIP 15.5 %vol	2.35	not degrade
		TTIP 20 %vol	2.94	not degrade
	vary aging time	Age 0 min	not degrade	not degrade
		Age 15 min	2.35	not degrade
		Age 30 min	not degrade	not degrade
	vary voltage	Voltage 22 kV	not degrade	not degrade
		Voltage 24 kV	2.35	not degrade
		Voltage 26 kV	not degrade	not degrade
Ethanol solvent	vary PVP	PVP 10 %wt	not degrade	7.18
		PVP 11.5 %wt	1.79	10.41
		PVP 13 %wt	6.75	6.18
	vary TTIP	TTIP 11 %vol	not degrade	6.32
		TTIP 15.5 %vol	1.79	10.41
		TTIP 20 %vol	not degrade	5.26
	vary aging time	Age 0 min	6.12	not degrade
		Age 15 min	1.79	10.41
		Age 30 min	not degrade	5.07
	vary voltage	Voltage 22 kV	not degrade	10.41
		Voltage 24 kV	1.79	10.41
		Voltage 26 kV	not degrade	10.41

Then, UV-B lamp were used to further the investigation of photocatalytic activity of the resultant photocatalysts. PVP 11.5wt%/TTIP 15.5wt%/Age 15 min/24 kV was used to represent this studied due to the highest degradation percentage. The degradation percentage of PVP 11.5wt%/TTIP 15.5wt%/Age 15 min/24 kV was shown in Table 4.37.

Table 4.37. Degradation percentage of PVP 11.5wt%/TTIP 15.5wt%/Age 15 min/24 kV in various photocatalyst type with both UV-A and UV-B lamp.

UV lamp type	Photocatalysts type	%degradation
UV-A lamp	Coaxial nanofibers	1.79
	Sheath nanofibers	33.55
	P25 commercial powder	53.22
	Sheath solution's powder	10.41
UV-B lamp	Coaxial nanofibers	2.23
	Sheath nanofibers	36.60
	P25 commercial powder	82.06
	Sheath solution's powder	22.45

According to Table 4.37., the degradation percentage of photocatalysts by using UV-B lamp is higher than UV-A. The degradation percentage of photocatalysts from the highest to the lowest are P25 commercial powder > sheath nanofibers > sheath solution’s powder > coaxial nanofibers.

The XRD patterns were used to confirmed the degradation percentage of various photocatalysts type.

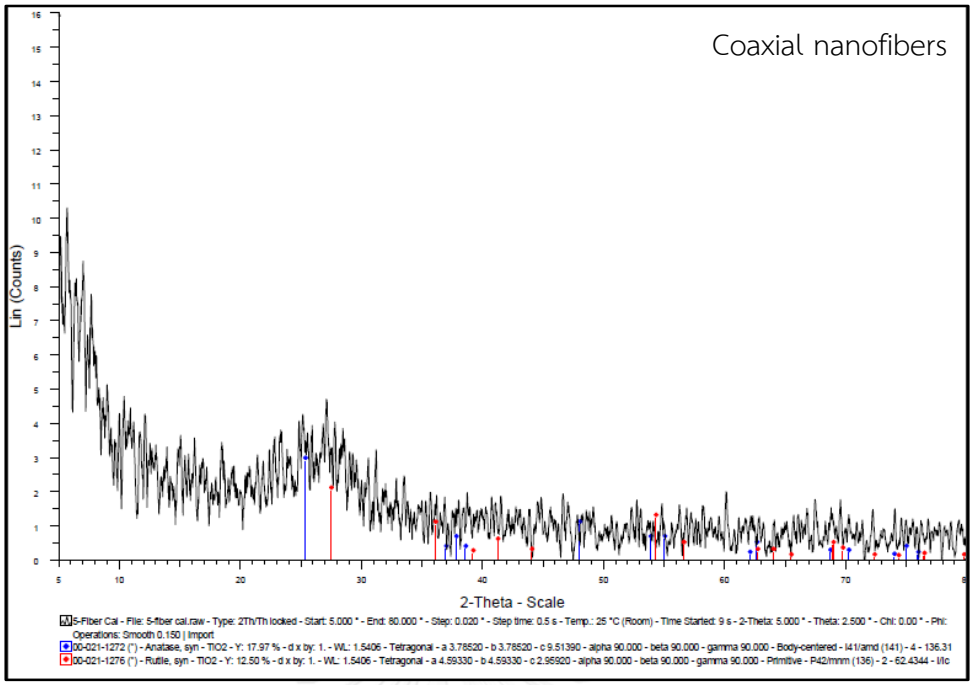

Figure 4.49. XRD patterns of coaxial nanofibers.

According to Figure 4.49., the overall structure of coaxial nanofibers were amorphous. Therefore, the degradation percentage of coaxial nanofibers was the lowest one.

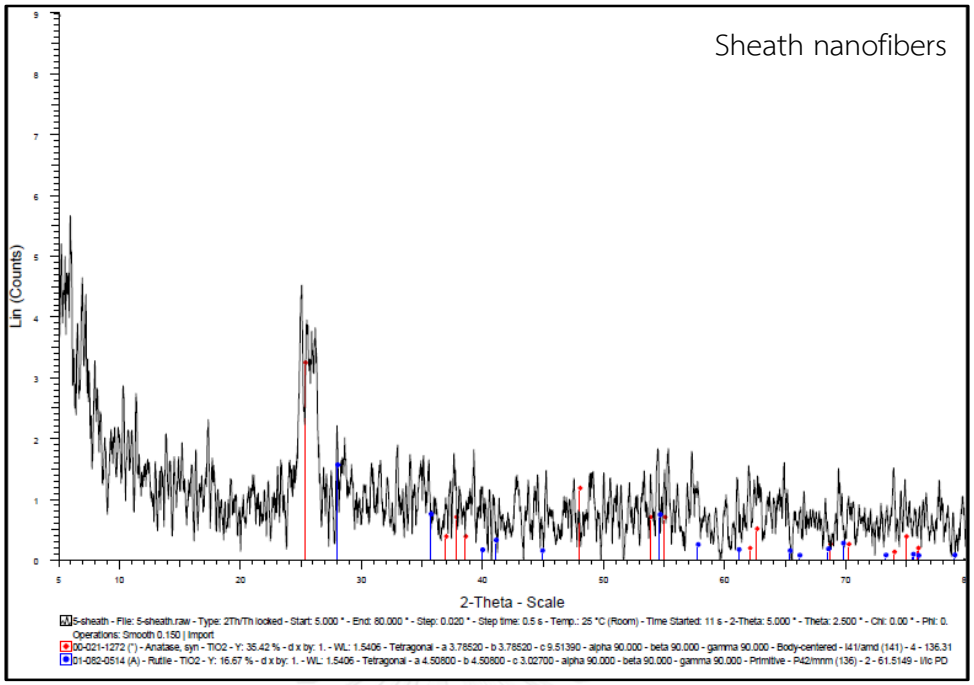

Figure 4.50. XRD patterns of sheath nanofibers.

According to Figure 4.50., the ratio of anatase and rutile of sheath nanofibers was 35.42% : 16.67%. Since, the peaks were not sharp, therefore the crystallization will be minimal. With low crystallization, the degradation percentage will be low.

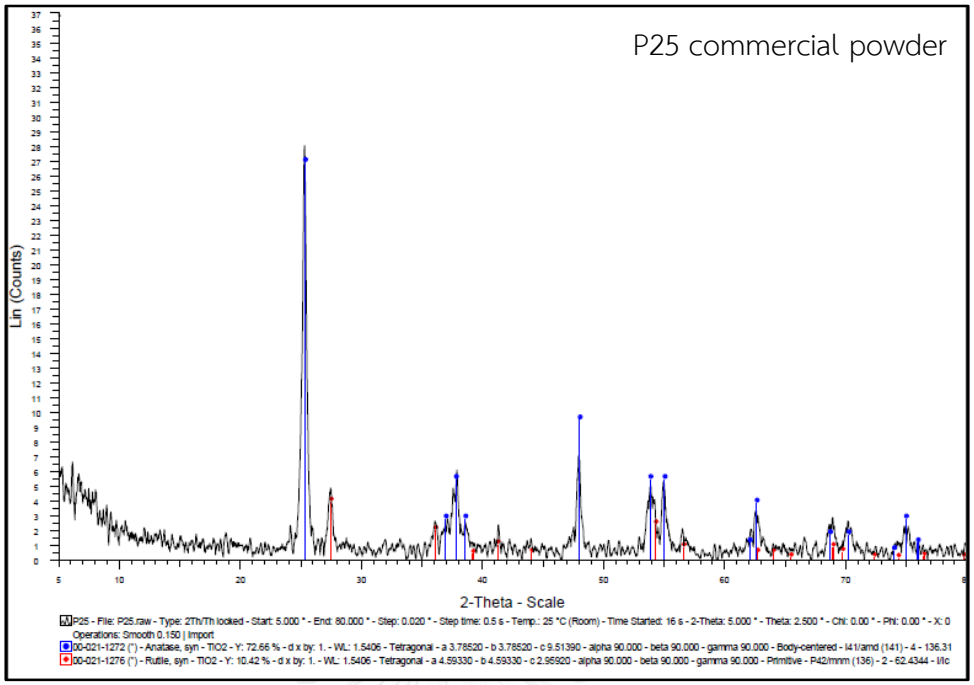

Figure 4.51. XRD patterns of P25 commercial powder.

According to Figure 4.51., the ratio of anatase and rutile of P25 commercial powder was 72.66% : 10.42%. The sharp peaks and high percentage of anatase and rutile will increase the degradation percentage.

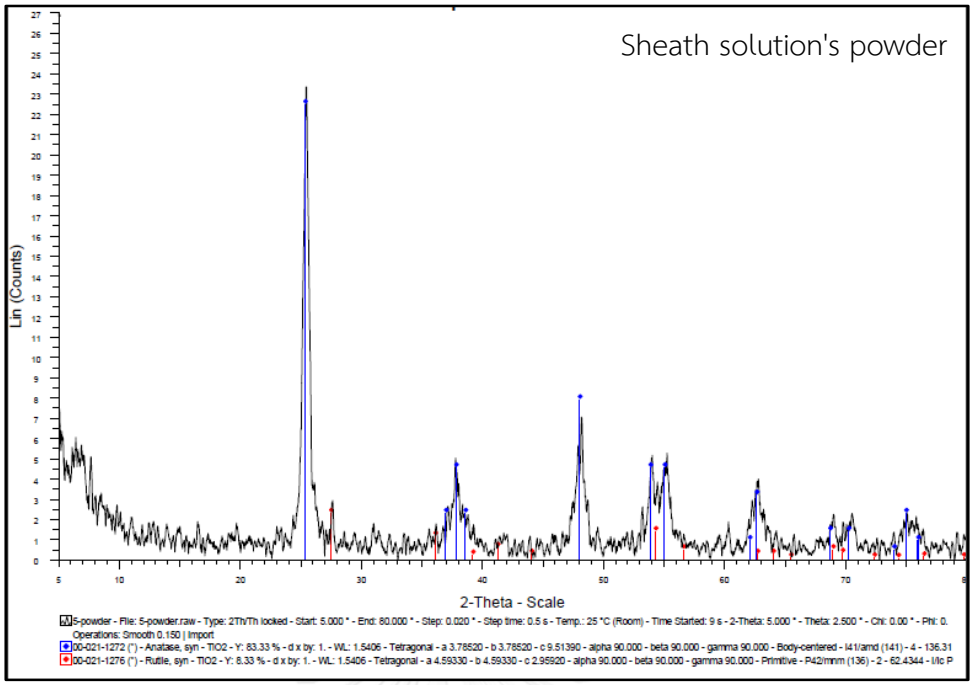

Figure 4.52. XRD patterns of sheath solution's powder.

According to Figure 4.52., the ratio of anatase and rutile of sheath solution's powder was 83.33% : 8.33%. The sharp peaks and high percentage of anatase and rutile will increase the degradation percentage, but in this case the degradation percentage of sheath solution's powder is not the highest corresponding to research paper of H.C. Ho and K.J. Wan (2013), the photocatalyst activity of TiO_2 nanofibers depended on preparation or operation conditions and PVP to TiO_2 ratio more than the ratio of anatase and rutile crystallization [78].

CHAPTER V

CONCLUSIONS

5.1. Summary of the results

5.1.1. TiO_2-PVP/PAN flexible nanofibers can be fabricated by coaxial electrospinning process followed by calcination.

5.1.2. Sol-gel process occurred only when using ethanol as solvent in titania-precusor solution.

5.1.3. After titania-precusor solution with ethanol solvent was aged for 15 min, it found out that sol-gel process was completed.

5.1.4. PAN is not soluble in ethanol. Thus, the mixed solution of PAN and ethanol was separated into two phases, solid and liquid immediately. The two phases were found to be swollen polymer and liquid layer due to the dissolution of PAN in ethanol.

5.1.5. TEM images of both DMF and ethanol in sheath solution confirmed the core/sheath structure of flexible nanofibers.

5.1.6. There is no core/sheath interface when using DMF as solvent in sheath solution and the component in sheath section is diffused into core section.

5.1.7. The core/sheath interface was clearly observed when using ethanol as solvent in sheath solution. The component in sheath section is only partly diffused into core section due to the interaction between PAN and ethanol.

5.1.8. The flexibility of the resultant calcined nanofibers was measured by bending fibermats to the curvature radius of 3.4 mm and 1.3 mm and they were very flexible and easily bent to be curved.

5.1.9. The nanofibers with DMF in sheath are larger and more uniform in size and no beads. On the other hand, nanofibers with ethanol in sheath are smaller and non uniform in size and there are beads occurred in some condition.

5.1.10. The spin coating film can investigate only the overall image of core/sheath interface behavior, but the results were similar with the others ones.

5.1.11. Either spin core first and followed by sheath or sheath first and followed by core, the behavior of core/sheath interface are the same.

5.1.12. If the first layer of the spin coat film was dried up before spinning the second one, then the core/sheath interface would be clearly observed. It also shows that core and sheath will interact only when it was a wet solution.

5.1.13. The photocatalytic efficiency of both nanofibers and powder when ethanol in sheath is higher than the one of DMF in sheath due to its structure.

5.1.14. The ratio of PVP to TiO_2 affects the activity of photocatalytic degradation more than TiO_2 crystalline phase.

5.2. Conclusions

Flexible core/sheath nanofibers were successfully fabricated by coaxial electrospinning process in this work. There is no core/sheath interface when using DMF as solvent in sheath solution. The diffusion of sheath section occurred and titania was trapped into core section, this decreased degradation efficiency. Sheath solution was successfully prepared using ethanol as solvent. At core/sheath interface ethanol interact with PAN, sheath section could not diffuse into core section and this improves degradation efficiency.

REFERENCES

1. Ehrampoosh, M.H., G.R. Moussavi, M.T. Ghaneian, S. Rahimi, and M. Ahmadian, *Removal of methylene blue dye from textile simulated sample using tubular reactor and TiO2/UV-C photocatalytic process.* Iranian Journal of Environmental Health Science & Engineering, 2011. **8**(1): pp. 34-40.
2. Hwang, K.-J., J.-W. Lee, W.-G. Shim, H.D. Jang, S.-I. Lee, and S.-J. Yoo, *Adsorption and photocatalysis of nanocrystalline TiO< sub> 2</sub> particles prepared by sol–gel method for methylene blue degradation.* Advanced Powder Technology, 2012. **23**(3): pp. 414-418.
3. Mohapatra, D.P., S.K. Brar, R. Daghrir, R.D. Tyagi, P. Picard, R.Y. Surampalli, and P. Drogui, *Photocatalytic degradation of carbamazepine in wastewater by using a new class of whey-stabilized nanocrystalline TiO< sub> 2</sub> and ZnO.* Science of The Total Environment, 2014. **485**: pp. 263-269.
4. Kango, S., S. Kalia, A. Celli, J. Njuguna, Y. Habibi, and R. Kumar, *Surface modification of inorganic nanoparticles for development of organic–inorganic nanocomposites—A review.* Progress in Polymer Science, 2013. **38**(8): pp. 1232-1261.
5. Zuo, R., G. Du, W. Zhang, L. Liu, Y. Liu, L. Mei, and Z. Li, *Photocatalytic degradation of methylene blue using TiO2 impregnated diatomite.*
6. Biswas, A., H. Park, and W.M. Sigmund, *Flexible ceramic nanofibermat electrospun from TiO< sub> 2</sub>–SiO< sub> 2</sub> aqueous sol.* Ceramics International, 2012. **38**(1): pp. 883-886.
7. Li, Q., D.J.G. Satur, H. Kim, and H.G. Kim, *Preparation of sol–gel modified electrospun TiO< sub> 2</sub> nanofibers for improved photocatalytic decomposition of ethylene.* Materials Letters, 2012. **76**: pp. 169-172.

8. Miao, J., M. Miyauchi, T.J. Simmons, J.S. Dordick, and R.J. Linhardt, *Electrospinning of nanomaterials and applications in electronic components and devices.* Journal of nanoscience and nanotechnology, 2010. **10**(9): pp. 5507-5519.

9. Yu, D.G., X. Wang, X.Y. Li, W. Chian, Y. Li, and Y.Z. Liao, *Electrospun biphasic drug release polyvinylpyrrolidone/ethyl cellulose core/sheath nanofibers.* Acta biomaterialia, 2013. **9**(3): pp. 5665-5672.

10. Du, P., L. Song, J. Xiong, N. Li, Z. Xi, L. Wang, D. Jin, S. Guo, and Y. Yuan, *Coaxial electrospun TiO< sub> 2</sub>/ZnO core–sheath nanofibers film: Novel structure for photoanode of dye-sensitized solar cells.* Electrochimica Acta, 2012. **78**: pp. 392-397.

11. Jiang, Y.-N., H.-Y. Mo, and D.-G. Yu, *Electrospun drug-loaded core–sheath PVP/zein nanofibers for biphasic drug release.* International journal of pharmaceutics, 2012. **438**(1): pp. 232-239.

12. Lu, Y., Y. Li, S. Zhang, G. Xu, K. Fu, H. Lee, and X. Zhang, *Parameter study and characterization for polyacrylonitrile nanofibers fabricated via centrifugal spinning process.* European Polymer Journal, 2013. **49**(12): pp. 3834-3845.

13. Lee, S., J. Kim, B.-C. Ku, J. Kim, and H.-I. Joh, *Structural evolution of polyacrylonitrile fibers in stabilization and carbonization.* Advances in Chemical Engineering and Science, 2012. **2**: pp. 275.

14. Cheng, C., J. Wu, Y. Xiao, Y. Chen, L. Fan, M. Huang, J. Ling, J. Wang, Z. Tang, and G. Yue, *Polyvinyl pyrrolidone aided preparation of TiO< sub> 2</sub> films used in flexible dye-sensitized solar cells.* Electrochimica Acta, 2011. **56**(21): pp. 7256-7260.

15. Patil, K.R., S.D. Sathaye, Y.B. Khollam, S.B. Deshpande, N.R. Pawaskar, and A.B. Mandale, *Preparation of TiO< sub> 2</sub> thin films by modified spin-coating method using an aqueous precursor.* Materials Letters, 2003. **57**(12): pp. 1775-1780.

16. Wang, X., F. Shi, X. Gao, C. Fan, W. Huang, and X. Feng, *A sol–gel dip/spin coating method to prepare titanium oxide films.* Thin Solid Films, 2013. **548**: pp. 34-39.

17. Umar, M. and H.A. Aziz, *Photocatalytic degradation of organic pollutants in water.* 2013.

18. Rives, V., *Morphology/Tailored Titania Nanoparticles.* New and Future Developments in Catalysis: Catalysis by Nanoparticles, 2013.

19. Meng, X., D.-W. Shin, S.M. Yu, J.H. Jung, H.I. Kim, H.M. Lee, Y.-H. Han, V. Bhoraskar, and J.-B. Yoo, *Growth of hierarchical TiO 2 nanostructures on anatase nanofibers and their application in photocatalytic activity.* CrystEngComm, 2011. **13**(8): pp. 3021-3029.

20. Pei, C.C. and W.W.-F. Leung, *Enhanced photocatalytic activity of electrospun TiO< sub> 2</sub>/ZnO nanofibers with optimal anatase/rutile ratio.* Catalysis Communications, 2013. **37**: pp. 100-104.

21. Landmann, M., E. Rauls, and W.G. Schmidt, *The electronic structure and optical response of rutile, anatase and brookite TiO2.* Journal of physics: Condensed matter, 2012. **24**(19): pp. 195503.

22. Li, C.-J. and G.-R. Xu, *Electrospinning technique in the nano-photocatalyst research.* e-Polymers, 2011. **11**(1): pp. 127-135.

23. Nakata, K. and A. Fujishima, *TiO< sub> 2</sub> photocatalysis: Design and applications.* Journal of Photochemistry and Photobiology C: Photochemistry Reviews, 2012. **13**(3): pp. 169-189.

24. Nataraj, S.K., K.S. Yang, and T.M. Aminabhavi, *Polyacrylonitrile-based nanofibers—a state-of-the-art review.* Progress in polymer science, 2012. **37**(3): pp. 487-513.

25. Im, J.S., M.I. Kim, and Y.-S. Lee, *Preparation of PAN-based electrospun nanofiber webs containing TiO< sub> 2</sub> for photocatalytic degradation.* Materials Letters, 2008. **62**(21): pp. 3652-3655.

26. Dhakate, S.R., A. Gupta, A. Chaudhari, J. Tawale, and R.B. Mathur, *Morphology and thermal properties of PAN copolymer based electrospun nanofibers.* Synthetic Metals, 2011. **161**(5): pp. 411-419.

27. Chen, J.-Y., H.-C. Chen, J.-N. Lin, and C. Kuo, *Effects of polymer media on electrospun mesoporous titania nanofibers.* Materials chemistry and physics, 2008. **107**(2): pp. 480-487.

28. Cao, H., P. Du, L. Song, J. Xiong, J. Yang, T. Xing, X. Liu, R. Wu, M. Wang, and X. Shao, *Co-electrospinning fabrication and photocatalytic performance of TiO< sub> 2</sub>/SiO< sub> 2</sub> core/sheath nanofibers with tunable sheath thickness.* Materials Research Bulletin, 2013. **48**(11): pp. 4673-4678.

29. Drabik, M., J. Touskova, J. Hanus, H. Kobayashi, and H. Biederman, *Properties of composite films of titania nanofibers and Safranin O dye.* Synthetic Metals, 2010. **160**(23): pp. 2564-2572.

30. Thomas, S., R. Shanks, and C. Sarathchandran, *Nanostructured Polymer Blends*. Vol. 1. 2013: William Andrew.

31. Kaewsaenee, J., P. Visal-athaphand, P. Supaphol, and V. Pavarajarn, *Fabrication and characterization of neat and aluminium-doped titanium (IV) oxide fibers prepared by combined sol–gel and electrospinning techniques.* Ceramics International, 2010. **36**(7): pp. 2055-2061.

32. Kao, L.-H., H.-K. Lin, F.-J. Chuang, and W.-T. Hsu, *Electrospun hierarchical cancellous-bone-like microstructures composed of a crystalline TiO< sub> 2</sub> nanonet.* Materials Letters, 2012. **82**: pp. 64-66.

33. Liu, S., B. Liu, K. Nakata, T. Ochiai, T. Murakami, and A. Fujishima, *Electrospinning preparation and photocatalytic activity of porous TiO 2 nanofibers.* Journal of Nanomaterials, 2012. **2012**: pp. 17.

34. Chen, R., C. Huang, Q. Ke, C. He, H. Wang, and X. Mo, *Preparation and characterization of coaxial electrospun thermoplastic polyurethane/collagen compound nanofibers for tissue engineering applications.* Colloids and Surfaces B: Biointerfaces, 2010. **79**(2): pp. 315-325.

35. Choi, K.-I., S. Ho Lee, J.-Y. Park, D.-Y. Choi, C.-H. Hwang, I.-H. Lee, and M. Hwa Chang, *Fabrication and characterization of hollow TiO< sub> 2</sub> fibers by microemulsion electrospinning for photocatalytic reactions.* Materials Letters, 2013. **112**: pp. 113-116.

36. Salehi, M., H. Hashemipour, and M. Mirzaee, *Experimental Study of Influencing Factors and Kinetics in Catalytic Removal of Methylene Blue with TiO< SUB> 2</SUB> Nanopowder.* American journal of environmental engineering, 2012. **2**(1): pp. 1-7.

37. Hatat-Fraile, M., J. Mendret, M. Rivallin, and S. Brosillon, *Effect of hydrodynamics during sol–gel synthesis of TiO< sub> 2</sub> nanoparticles: From morphology to photocatalytic properties.* Chemical Engineering Research and Design, 2013. **91**(12): pp. 2389-2400.

38. Akpan, U.G. and B.H. Hameed, *The advancements in sol–gel method of doped-TiO< sub> 2</sub> photocatalysts.* Applied Catalysis A: General, 2010. **375**(1): pp. 1-11.

39. Choi, J.S., S.W. Lee, L. Jeong, S.-H. Bae, B.C. Min, J.H. Youk, and W.H. Park, *Effect of organosoluble salts on the nanofibrous structure of electrospun poly (3-hydroxybutyrate-< i> co</i>-3-hydroxyvalerate).* International journal of biological macromolecules, 2004. **34**(4): pp. 249-256.

40. Ramakrishna, S., K. Fujihara, W.-E. Teo, T.-C. Lim, and Z. Ma, *An introduction to electrospinning and nanofibers*. Vol. 90. 2005: World Scientific.

41. Garcia-Gomez, N.A., D.I. Garcia-Gutierrez, S. Sepulveda-Guzman, and E.M. Sanchez, *Enhancement of electrochemical properties on TiO2/carbon nanofibers by electrospinning process.* Journal of Materials Science: Materials in Electronics, 2013. **24**(10): pp. 3976-3984.

42. Tan, A.W., B. Pingguan-Murphy, R. Ahmad, and S.A. Akbar, *Advances in fabrication of TiO2 nanofiber/nanowire arrays toward the cellular response in biomedical implantations: a review.* Journal of Materials Science, 2013. **48**(24): pp. 8337-8353.

43. Elahi, M.F., W. Lu, G. Guoping, and F. Khan, *Core-shell Fibers for Biomedical Applications-A Review.* J Bioengineer & Biomedical Sci 3: 121. doi, 2013.

44. Bedford, N.M. and A.J. Steckl, *Photocatalytic self cleaning textile fibers by coaxial electrospinning.* ACS Applied Materials & Interfaces, 2010. **2**(8): pp. 2448-2455.

45. Tian, L., S. Zi-qiang, W. Jian-quan, and G. Mu-jia, *Fabrication of hydroxyapatite nanoparticles decorated cellulose triacetate nanofibers for protein adsorption by coaxial electrospinning.* Chemical Engineering Journal, 2014.

46. Lin, C.-H., J.-H. Chao, C.-H. Liu, J.-C. Chang, and F.-C. Wang, *Effect of calcination temperature on the structure of a Pt/TiO2 (B) nanofiber and its photocatalytic activity in generating H2.* Langmuir, 2008. **24**(17): pp. 9907-9915.

47. Ahmed, S., M.G. Rasul, W.N. Martens, R. Brown, and M.A. Hashib, *Heterogeneous photocatalytic degradation of phenols in wastewater: a review on current status and developments.* Desalination, 2010. **261**(1): pp. 3-18.

48. Lee, K.I., J. Li, B. Fei, and J.H. Xin, *Mechanism study of heat stabilization of polyacrylonitrile nanofibers against alkaline hydrolysis.* Polymer Degradation and Stability, 2014. **105**: pp. 80-85.

49. Porbeni, F.E., E.M. Edeki, I.D. Shin, and A.E. Tonelli, *Formation and characterization of the inclusion complexes between poly (dimethylsiloxane) and polyacrylonitrile with γ-cyclodextrin.* Polymer, 2001. **42**(16): pp. 6907-6912.

50. Ouyang, Q., L. Cheng, H. Wang, and K. Li, *Mechanism and kinetics of the stabilization reactions of itaconic acid-modified polyacrylonitrile.* Polymer Degradation and Stability, 2008. **93**(8): pp. 1415-1421.

51. Zhu, H., M. Du, M. Zou, C. Xu, N. Li, and Y. Fu, *Facile and green synthesis of well-dispersed Au nanoparticles in PAN nanofibers by tea polyphenols.* Journal of Materials Chemistry, 2012. **22**(18): pp. 9301-9307.

52. Jacob, M.M.E. and A.K. Arof, *FTIR studies of DMF plasticized polyvinyledene fluoride based polymer electrolytes.* Electrochimica acta, 2000. **45**(10): pp. 1701-1706.

53. Deng, S., R. Bai, and J.P. Chen, *Behaviors and mechanisms of copper adsorption on hydrolyzed polyacrylonitrile fibers.* Journal of colloid and interface science, 2003. **260**(2): pp. 265-272.

54. Gezici, O., I. Demir, A. Demircan, N. Ünlü, and M. Karaarslan, *Subtractive-FTIR spectroscopy to characterize organic matter in lignite samples from different depths.* Spectrochimica Acta Part A: Molecular and Biomolecular Spectroscopy, 2012. **96**: pp. 63-69.

55. Nhlapo, N.S., W.W. Focke, and E. Vuorinen, *TGA–FTIR study of the vapors released by triethylamine–acetic acid mixtures.* Thermochimica Acta, 2012. **546**: pp. 113-119.

56. Shin, H.K., M. Park, P.H. Kang, H.-S. Choi, and S.-J. Park, *Preparation and characterization of polyacrylonitrile-based carbon fibers produced by electron beam irradiation pretreatment.* Journal of Industrial and Engineering Chemistry, 2014. **20**(5): pp. 3789-3792.

57. Cetiner, S., H. Karakas, R. Ciobanu, M. Olariu, N.U. Kaya, C. Unsal, F. Kalaoglu, and A.S. Sarac, *Polymerization of pyrrole derivatives on polyacrylonitrile matrix, FTIR–ATR and dielectric spectroscopic characterization of composite thin films.* Synthetic Metals, 2010. **160**(11): pp. 1189-1196.

58. Yu, M., L. Sun, W. Li, Z. Lan, B. Li, L. Tan, M. Li, and X. Yang, *Investigation of structure and dissolution properties of a solid dispersion of lansoprazole in polyvinylpyrrolidone.* Journal of Molecular Structure, 2011. **1005**(1): pp. 70-77.

59. Shanmugam, N., S. Cholan, N. Kannadasan, K. Sathishkumar, and G. Viruthagiri, *Effect of polyvinylpyrrolidone as capping agent on Ce 3+ doped flowerlike ZnS nanostructure.* Solid State Sciences, 2014. **28**: pp. 55-60.

60. Ahn, K.-H., Y.-B. Park, and D.-W. Park, *Kinetic and mechanistic study on the chemical vapor deposition of titanium dioxide thin films by in situ FT-IR using TTIP.* Surface and Coatings Technology, 2003. **171**(1): pp. 198-204.

61. El-Rehim, H.A.A., E.-S.A. Hegazy, A.A. Hamed, and A.E. Swilem, *Controlling the size and swellability of stimuli-responsive polyvinylpyrrolidone–poly (acrylic acid) nanogels synthesized by gamma radiation-induced template polymerization.* European Polymer Journal, 2013. **49**(3): pp. 601-612.

62. Wang, W. and A. Wang, *Synthesis and swelling properties of pH-sensitive semi-IPN superabsorbent hydrogels based on sodium alginate-g-poly (sodium acrylate) and polyvinylpyrrolidone.* Carbohydrate polymers, 2010. **80**(4): pp. 1028-1036.

63. Seoudi, R., A.A. Fouda, and D.A. Elmenshawy, *Synthesis, characterization and vibrational spectroscopic studies of different particle size of gold nanoparticle capped with polyvinylpyrrolidone.* Physica B: Condensed Matter, 2010. **405**(3): pp. 906-911.

64. Wei, S.F., J.S. Lian, and Q. Jiang, *Controlling growth of ZnO rods by polyvinylpyrrolidone (PVP) and their optical properties.* Applied Surface Science, 2009. **255**(15): pp. 6978-6984.

65. El-Newehy, M.H., A. Alamri, and S.S. Al-Deyab, *Optimization of amine-terminated polyacrylonitrile synthesis and characterization.* Arabian Journal of Chemistry, 2014. **7**(2): pp. 235-241.

66. Fujii, K., Y. Kitamoto, M. Hara, O. Odawara, and H. Wada, *Optical properties of silica-coated Y 2 O 3: Er, Yb nanoparticles in the presence of polyvinylpyrrolidone.* Journal of Luminescence, 2014. **156**: pp. 8-15.

67. Mirzaee, S., S. Mahdavifar, and S.H. Hekmatara, *Synthesis, characterization and Monte Carlo simulation of CoFe 2 O 4/Polyvinylpyrrolidone nanocomposites: The coercivity investigation.* Journal of Magnetism and Magnetic Materials, 2015. **393**: pp. 1-7.

68. Cho, C.W., D. Cho, Y.-G. Ko, and O.H. Kwon, *Stabilization, carbonization, and characterization of PAN precursor webs processed by electrospinning technique.* Carbon Letters, 2007. **8**(4): pp. 313-320.

69. Miao, P., D. Wu, K. Zeng, G. Xu, C.e. Zhao, and G. Yang, *Influence of electron beam pre-irradiation on the thermal behaviors of polyacrylonitrile.* Polymer Degradation and Stability, 2010. **95**(9): pp. 1665-1671.

70. Zeitler, V.A. and C.A. Brown, *The infrared spectra of some Ti-O-Si, Ti-O-Ti and Si-O-Si compounds.* The Journal of Physical Chemistry, 1957. **61**(9): pp. 1174-1177.

71. Daneshfar, A., T. Matsuura, D. Emadzadeh, Z. Pahlevani, and A.F. Ismail, *Urease-carrying electrospun polyacrylonitrile mat for urea hydrolysis.* Reactive and Functional Polymers, 2015. **87**: pp. 37-45.

72. Zhang, Y., L. Deng, G. Zhang, and H. Gan, *Facile synthesis and photocatalytic property of bicrystalline TiO 2/rectorite composites.* Colloids and Surfaces A: Physicochemical and Engineering Aspects, 2011. **384**(1): pp. 137-144.

73. Lee, Y. and M. Kang, *The optical properties of nanoporous structured titanium dioxide and the photovoltaic efficiency on DSSC.* Materials Chemistry and Physics, 2010. **122**(1): pp. 284-289.

74. Simonsen, M.E. and E.G. Søgaard, *Sol–gel reactions of titanium alkoxides and water: influence of pH and alkoxy group on cluster formation and properties of the resulting products.* Journal of sol-gel science and technology, 2010. **53**(3): pp. 485-497.

75. Miller-Chou, B.A. and J.L. Koenig, *A review of polymer dissolution.* Progress in Polymer Science, 2003. **28**(8): pp. 1223-1270.

76. Li, Y., Y. Yu, L. Wu, and J. Zhi, *Processable polyaniline/titania nanocomposites with good photocatalytic and conductivity properties prepared via peroxo-titanium complex catalyzed emulsion polymerization approach.* Applied Surface Science, 2013. **273**: pp. 135-143.

77. Xu, G., X.L. Wang, and G.Z. Liu, *Facile solvothermal synthesis of abnormal growth of one-dimensional ZnO nanostructures by ring-opening reaction of polyvinylpyrrolidone.* Applied Surface Science, 2015. **329**: pp. 137-142.

78. Chun, H.-H. and W.-K. Jo, *Polymer material-supported titania nanofibers with different polyvinylpyrrolidone to TiO< sub> 2</sub> ratios for degradation of vaporous trichloroethylene.* Journal of Industrial and Engineering Chemistry, 2014. **20**(3): pp. 1010-1015.

APPENDIX

APPENDIX A

FTIR TRANSMITTANCE SPECTRA

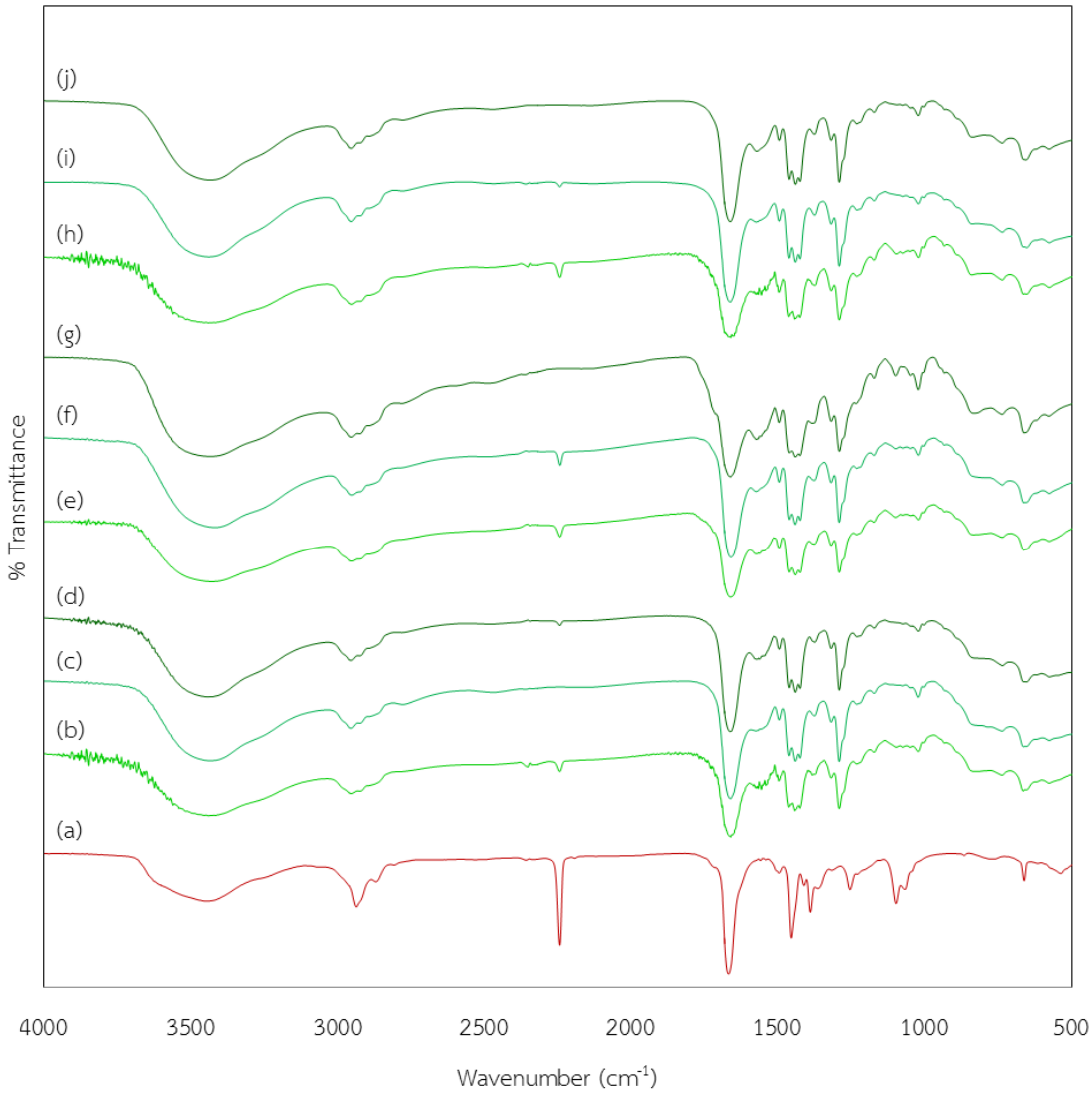

Figure A.1. FTIR transmittance spectra of (a) PAN 8wt% core solution, (b) gel of PAN 8wt%/PVP 10wt%, (c) liquid phase of PAN 8wt%/PVP 10wt%, (d) PVP 10wt% sheath solution, (e) gel of PAN 8wt%/PVP 11.5wt%, (f) liquid phase of PAN 8wt%/PVP 11.5wt%, (g) PVP 11.5wt% sheath solution, (h) gel of PAN 8wt%/PVP 13wt%, (i) liquid

phase of PAN 8wt%/PVP 13wt% and (j) PVP 13wt% sheath solution – All DMF solvent.

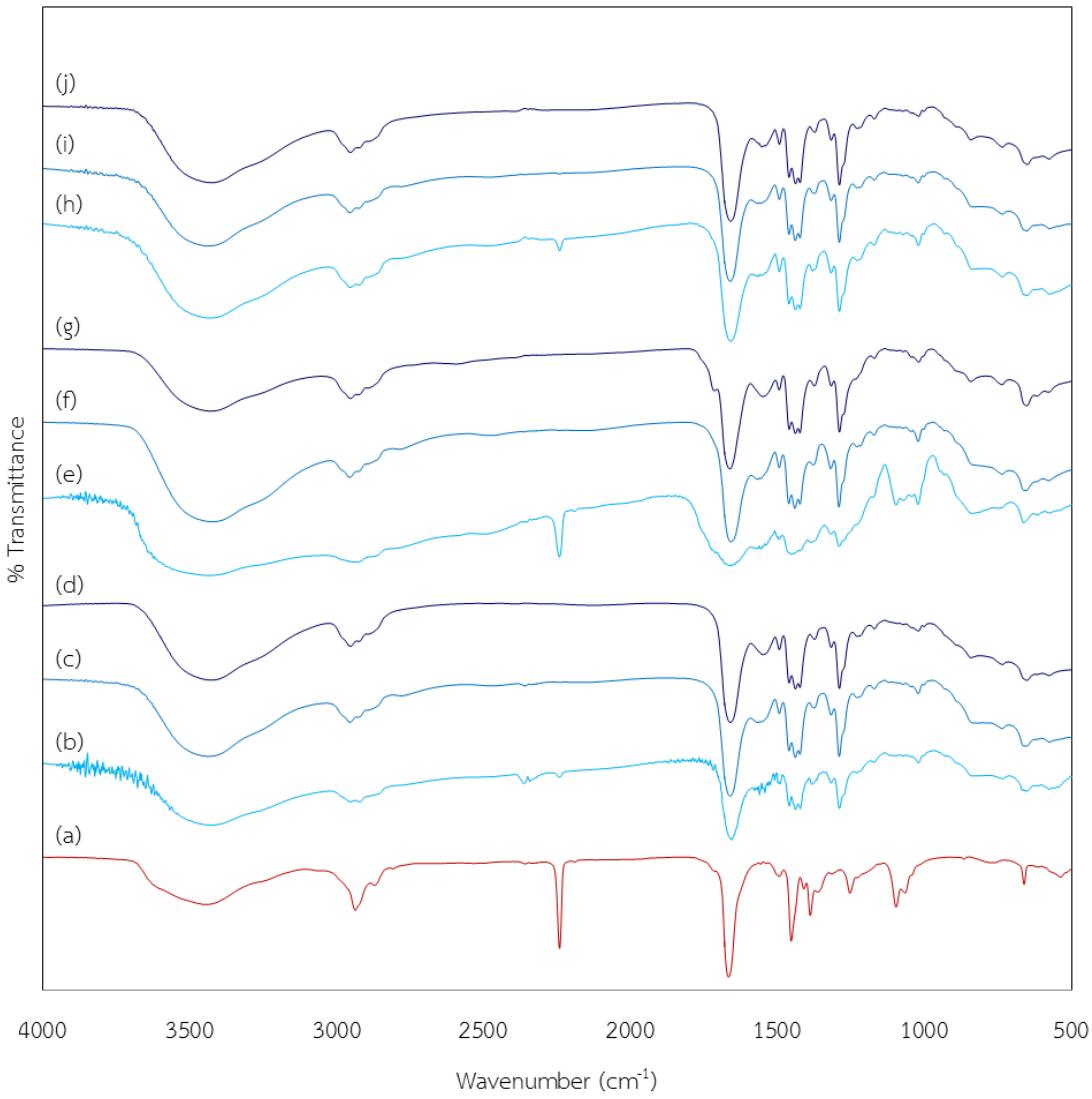

Figure A.2. FTIR transmittance spectra of (a) PAN 8wt% core solution, (b) solid phase of PAN 8wt%/PVP 10wt%, (c) liquid phase of PAN 8wt%/PVP 10wt%, (d) PVP 10wt% sheath solution, (e) solid phase of PAN 8wt%/PVP 11.5wt%, (f) liquid phase of PAN 8wt%/PVP 11.5wt%, (g) PVP 11.5wt% sheath solution, (h) solid phase of PAN 8wt%/PVP 13wt%, (i) liquid phase of PAN 8wt%/PVP 13wt% and (j) PVP 13wt% sheath solution – All ethanol solvent.

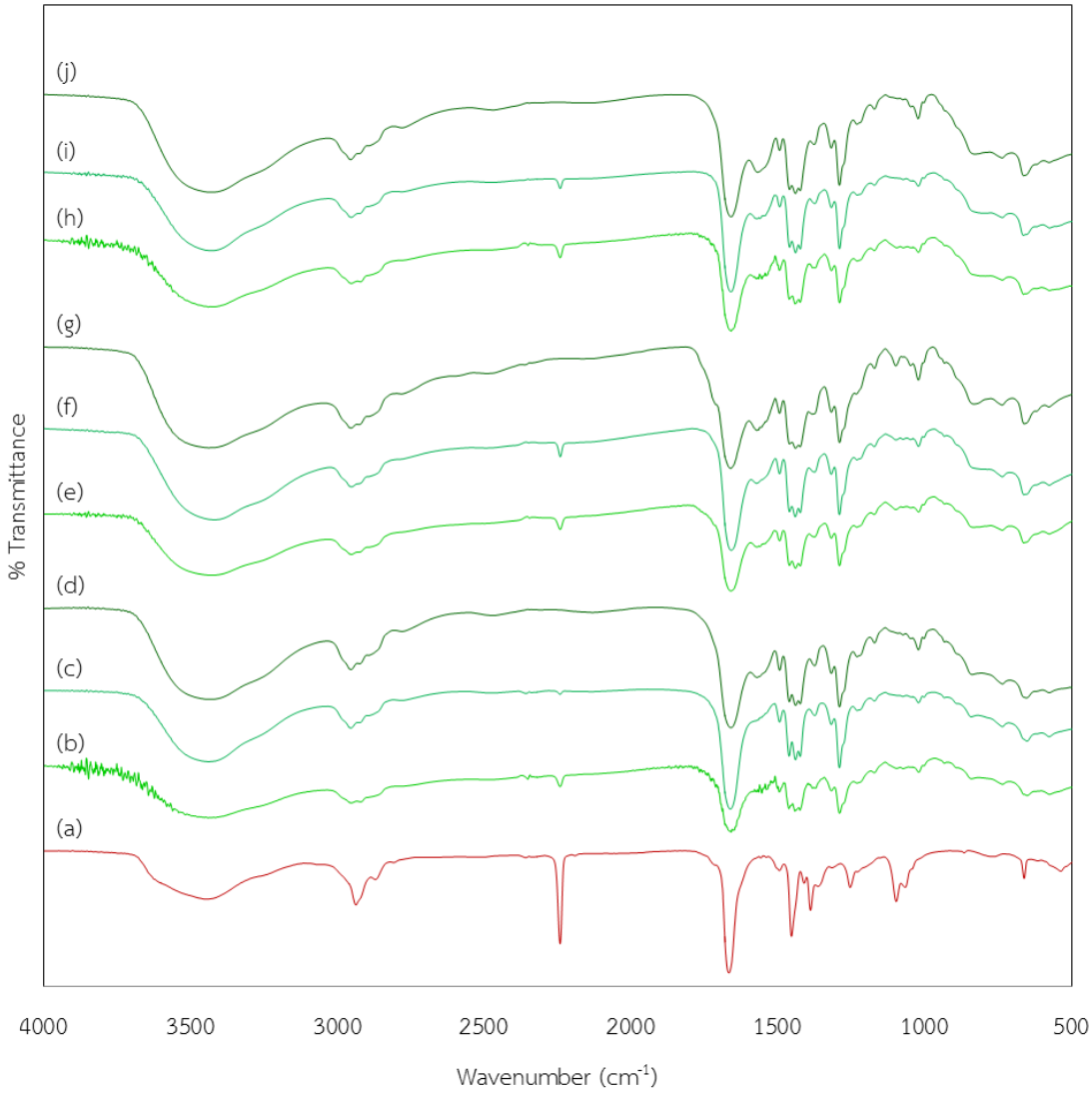

Figure A.3. FTIR transmittance spectra of (a) PAN 8wt% core solution, (b) gel of PAN 8wt%/TTIP 11vol%, (c) liquid phase of PAN 8wt%/TTIP 11vol%, (d) TTIP 11vol% sheath solution, (e) gel of PAN 8wt%/TTIP 15.5vol%, (f) liquid phase of PAN 8wt%/TTIP 15.5vol%, (g) TTIP 15.5vol% sheath solution, (h) gel of PAN 8wt%/TTIP 20vol%, (i) liquid phase of PAN 8wt%/TTIP 20vol% and (j) TTIP 20vol% sheath solution – All DMF solvent.

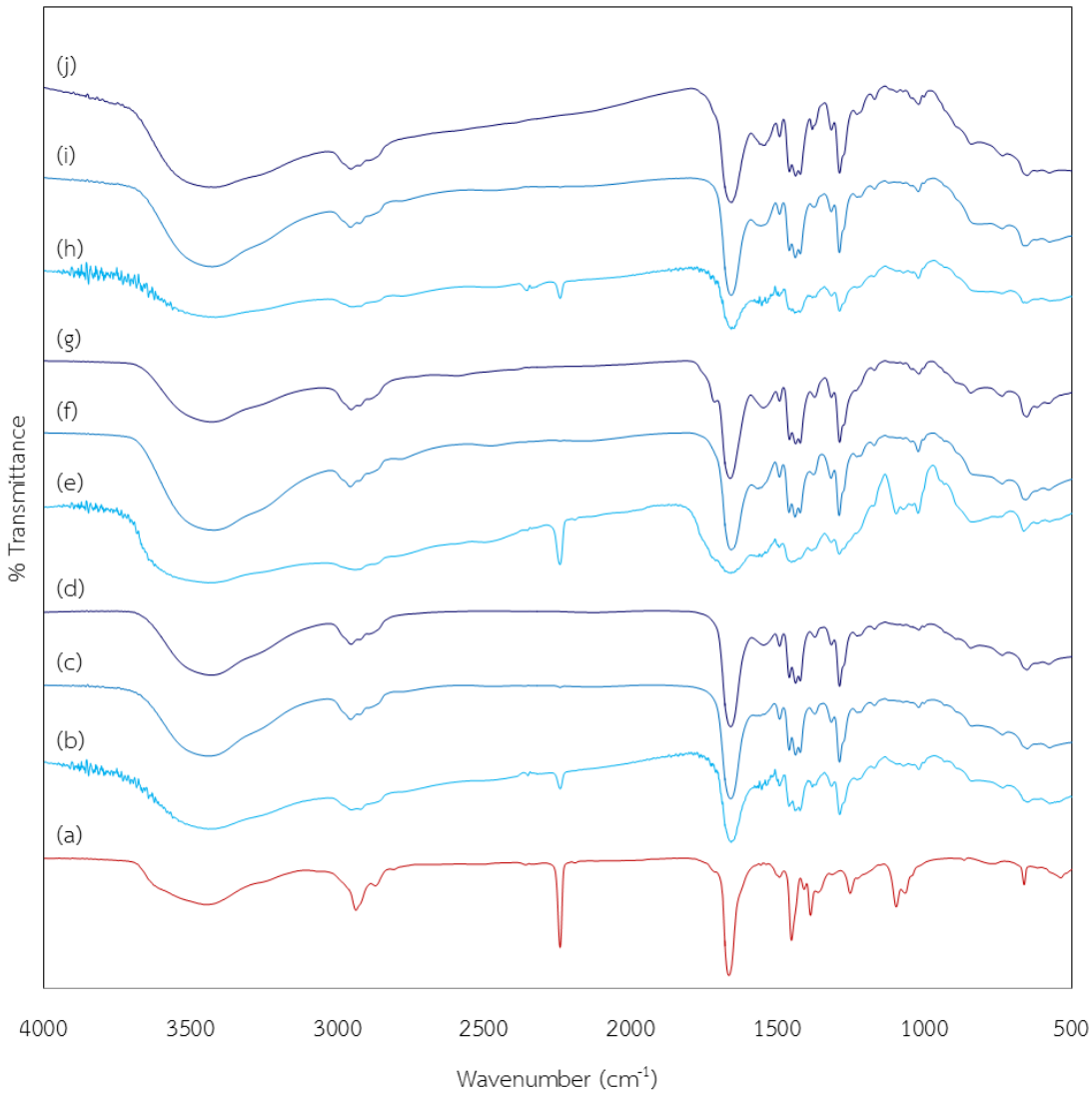

Figure A.4. FTIR transmittance spectra of (a) PAN 8wt% core solution, (b) solid phase of PAN 8wt%/TTIP 11vol%, (c) liquid phase of PAN 8wt%/TTIP 11vol%, (d) TTIP 11vol% sheath solution, (e) solid phase of PAN 8wt%/TTIP 15.5vol%, (f) liquid phase of PAN 8wt%/TTIP 15.5vol%, (g) TTIP 15.5vol% sheath solution, (h) solid phase of PAN 8wt%/TTIP 20vol%, (i) liquid phase of PAN 8wt%/TTIP 20vol% and (j) TTIP 20vol% sheath solution – All ethanol solvent.

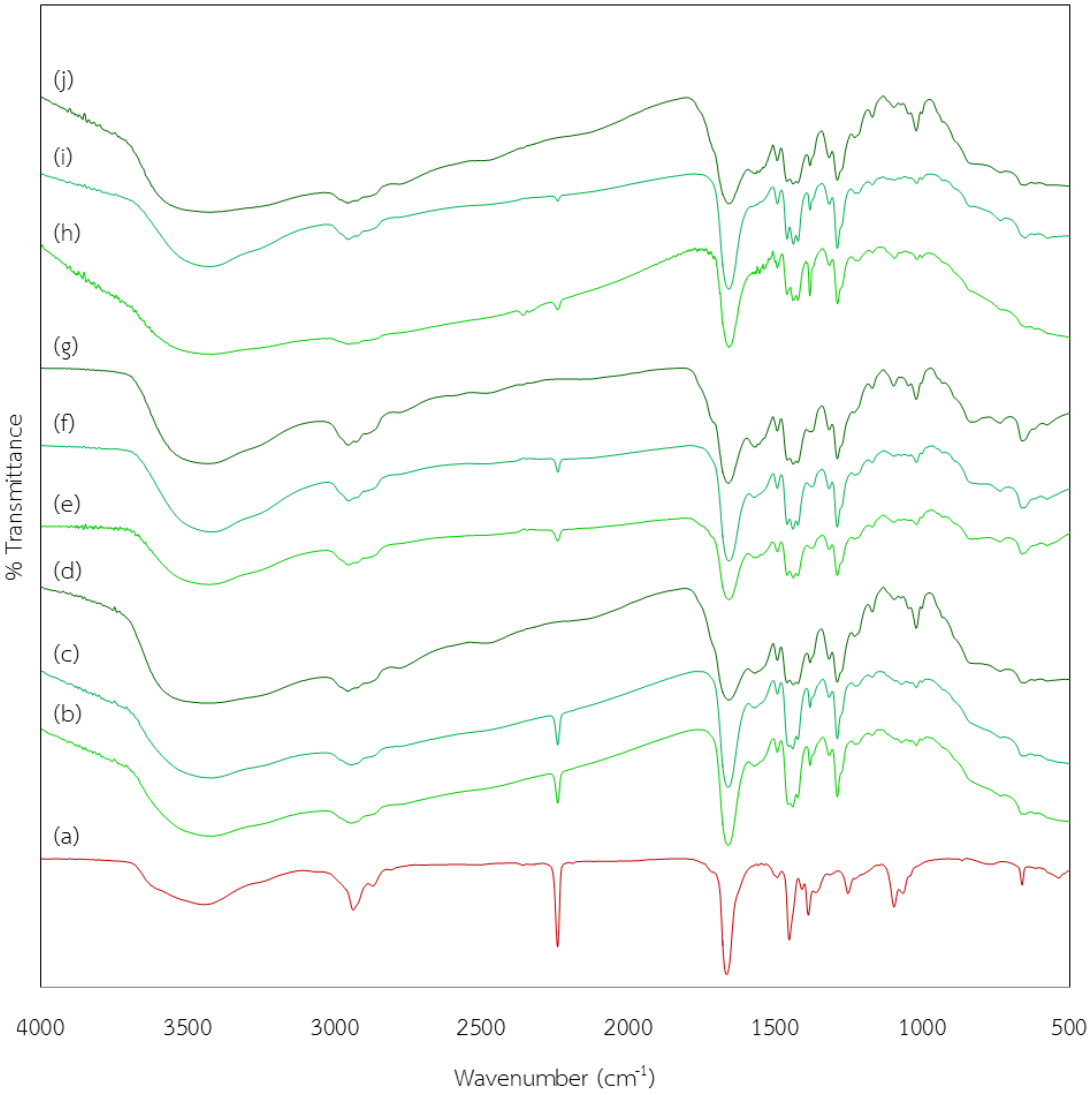

Figure A.5. FTIR transmittance spectra of (a) PAN 8wt% core solution, (b) gel of PAN 8wt%/age 0 min, (c) liquid phase of PAN 8wt%/age 0 min, (d) age 0 min sheath solution, (e) gel of PAN 8wt%/age 15 min, (f) liquid phase of PAN 8wt%/age 15 min, (g) age 15 min sheath solution, (h) gel of PAN 8wt%/age 30 min, (i) liquid phase of PAN 8wt%/age 30 min and (j) age 30 min sheath solution – All DMF solvent.

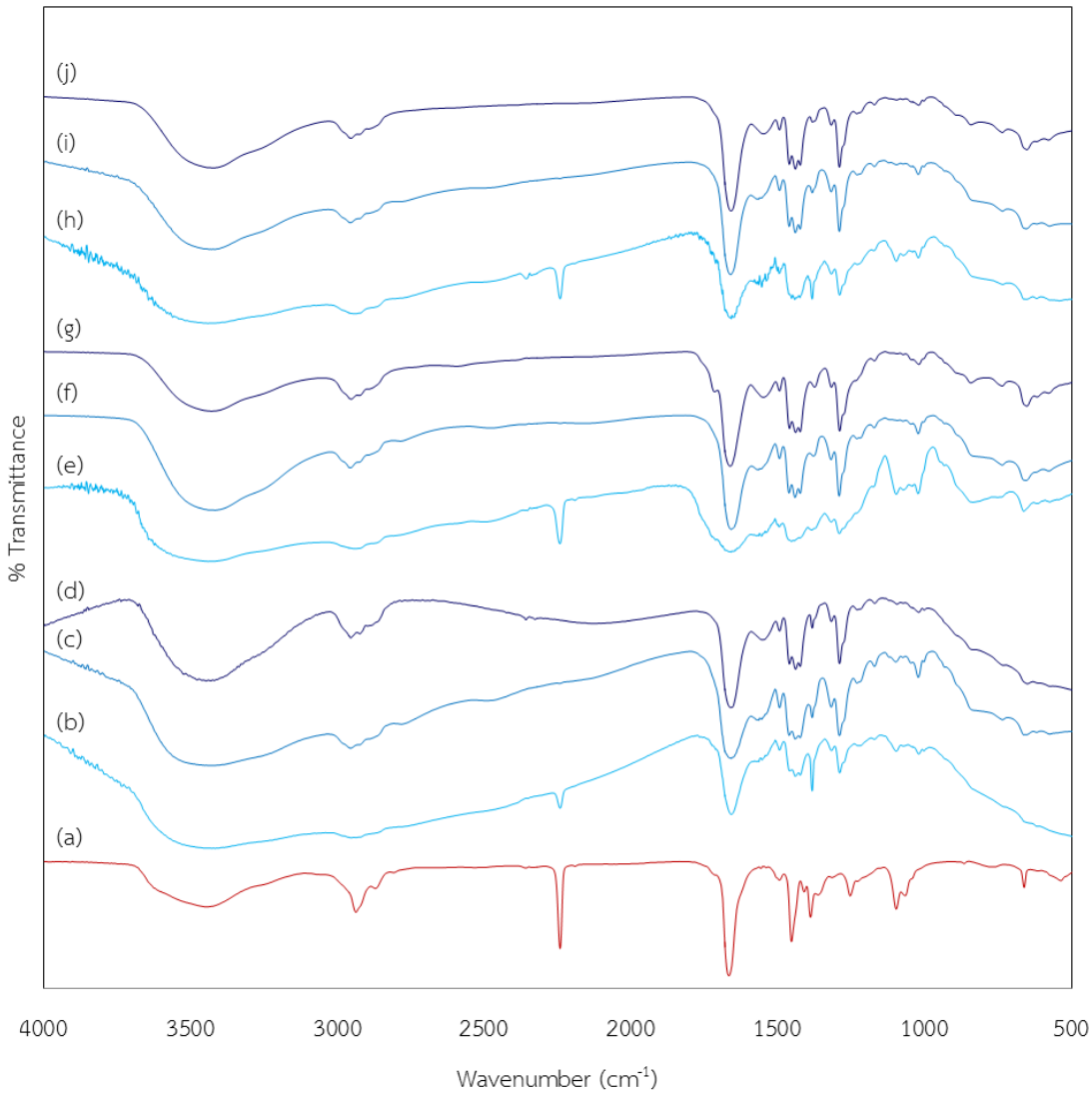

Figure A.6. FTIR transmittance spectra of (a) PAN 8wt% core solution, (b) solid phase of PAN 8wt%/age 0 min, (c) liquid phase of PAN 8wt%/age 0 min, (d) age 0 min sheath solution, (e) solid phase of PAN 8wt%/age 15 min, (f) liquid phase of PAN 8wt%/age 15 min, (g) age 15 min sheath solution, (h) solid phase of PAN 8wt%/age 30 min, (i) liquid phase of PAN 8wt%/age 30 min and (j) age 30 min sheath solution – All ethanol solvent.

APPENDIX B

FTIR SPECTRA AND TABLE OF PEAK WHICH USED TO COMPARE THE STRUCTURE OF ELECTROSPINNING NANOFIBERS AND SPIN COATING FILMS.

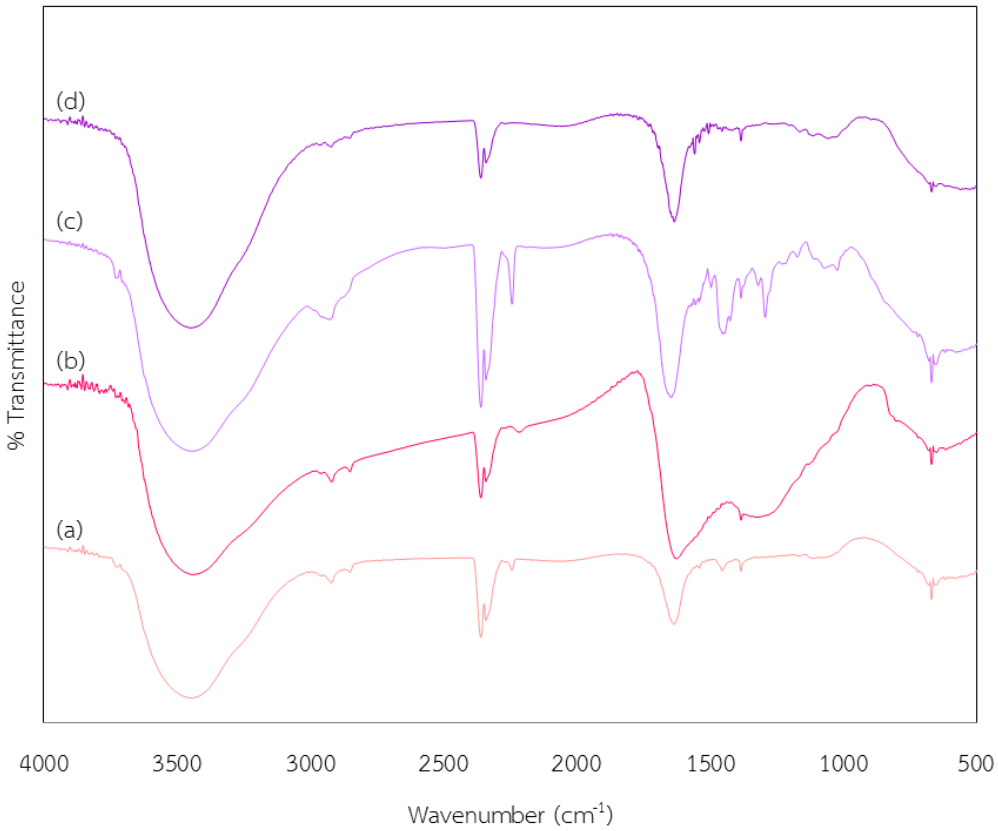

Figure B.1. FTIR transmittance spectra of PAN 8wt%/PVP 10wt% (a) nanofiber, (b) calcined nanofiber, (c) film and (d) calcined film – All DMF solvent.

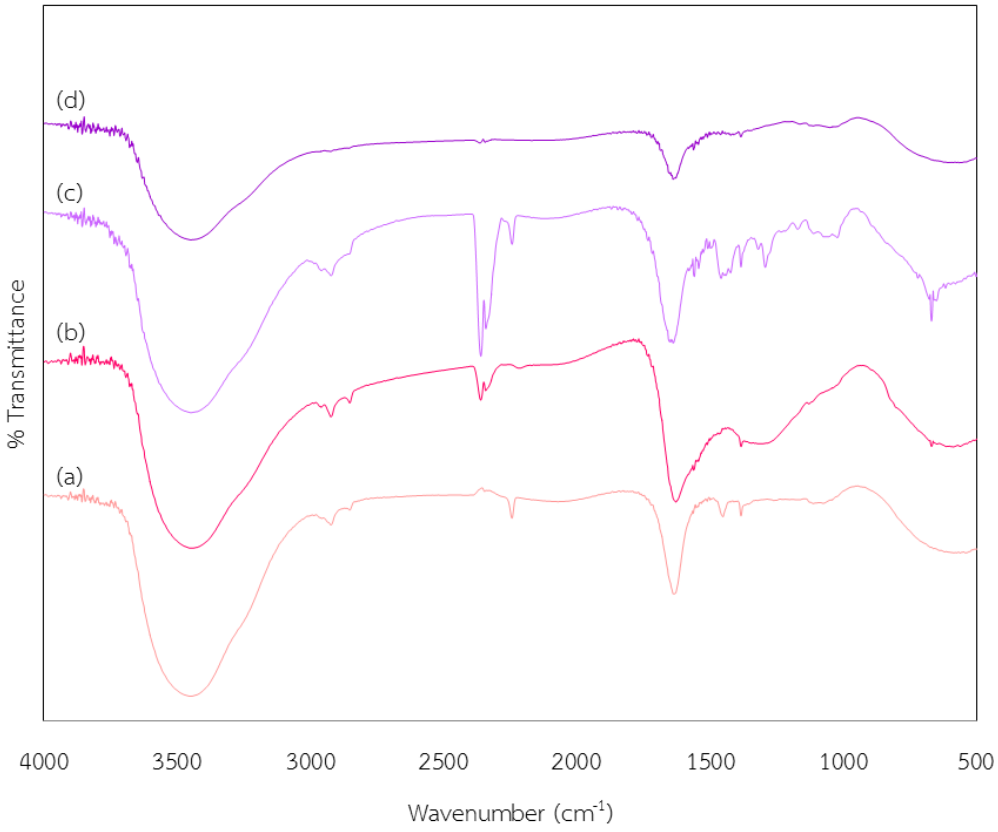

Figure B.2. FTIR transmittance spectra of PAN 8wt%/PVP 11.5wt% (a) nanofiber, (b) calcined nanofiber, (c) film and (d) calcined film – All DMF solvent.

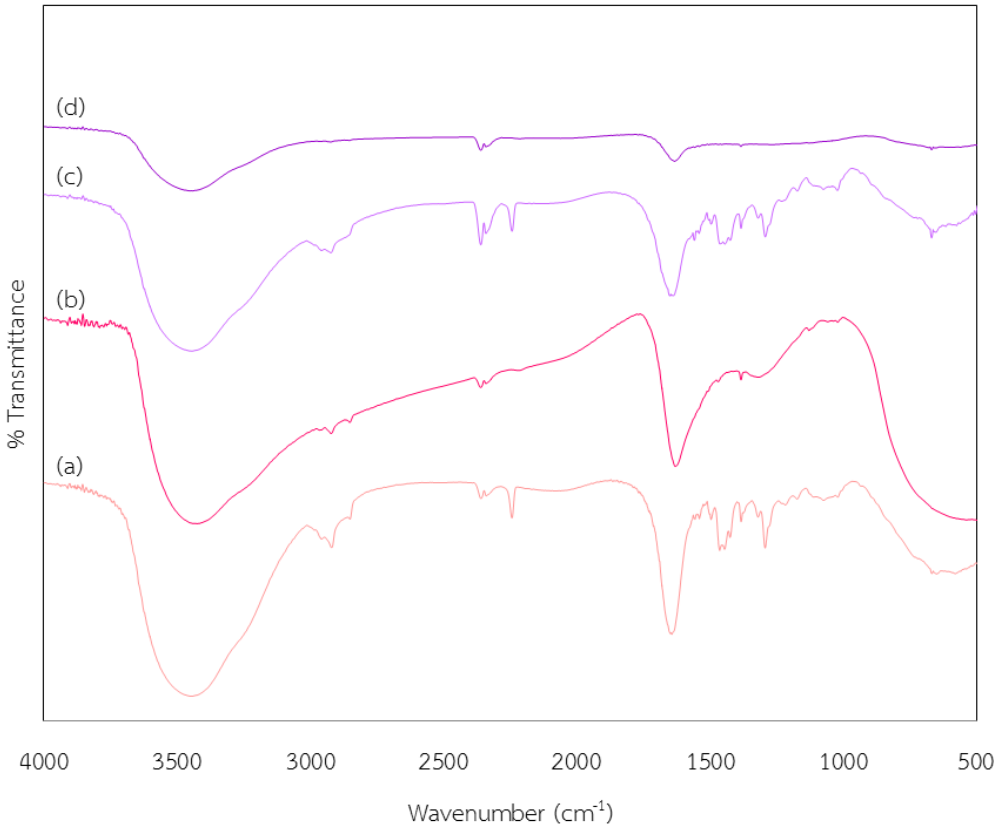

Figure B.3. FTIR transmittance spectra of PAN 8wt%/PVP 13wt% (a) nanofiber, (b) calcined nanofiber, (c) film and (d) calcined film – All DMF solvent.

Table B.1. FTIR spectra of Figure

PVP 10wt%				PVP 11.5wt%				PVP 15wt%			
(a)	(b)	(c)	(d)	(a)	(b)	(c)	(d)	(a)	(b)	(c)	(d)
Fiber	Cal. fiber	Film	Cal. film	Fiber	Cal. fiber	Film	Cal. film	Fiber	Cal. fiber	Film	Cal. film
3440	3440	3440	3440	3451	3440	3450	3450	3442	3440	3442	3452
2922	2920	2924	2923	2957	2958	2957			2966		2966
2852	2851		2853	2986				2957		2957	
2360	2360	2360	2360	2923	2923	2923		2920	2923	2923	2923
2341	2341	2341	2341	2852	2852			2851	2852		2853
2243		2243			2360	2360	2363	2360	2360	2360	2360
	2217			2346	2342	2341	2344	2340	2341	2341	2341
		1648	1647	2243		2243		2243		2243	
1633	1629				2214				2217		2213
1541		1540	1540	1635	1628	1638	1638	1643		1643	
1523		1523	1523	1563	1561	1569	1562		1630		1633
1506	1505		1505	1552	1552	1551	1552	1556		1558	1556
1496		1496	1496	1544	1543	1542	1543	1540		1541	1540
1454	1454	1454	1454	1533	1533	1532	1532	1496		1496	1496
	1425	1425	1425	1526		1525	1525	1464	1470	1463	1471
1383	1383	1383	1384	1510	1510	1508	1510	1445		1444	
1319		1319		1500	1500	1498		1425		1424	
1294		1293		1451	1450	1458	1449	1383	1383	1383	1384
		1231			1440	1440	1440	1320	1317	1319	
1166		1165	1163	1423		1423	1422	1293		1292	
1113			1113	1383	1383	1384	1384			1231	
		1073				1319		1217			

		1022				1292		1173		1172	
719	718	719		1165		1171	1163		1128		1128
677	677	677	676		1128			1074		1074	
669	668	668	668	1112		1111			1059		
651	650	651	651	1075		1073		1020	1021	1022	
617	616	617					1051	667		668	668
						1022					
						719					
					668	669					
					648	650					

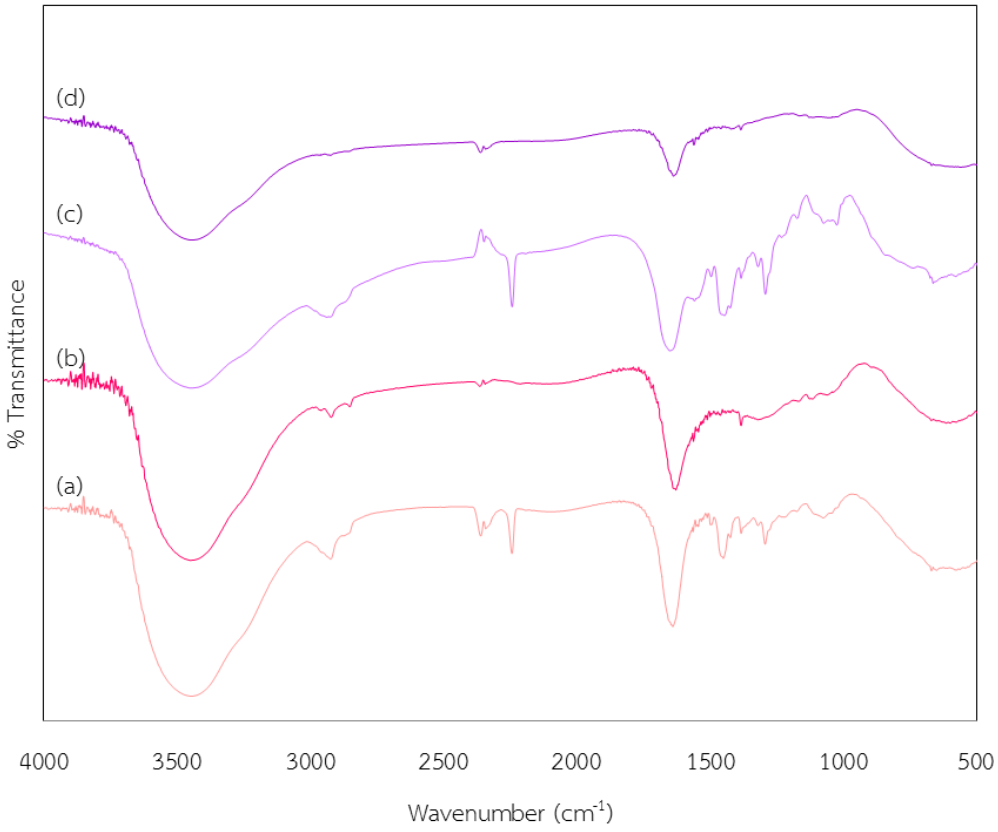

Figure B.4. FTIR transmittance spectra of PAN 8wt%/PVP 10wt% (a) nanofiber, (b) calcined nanofiber, (c) film and (d) calcined film – All ethanol solvent.

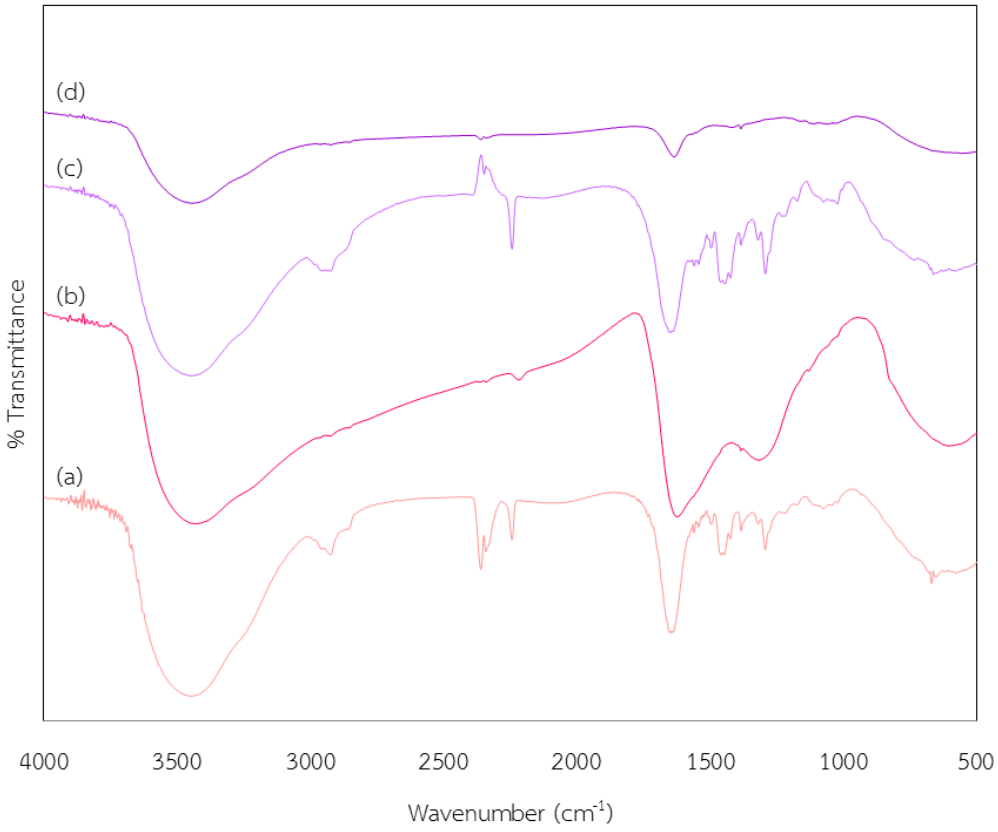

Figure B.5. FTIR transmittance spectra of PAN 8wt%/PVP 11.5wt% (a) nanofiber, (b) calcined nanofiber, (c) film and (d) calcined film – All ethanol solvent.

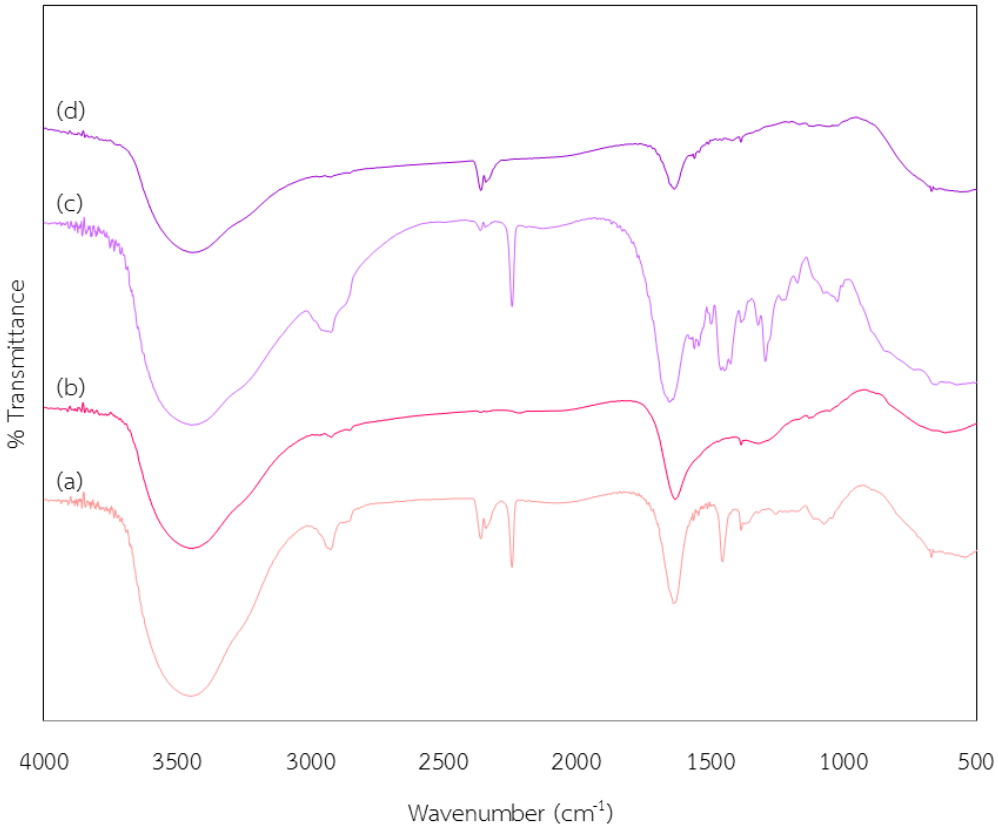

Figure B.6. FTIR transmittance spectra of PAN 8wt%/PVP 13wt% (a) nanofiber, (b) calcined nanofiber, (c) film and (d) calcined film – All ethanol solvent.

Table B.2. FTIR spectra which used to compare the structure of electrospinning nanofibers and spin coating films in topic 4.3.

PVP 10wt%				PVP 11.5wt%				PVP 15wt%			
(a)	(b)	(c)	(d)	(a)	(b)	(c)	(d)	(a)	(b)	(c)	(d)
Fiber	Cal. fiber	Film	Cal. film	Fiber	Cal. fiber	Film	Cal. film	Fiber	Cal. fiber	Film	Cal. film
3447	3451	3441	3440	3450	3425	3443	3442	3451	3442	3345	3441
		2984				2985				2990	
2958	2958		2957				2967		2967		2967
		2938		2957	2957	2957				2957	
2924	2922	2925	2924			2936		2935		2940	
2879		2872		2924	2924	2924	2923	2924	2922		2923
	2852		2849	2878		2872		2878		2875	
2360	2363		2361		2849		2853		2853		2852
2342	2344	2348	2343	2360	2366		2360	2360	2361	2361	2360
2243		2243		2341	2341	2348	2341	2341	2339	2343	2341
	2213			2243		2243		2243		2243	
		1650			2217				2217		
1639			1637	1645		1646				1651	
	1628						1634	1635	1631		1634
1563	1562	1558	1561		1623			1562		1568	
1552	1552		1552			1568	1563	1552		1558	1558
1544	1543		1543	1561		1558		1543		1542	1541
1526	1526		1525	1551			1552	1525			
1510	1510		1509	1542		1542		1510			1506
1494	1494	1496	1499	1525				1499		1495	
	1461		1459	1494		1497					1471
1450				1460		1460		1453		1458	1456
	1440	1445		1448		1444				1445	

1423	1423	1424	1421			1423		1423		1423	
1383	1383	1383	1384				1414				1415
1320	1320	1319		1383	1383	1383	1384	1383	1383	1383	1384
1293		1292		1320	1318	1320		1317	1318	1319	
		1231		1293		1292		1294		1292	
1219	1218		1212	1235		1230		1252			
1174		1173		1218			1212	1230		1230	
	1167		1163	1173		1173		1206			
	1130		1130				1161	1176		1172	
			1127		1129		1127		1165		1162
	1115			1112					1127		1127
1075		1073		1075		1074		1110	1115		1113
	1061			1041		1041	1059	1073		1073	
		1050	1051		1031				1053		1058
1041	1036			1022		1022	1021	1042			
		1024	1024	1003		1003				1022	
1018						836				1003	
		838				734				839	
		737		718						738	
717				668			667	669	668		668
669	669	662	668			662				651	
650				650		650		617	618		
617				616		611				574	
576		577			597						561
			557	576		577					
							557				

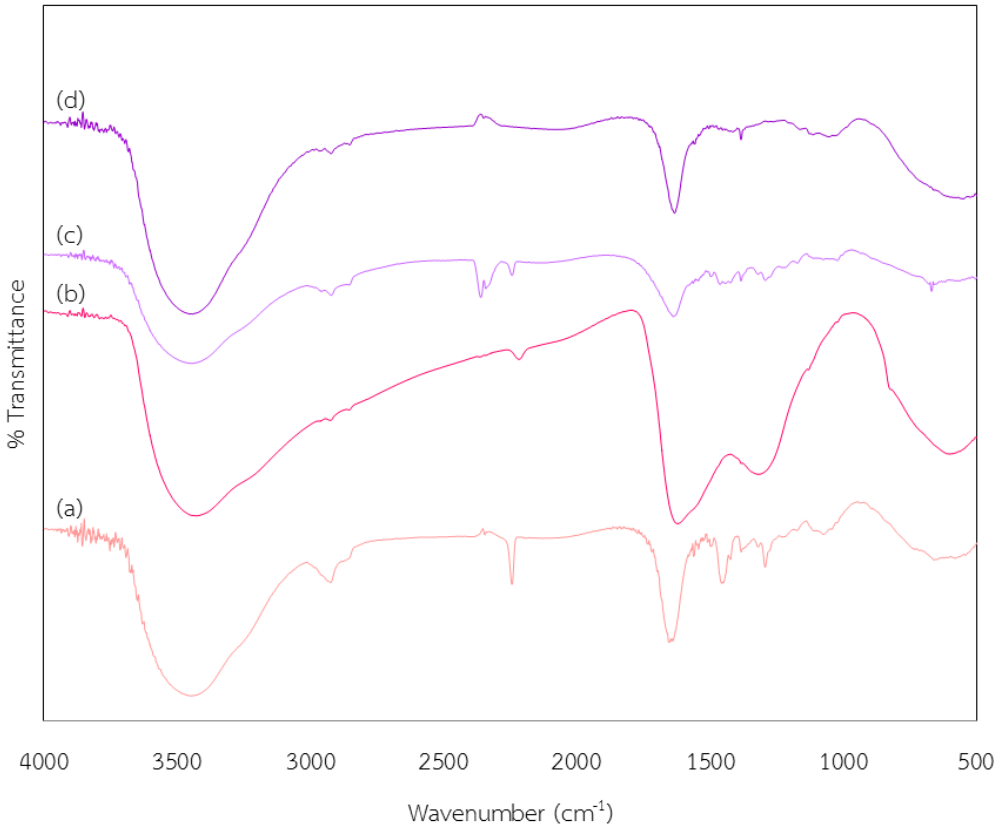

Figure B.7. FTIR transmittance spectra of PAN 8wt%/TTIP 11vol% (a) nanofiber, (b) calcined nanofiber, (c) film and (d) calcined film – All DMF solvent.

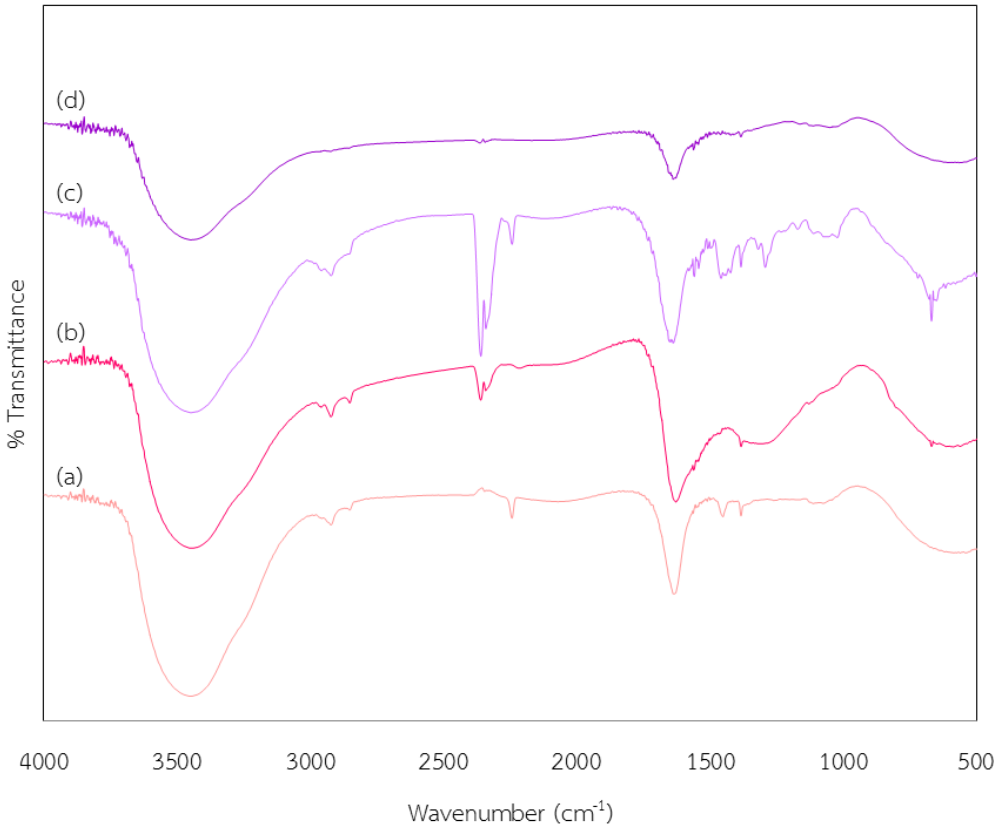

Figure B.8. FTIR transmittance spectra of PAN 8wt%/TTIP 15.5vol% (a) nanofiber, (b) calcined nanofiber, (c) film and (d) calcined film – All DMF solvent.

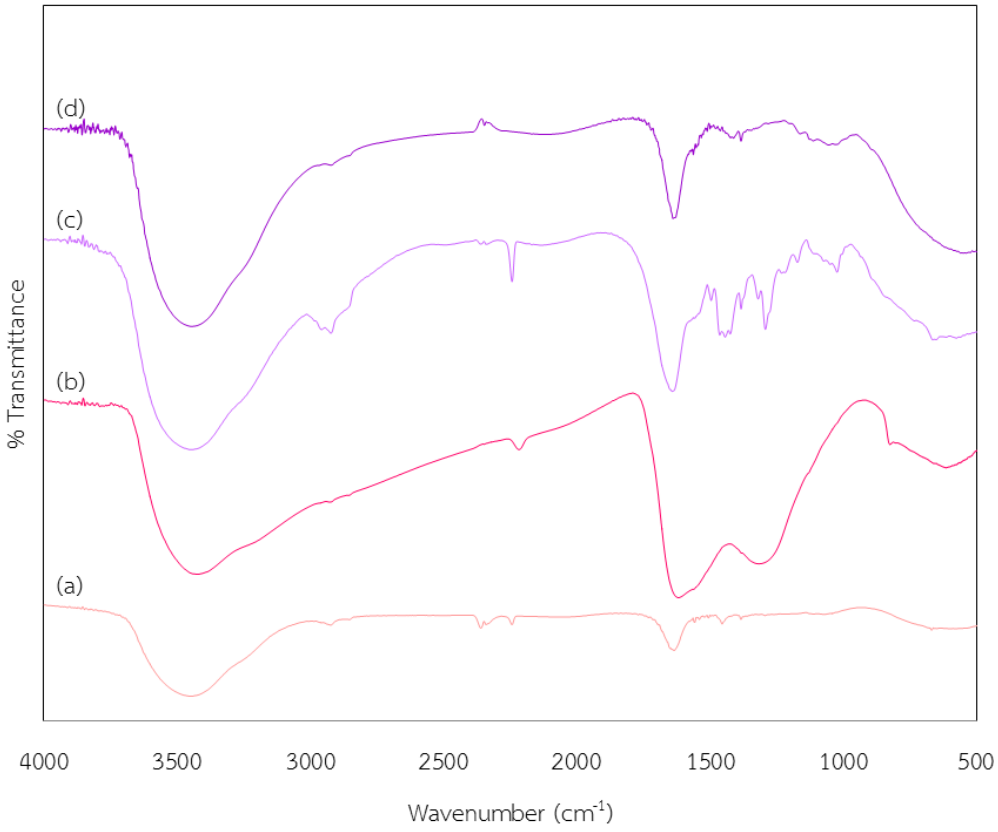

Figure B.9. FTIR transmittance spectra of PAN 8wt%/TTIP 20vol% (a) nanofiber, (b) calcined nanofiber, (c) film and (d) calcined film – All DMF solvent.

Table B.3. FTIR spectra which used to compare the structure of electrospinning nanofibers and spin coating films in topic 4.4.

TTIP 11vol%				TTIP 15.5vol%				TTIP 20vol%			
(a)	(b)	(c)	(d)	(a)	(b)	(c)	(d)	(a)	(b)	(c)	(d)
Fiber	Cal. fiber	Film	Cal. film	Fiber	Cal. fiber	Film	Cal. film	Fiber	Cal. fiber	Film	Cal. film
3450	3426	3451	3452	3451	3440	3450	3450	3452	3425	3442	3440
		2990		2957	2958	2957				3030	
	2969		2967	2986					2963		2969
		2957		2923	2923	2923				2957	
2940				2852	2852			2923	2925	2923	2923
2924	2925	2922	2923		2360	2360	2363	2853	2852	2857	2852
2881				2346	2342	2341	2344	2360		2360	
	2854	2854	2853	2243		2243		2341	2342	2340	2346
	2363	2360			2214			2243		2243	
2345			2349	1635	1628	1638	1638		2217		
	2339	2341		1563	1561	1569	1562	1643		1642	1639
2243		2243		1552	1552	1551	1552		1617		
	2217			1544	1543	1542	1543	1557	1562	1556	1562
1646				1533	1533	1532	1532	1551			1552
		1638	1633	1526		1525	1525	1540			1544
	1622			1510	1510	1508	1510				1526
1561		1562		1500	1500	1498		1496		1496	1494
		1552	1556	1451	1450	1458	1449			1463	
1546					1440	1440	1440	1454			
1543		1543	1540	1423		1423	1422			1443	
1525			1523	1383	1383	1384	1384			1424	1423
1494		1494	1496			1319					1412
1457		1461				1292		1383	1383	1383	1383

1450			1453	1165		1171	1163	1318	1314	1319	
		1441	1443		1128			1293		1292	
1423		1423	1425	1112		1111		1227		1231	
			1414	1075		1073				1218	
1383	1383	1383	1383				1051				1203
1320	1318	1320				1022		1175		1172	
1293		1292				719					1162
1229		1230			668	669		1112		1109	1113
		1218			648	650		1074		1073	
			1203					1045		1049	1054
1174		1172						1021		1023	1027
	1130		1130							1005	
1112		1112	1113						824		
1074		1075								733	
			1053					668	668	664	
1041									613		
1018		1022	1021					582			
		1003								575	
	823										558
738		738									
		668	668								
658											
		617									
	604										
576		574	575								

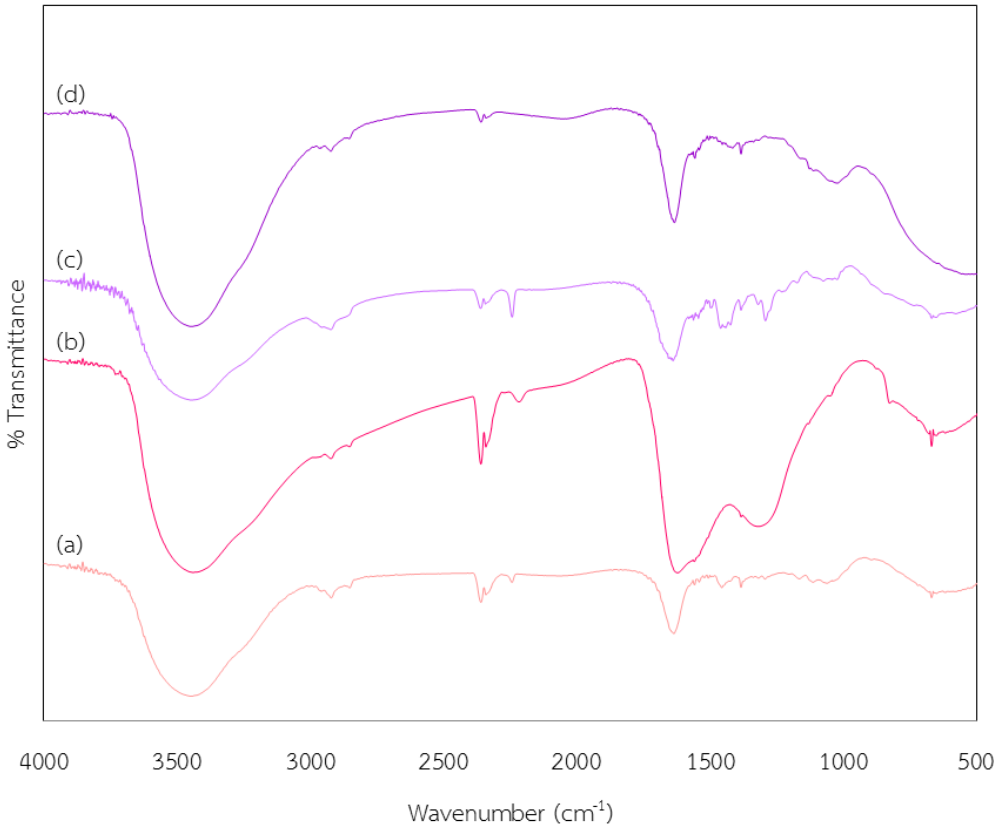

Figure B.10. FTIR transmittance spectra of PAN 8wt%/TTIP 11vol% (a) nanofiber, (b) calcined nanofiber, (c) film and (d) calcined film – All ethanol solvent.

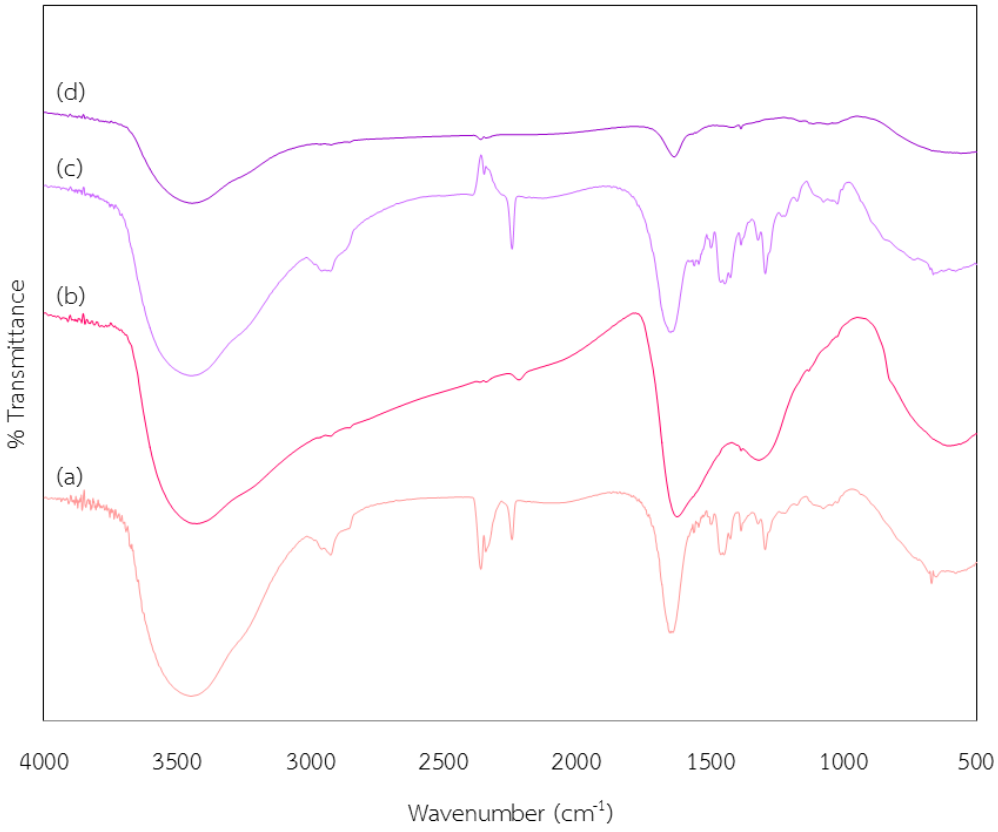

Figure B.11. FTIR transmittance spectra of PAN 8wt%/TTIP 15.5vol% (a) nanofiber, (b) calcined nanofiber, (c) film and (d) calcined film – All ethanol solvent.

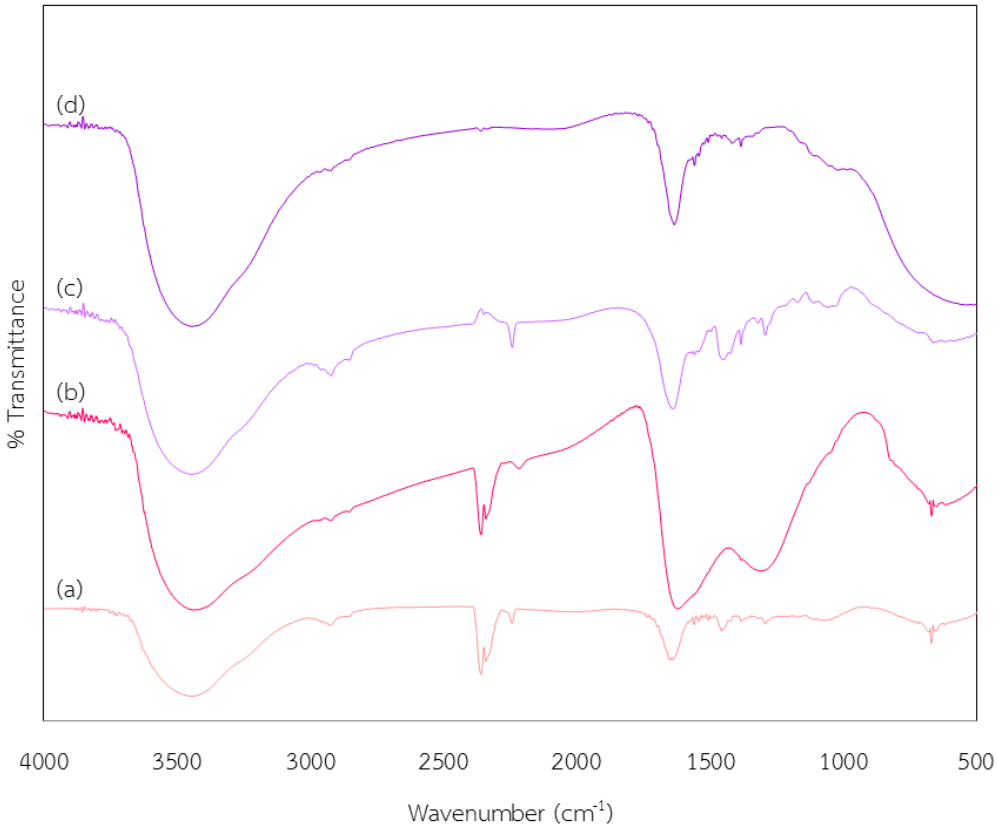

Figure B.12. FTIR transmittance spectra of PAN 8wt%/TTIP 20vol% (a) nanofiber, (b) calcined nanofiber, (c) film and (d) calcined film – All ethanol solvent.

Table B.4. FTIR spectra which used to compare the structure of electrospinning nanofibers and spin coating films in topic 4.5.

TTIP 11vol%				TTIP 15.5vol%				TTIP 20vol%			
(a)	(b)	(c)	(d)	(a)	(b)	(c)	(d)	(a)	(b)	(c)	(d)
Fiber	Cal. fiber	Film	Cal. film	Fiber	Cal. fiber	Film	Cal. film	Fiber	Cal. fiber	Film	Cal. film
3442	3441	3447	3442	3450	3425	3443	3442	3447	3441	3441	3442
2986	2986	2984				2985		2985	2987	2986	
			2967				2967				2967
2957		2957		2957	2957	2957		2957		2957	
2922	2923	2923	2923			2936		2924	2923	2923	2923
2852	2852	2857	2854	2924	2924	2924	2923	2854	2853	2853	2854
2360	2360	2361	2360	2878		2872		2360	2360		2359
2341	2341	2343	2341		2849		2853			2348	
2243		2243		2360	2366		2360	2341	2341		2339
	2217			2341	2341	2348	2341	2243		2242	
1636		1639	1634	2243		2243			2217		
	1623				2217			1638		1642	1634
1558	1559	1562	1556	1645		1646			1622		
		1552					1634	1559		1557	1558
1541		1543	1540		1623			1551			
1523		1525	1523			1568	1563	1542		1541	1541
1506				1561		1558		1524			1523
1497		1494	1496	1551			1552	1508			
1455		1460	1454	1542		1542		1498			1497
		1441	1443	1525				1457		1454	1456
		1423	1425	1494		1497				1425	
			1415	1460		1460					1416
1383	1383	1383	1383	1448		1444		1383	1382	1384	1384

1337						1423		1319		1320	
1318	1318	1319					1414		1311		
1293		1292		1383	1383	1383	1384	1293		1292	
		1230		1320	1318	1320				1230	
		1215	1212	1293		1292		1209		1212	1212
1206				1235		1230		1172		1171	
			1127	1218			1212				1162
		1174		1173		1173			1131		
1164							1161				1125
	1130				1129		1127	1112		1112	1110
1114		1115	1112	1112				1074		1074	
		1077		1075		1074			1047	1052	1050
1060				1041		1041	1059			1041	
	1050		1048		1031					1024	1019
1036		1041		1022		1022	1021			1003	
		1024	1023	1003		1003					985
		1003				836				932	
		935				734				897	
		897		718					873		
	875			668			667	719			
		735				662		669	668	663	
718				650		650		651	650		
668	668	668		616		611		617	617	617	
649	650	650			597					580	
615	616			576		577					
		576					557				

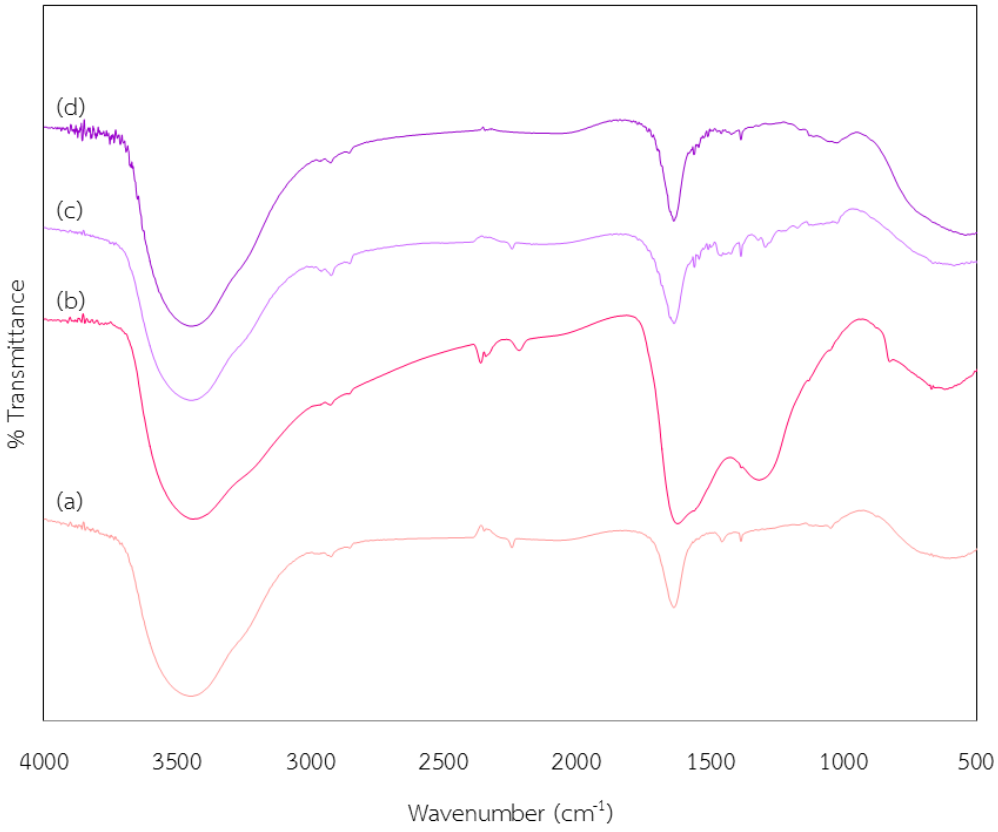

Figure B.13. FTIR transmittance spectra of PAN 8wt%/age 0 min (a) nanofiber, (b) calcined nanofiber, (c) film and (d) calcined film – All DMF solvent.

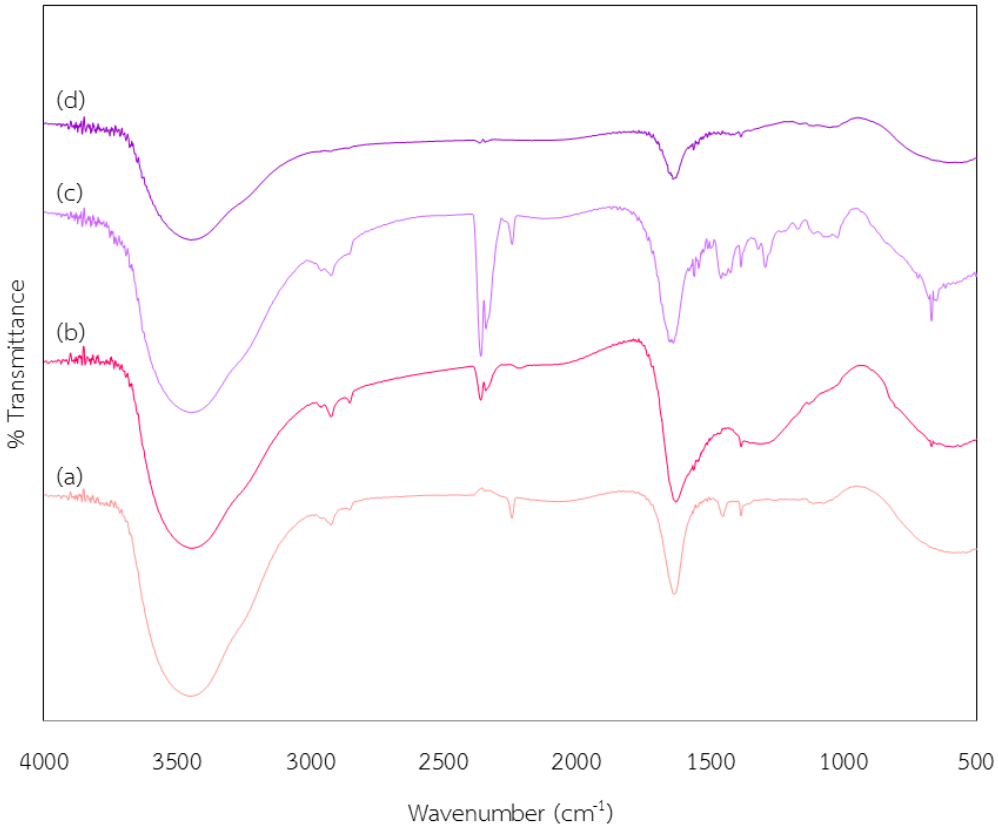

Figure B.14. FTIR transmittance spectra of PAN 8wt%/age 15 min (a) nanofiber, (b) calcined nanofiber, (c) film and (d) calcined film – All DMF solvent.

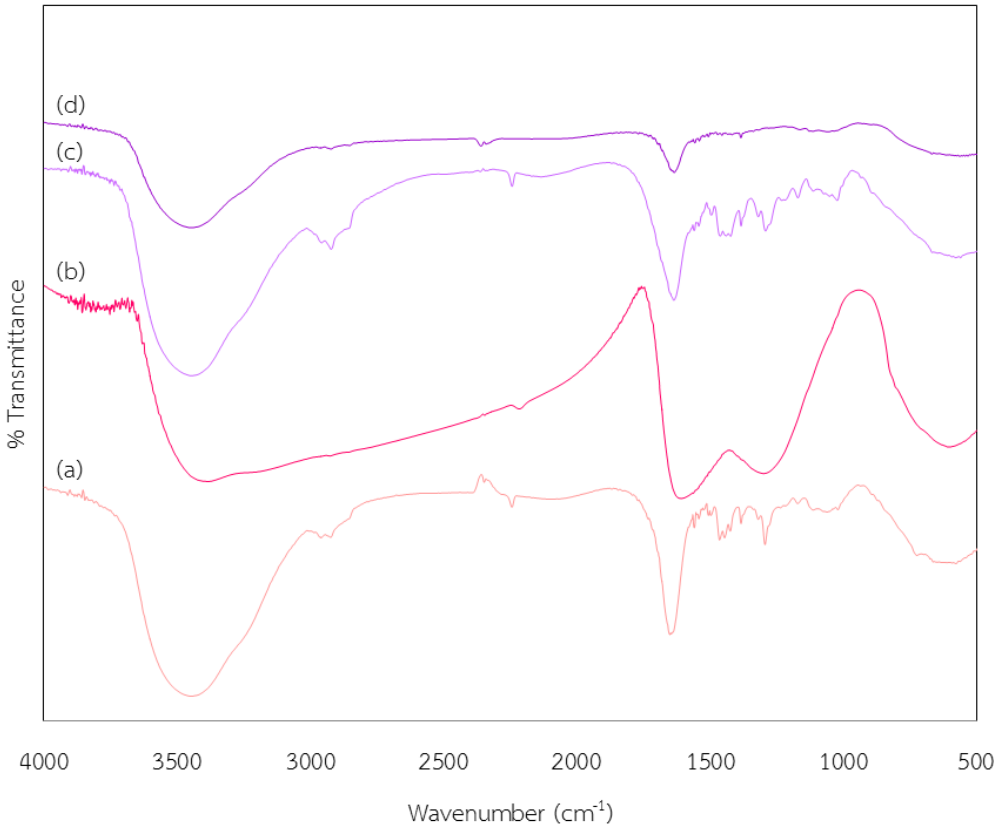

Figure B.15. FTIR transmittance spectra of PAN 8wt%/age 30 min (a) nanofiber, (b) calcined nanofiber, (c) film and (d) calcined film – All DMF solvent.

Table B.5. FTIR spectra which used to compare the structure of electrospinning nanofibers and spin coating films in topic 4.6.

Age 0 min				Age 15 min				Age 30 min			
(a)	(b)	(c)	(d)	(a)	(b)	(c)	(d)	(a)	(b)	(c)	(d)
Fiber	Cal. fiber	Film	Cal. film	Fiber	Cal. fiber	Film	Cal. film	Fiber	Cal. fiber	Film	Cal. film
3451	3441	3443	3449	3451	3440	3450	3450	3442	3385	3443	3442
2990		2986		2957	2958	2957		2986		2984	
2968	2969		2967	2986				2958	2963	2957	2967
		2958		2923	2923	2923		2924	2926	2922	2923
2923	2924	2922	2924	2852	2852			2852	2852	2854	2853
2852	2854	2853	2854		2360	2360	2363		2366	2362	2359
	2360			2346	2342	2341	2344	2347	2345	2344	2340
2347			2344	2243		2243		2243		2243	
	2341	2342			2214				2216		
2243		2243		1635	1628	1638	1638	1645			
	2216			1563	1561	1569	1562			1635	1634
1635		1635	1635	1552	1552	1551	1552		1609		
	1622			1544	1543	1542	1543	1559	1563	1559	1556
1562	1561	1558	1560	1533	1533	1532	1532	1551		1551	1545
1552		1551	1552	1526		1525	1525	1542		1542	1540
1542		1541	1542	1510	1510	1508	1510	1524			1523
		1524	1524	1500	1500	1498		1506			1506
1508		1506	1508	1451	1450	1458	1449	1497		1494	1496
		1497	1499		1440	1440	1440				1471
			1473	1423		1423	1422	1464		1461	
1455		1457	1457	1383	1383	1384	1384				1455
		1444				1319		1445			
		1421	1420			1292				1439	

1384	1382	1384	1384	1165		1171	1163	1424		1423	1418
			1340		1128				1397		
	1315	1319	1319	1112		1111		1383		1383	1384
1294		1292		1075		1073					1338
			1279				1051	1319		1319	1315
		1230				1022		1293	1298	1291	
1209		1212				719					1276
1174		1172			668	669		1235		1231	
			1160		648	650		1217		1217	
	1130	1127	1127					1171		1170	
		1114									1162
1078		1074									1127
1047	1050		1050					1113		1112	1114
		1041								1073	
1019		1023	1023					1060			1057
	876									1051	
	825							1020		1022	
662	669	663								1003	
		646						724			
	619							663			667
		583									614
			541						606		
								576			
										559	
											542

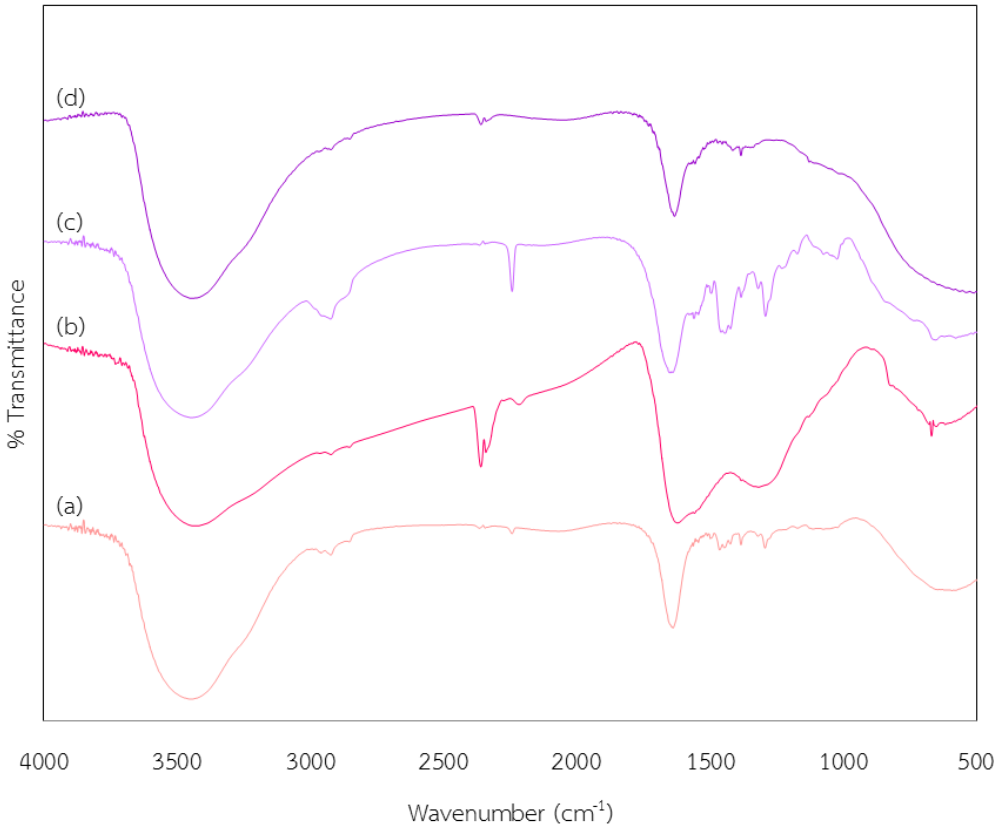

Figure B.16. FTIR transmittance spectra of PAN 8wt%/age 0 min (a) nanofiber, (b) calcined nanofiber, (c) film and (d) calcined film – All ethanol solvent.

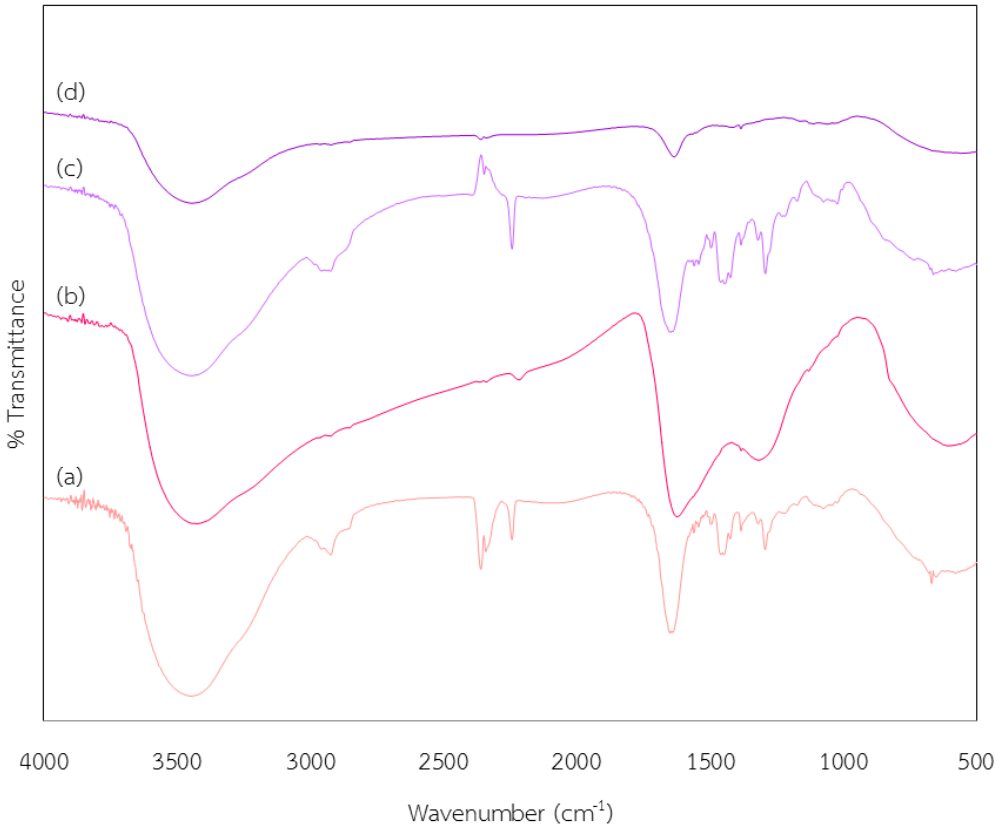

Figure B.17. FTIR transmittance spectra of PAN 8wt%/age 15 min (a) nanofiber, (b) calcined nanofiber, (c) film and (d) calcined film – All ethanol solvent.

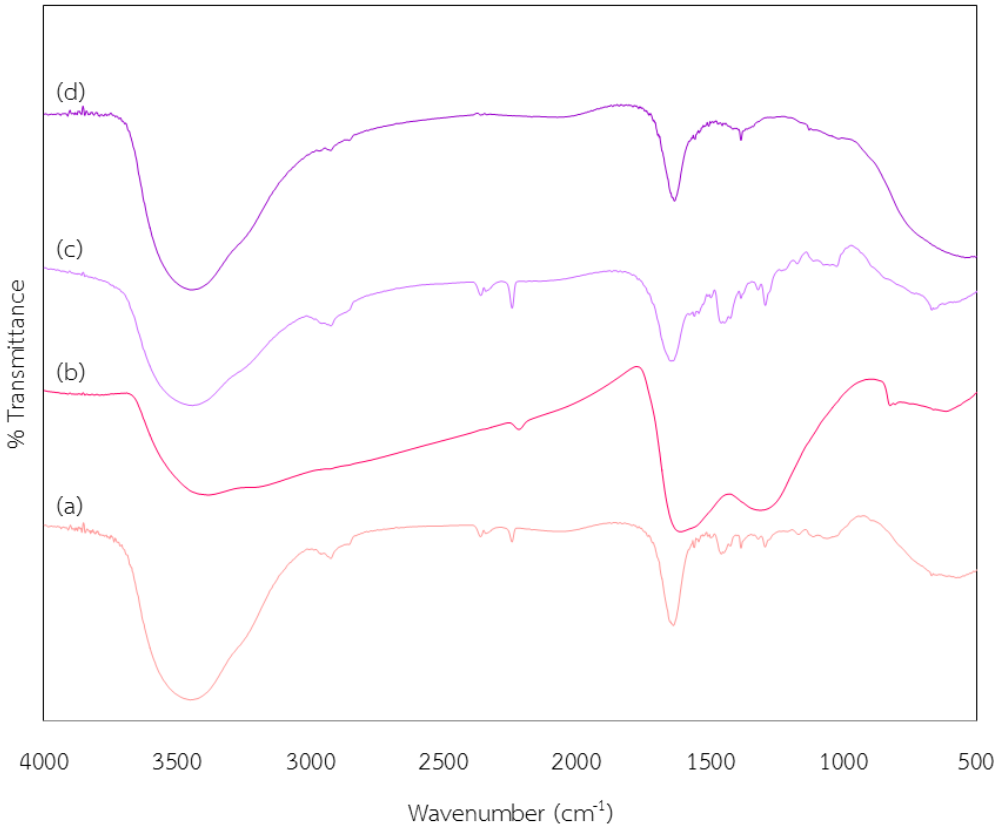

Figure B.18. FTIR transmittance spectra of PAN 8wt%/age 30 min (a) nanofiber, (b) calcined nanofiber, (c) film and (d) calcined film – All ethanol solvent.

Table B.6. FTIR spectra which used to compare the structure of electrospinning nanofibers and spin coating films in topic 4.7.

Age 0 min				Age 15 min				Age 30 min			
(a)	(b)	(c)	(d)	(a)	(b)	(c)	(d)	(a)	(b)	(c)	(d)
Fiber	Cal. fiber	Film	Cal. film	Fiber	Cal. fiber	Film	Cal. film	Fiber	Cal. fiber	Film	Cal. film
3451	3426	3443	3441	3450	3425	3443	3442	3451	3385	3442	3442
2958	2963	2956	2968			2985		2957		2957	2957
2923	2923	2924	2923				2967	2923	2923	2923	2924
		2875		2957	2957	2957				2869	
2853	2853		2853			2936		2854	2849		2853
2365	2360	2365	2359	2924	2924	2924	2923	2361	2357	2360	2361
2344	2341	2344	2340	2878		2872		2342		2341	2337
2243		2243			2849		2853	2243		2243	
	2216			2360	2366		2360		2217		
1639		1639		2341	2341	2348	2341			1645	
			1633	2243		2243		1638			1633
	1623				2217				1612		
1562	1559	1561	1556	1645		1646		1559	1556	1558	1556
1552		1551					1634	1551			
1543		1543	1540		1623			1542		1542	1540
1525			1523			1568	1563	1524			1523
1510		1509	1505	1561		1558		1507		1508	1505
1499		1495	1496	1551			1552	1498		1497	1496
1465				1542		1542		1457		1457	1454
		1458	1454	1525				1448		1445	1443
1445		1444	1443	1494		1497		1423		1423	
1423		1423		1460		1460					1414
			1414	1448		1444		1383		1383	1384

1384	1383	1383	1384			1423		1319		1319	
			1347				1414		1313		
1320	1318	1319		1383	1383	1383	1384	1293		1292	
1293		1291		1320	1318	1320				1230	
		1230		1293		1292		1206			
1217				1235		1230				1173	
1172		1172		1218			1212	1167			
	1130		1127	1173		1173					1127
1113		1112	1112				1161	1112		1112	1112
			1103		1129		1127			1074	
1075		1074		1112				1060			
		1047		1075		1074				1051	
1021		1023		1041		1041	1059	1024		1024	
			1015		1031						1017
		1003		1022		1022	1021		823		
	821			1003		1003			805		
	668					836		668	662	667	
	650	654				734				658	
	617	619		718					615	620	
		576		668			667	576		578	
						662					
				650		650					
				616		611					
					597						
				576		577					
							557				

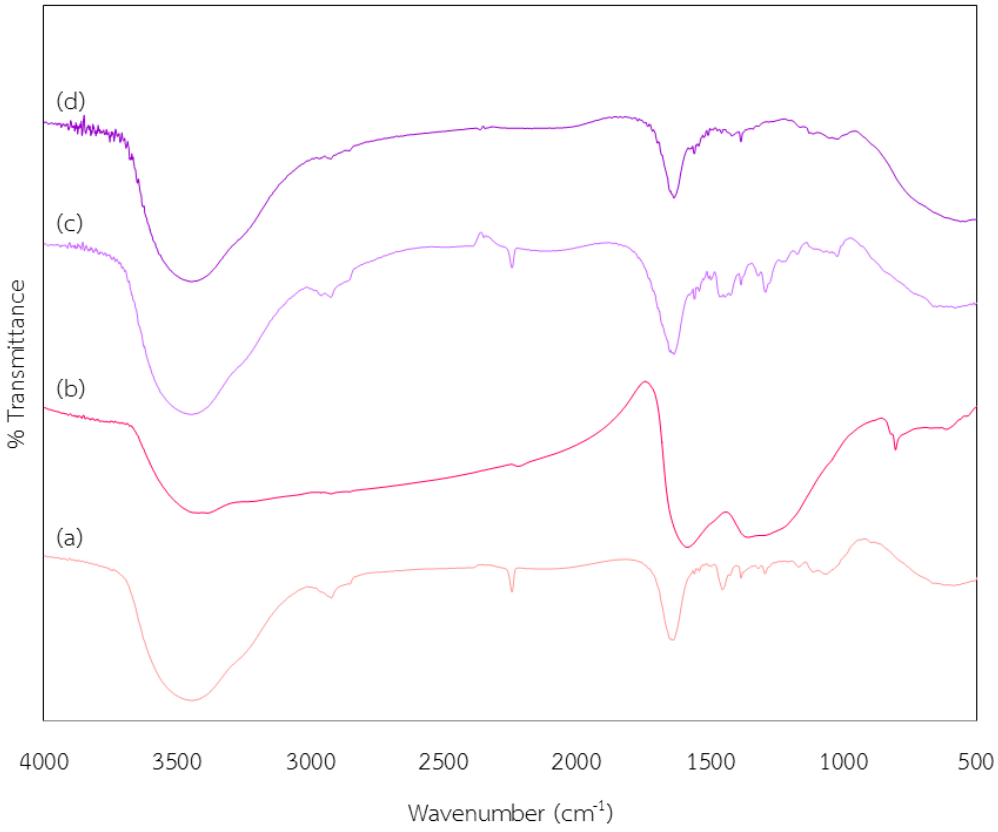

Figure B.19. FTIR transmittance spectra of PAN 8wt%/22 kV for electrospinning nanofibers and 3 V for spin coating films (a) nanofiber, (b) calcined nanofiber, (c) film and (d) calcined film – All DMF solvent.

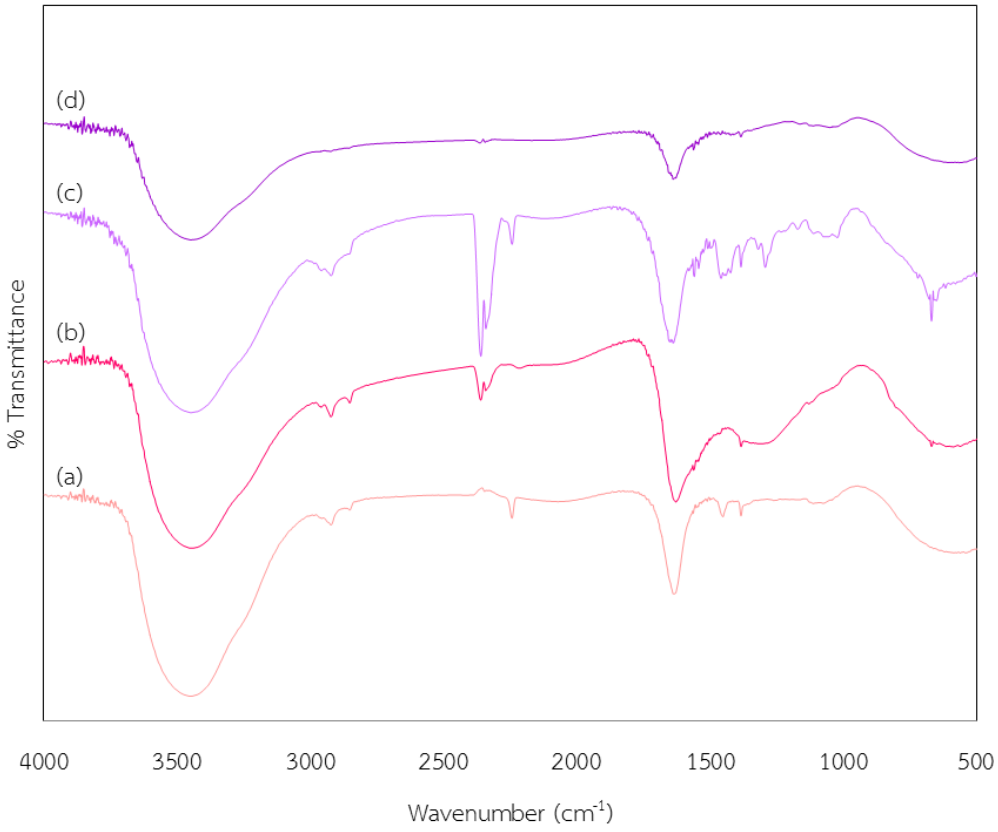

Figure B.20. FTIR transmittance spectra of PAN 8wt%/24 kV for electrospinning nanofibers and 5 V for spin coating films (a) nanofiber, (b) calcined nanofiber, (c) film and (d) calcined film – All DMF solvent.

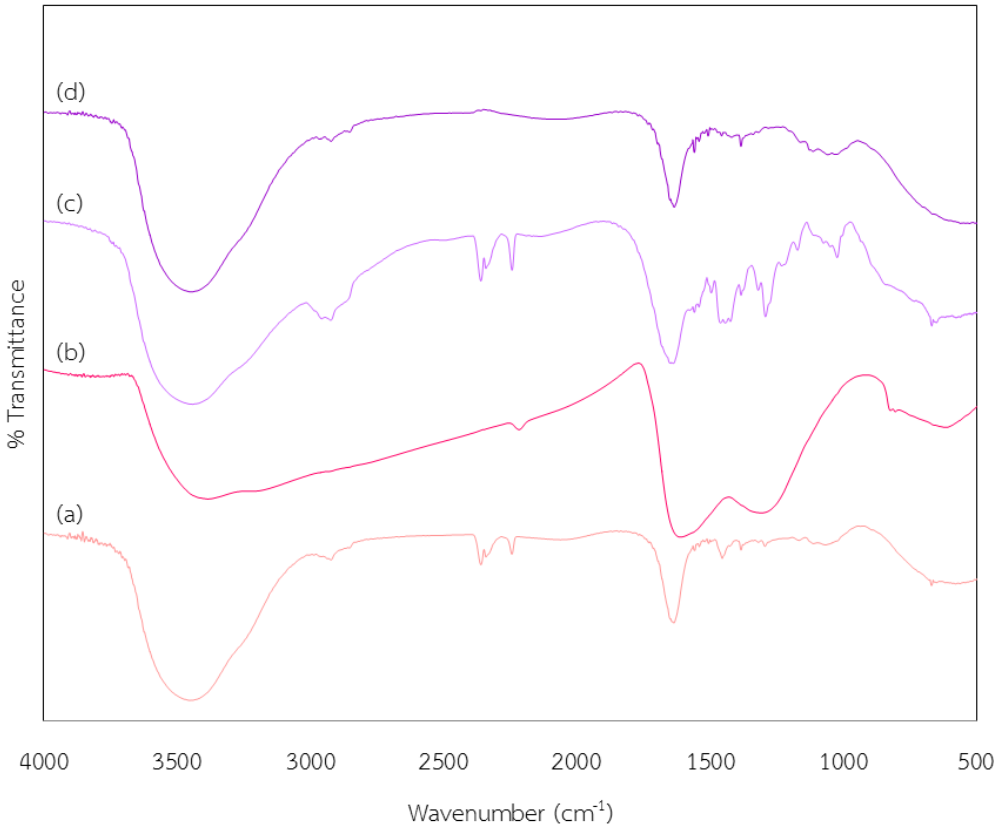

Figure B.21. FTIR transmittance spectra of PAN 8wt%/26 kV for electrospinning nanofibers and 7 V for spin coating films (a) nanofiber, (b) calcined nanofiber, (c) film and (d) calcined film – All DMF solvent.

Table B.7. FTIR spectra which used to compare the structure of electrospinning nanofibers and spin coating films in topic 4.8.

22 kV electrical potential				24 kV electrical potential				26 kV electrical potential			
(a)	(b)	(c)	(d)	(a)	(b)	(c)	(d)	(a)	(b)	(c)	(d)
Fiber	Cal. fiber	Film	Cal. film	Fiber	Cal. fiber	Film	Cal. film	Fiber	Cal. fiber	Film	Cal. film
3442	3385	3442	3450	3451	3440	3450	3450	3453	3385	3342	3442
		2986		2957	2958	2957		2986		2987	
2956	2960	2958	2357	2986						2957	2957
2922	2922	2923	2924	2923	2923	2923		2923	2919	2924	2923
2853	2853		2853	2852	2852			2853	2853		2853
			2362		2360	2360	2363	2360		2360	2360
		2348	2344	2346	2342	2341	2344	2341		2341	
2243	2220	2243		2243		2243		2243		2243	
1638		1635	1635		2214				2217		
	1585			1635	1628	1638	1638	1635		1637	1634
1559		1558	1559	1563	1561	1569	1562		1610		
1551		1551	1552	1552	1552	1551	1552			1576	
1541		1540	1542	1544	1543	1542	1543	1557		1558	1559
1523		1523	1523	1533	1533	1532	1532				1551
1505		1505	1507	1526		1525	1525	1540		1541	1541
1496		1496	1498	1510	1510	1508	1510	1519			1523
		1464	1472	1500	1500	1498		1505			1507
1453		1443	1457	1451	1450	1458	1449	1496		1496	1497
1425		1425			1440	1440	1440	1454		1460	1456
			1416	1423		1423	1422			1443	
1383		1383	1384	1383	1383	1384	1384	1425		1423	1419
	1356					1319		1383		1383	1384
1319		1319				1292					1338

1293		1292		1165		1171	1163	1319	1307	1319	1319
		1231			1128			1293		1291	1280
1207				1112		1111				1230	
1165		1172	1161	1075		1073		1165		1171	1160
			1127				1051				1126
1113			1113			1022		1111			1113
		1074				719		1068		1074	
1063					668	669				1048	1059
		1050	1050		648	650				1023	1029
		1022	1020						822		
	804								804		
	610	619						668			
			559					650			
									610	618	
								576			

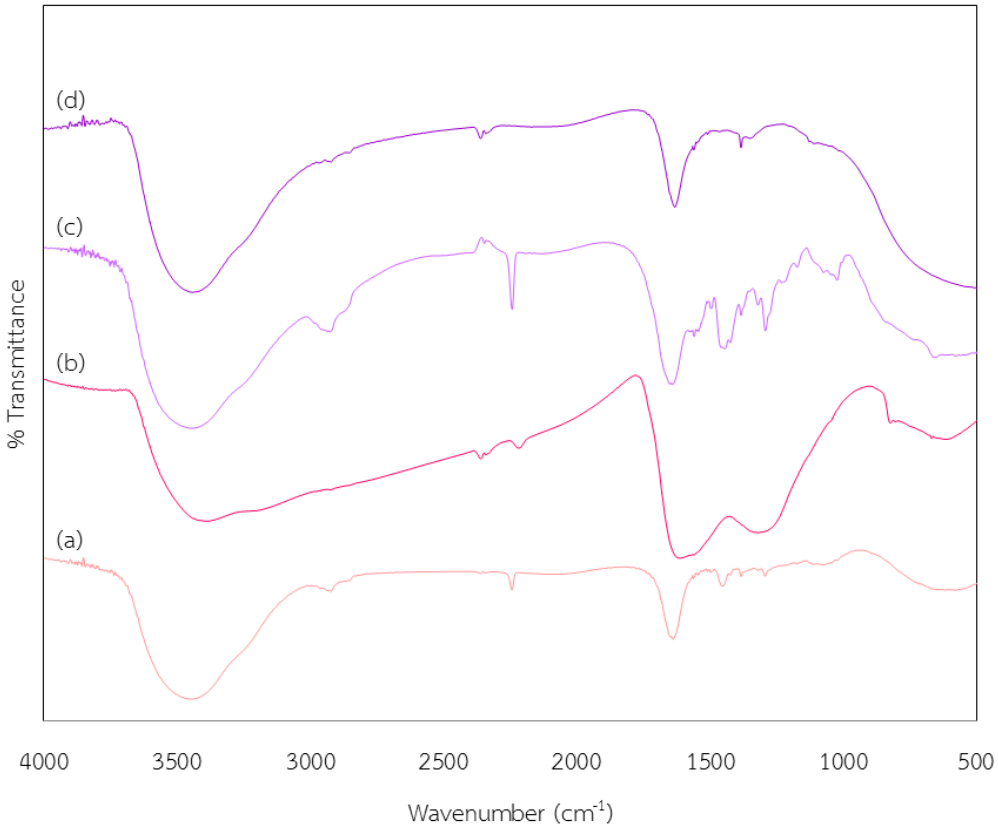

Figure B.22. FTIR transmittance spectra of PAN 8wt%/22 kV for electrospinning nanofibers and 3 V for spin coating films (a) nanofiber, (b) calcined nanofiber, (c) film and (d) calcined film – All ethanol solvent.

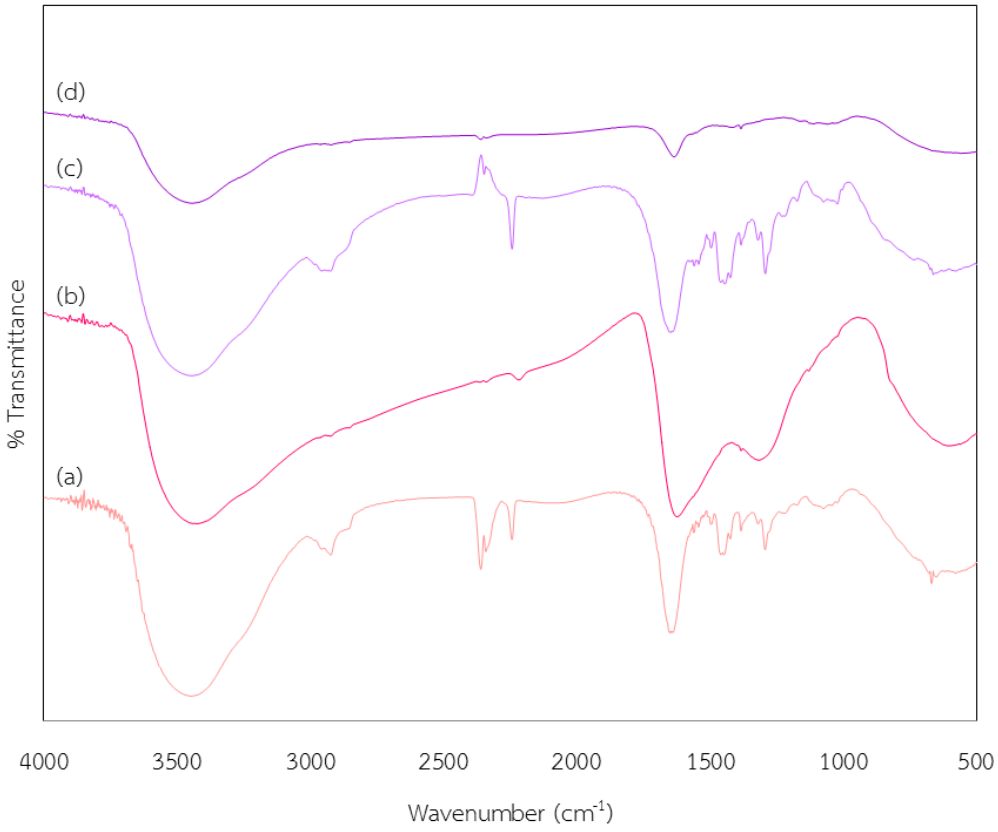

Figure B.23. FTIR transmittance spectra of PAN 8wt%/24 kV for electrospinning nanofibers and 5 V for spin coating films (a) nanofiber, (b) calcined nanofiber, (c) film and (d) calcined film – All ethanol solvent.

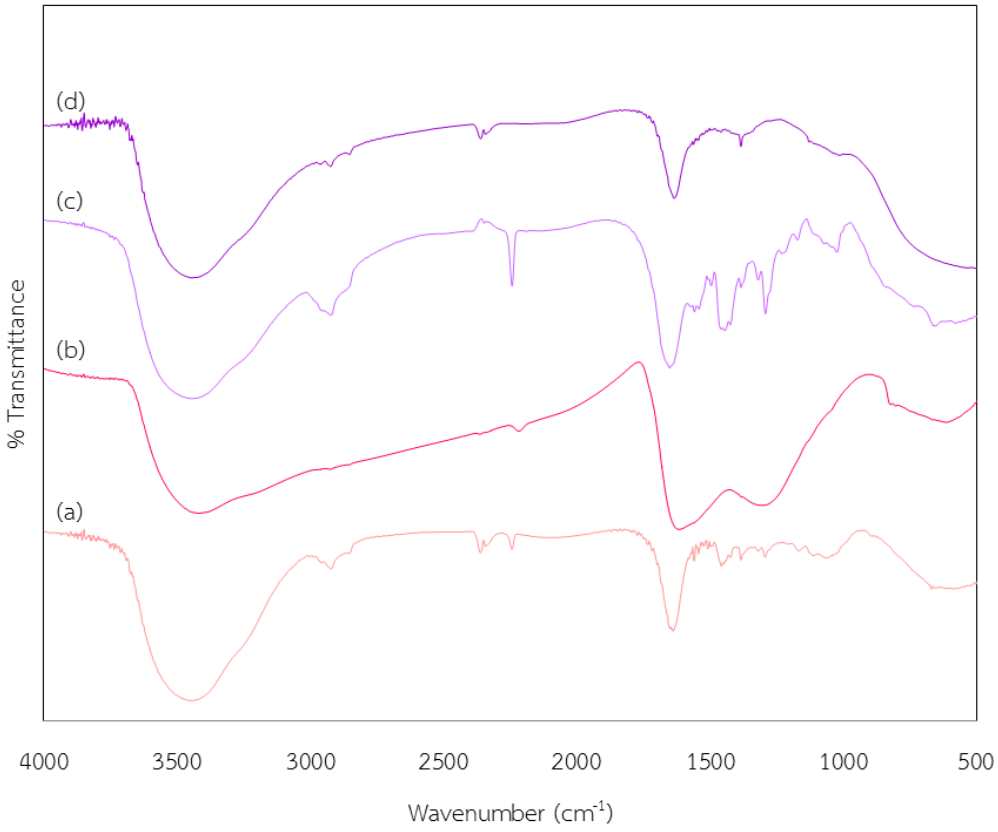

Figure B.24. FTIR transmittance spectra of PAN 8wt%/26 kV for electrospinning nanofibers and 7 V for spin coating films (a) nanofiber, (b) calcined nanofiber, (c) film and (d) calcined film – All ethanol solvent.

Table B.8. FTIR spectra which used to compare the structure of electrospinning nanofibers and spin coating films in topic 4.9.

22 kV electrical potential				24 kV electrical potential				26 kV electrical potential			
(a)	(b)	(c)	(d)	(a)	(b)	(c)	(d)	(a)	(b)	(c)	(d)
Fiber	Cal. fiber	Film	Cal. film	Fiber	Cal. fiber	Film	Cal. film	Fiber	Cal. fiber	Film	Cal. film
3451	3386	3451	3441	3450	3425	3443	3442	3447	3418	3442	3440
		2987				2985			2981	2987	
2957	2963		2957				2967	2957			2959
2923	2928	2924	2923	2957	2957	2957		2923	2925	2923	2924
		2872				2936				2875	
2849	2852		2854	2924	2924	2924	2923	2854	2852		2853
2363	2360		2361	2878		2872		2361	2364		2360
2344	2341	2347	2341		2849		2853	2343	2340	2347	2343
2243		2243		2360	2366		2360	2243		2243	
	2218			2341	2341	2348	2341		2217		
1639		1639	1632	2243		2243				1652	
	1613				2217			1638			1635
1562	1562	1559	1561	1645		1646			1615		
1552		1551	1551				1634	1559	1569	1567	1562
1543		1543			1623			1551		1558	1552
1525						1568	1563	1542		1542	1543
1509		1510	1509	1561		1558		1525			1524
1499		1495	1499	1551			1552	1508			1510
			1465	1542		1542		1498		1496	1499
1450		1445		1525				1457		1457	
1423		1423		1494		1497				1444	
1383		1383	1383	1460		1460		1423		1424	
			1350	1448		1444		1398			

1320	1319	1320				1423		1383	1386	1383	1384
1293		1292					1414	1339			
1230		1230		1383	1383	1383	1384	1319		1319	
1171		1173		1320	1318	1320			1307		
			1127	1293		1292		1293		1292	
1112			1115	1235		1230				1230	
1074		1074		1218			1212	1206			
		1047		1173		1173		1165		1172	
		1023					1161	1112			
	823				1129		1127	1061		1073	
	804			1112						1023	
668	668			1075		1074			822		
		652		1041		1041	1059	668	667	662	
	616				1031			653			
577		577		1022		1022	1021		611		
				1003		1003		577		578	
						836					
						734					
				718							
				668			667				
						662					
				650		650					
				616		611					
					597						
				576		577					
							557				

APPENDIX C

SEM-EDX MAPPING OF RESULTANT CORE/SHEATH FILMS.

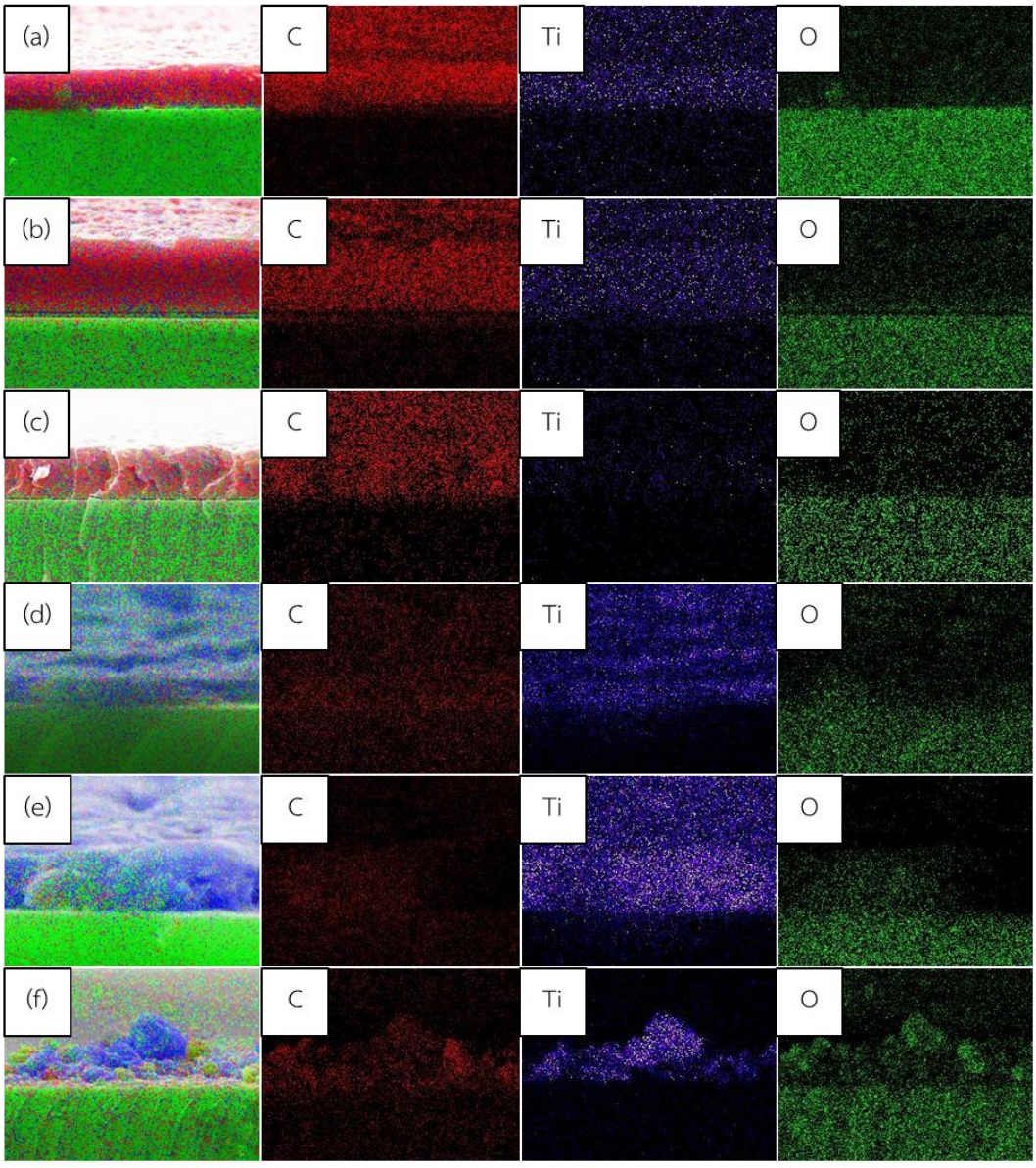

Figure C.1. SEM-EDX mapping of resultant core/sheath films (a) PAN 8wt%/PVP 10wt%, (b) PAN 8wt%/PVP 11.5wt%, (c) PAN 8wt%/PVP 13wt%, (d) calcined PAN 8wt%/PVP 10wt%, (e) calcined PAN 8wt%/PVP 11.5wt% and (f) calcined PAN 8wt%/PVP 13wt% – All DMF solvent.

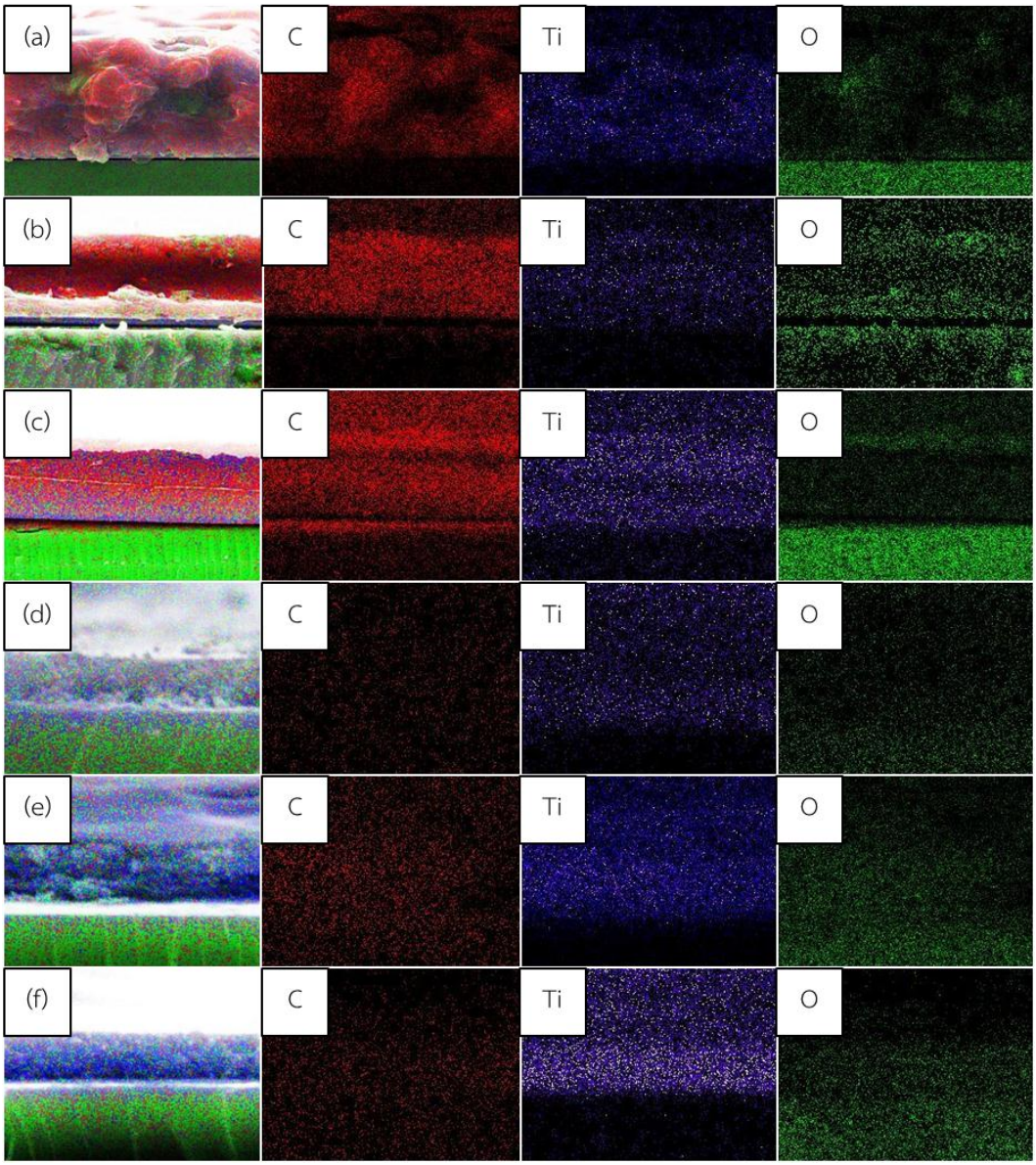

Figure C.2. SEM-EDX mapping of resultant core/sheath films (a) PAN 8wt%/PVP 10wt%, (b) PAN 8wt%/PVP 11.5wt%, (c) PAN 8wt%/PVP 13wt%, (d) calcined PAN 8wt%/PVP 10wt%, (e) calcined PAN 8wt%/PVP 11.5wt% and (f) calcined PAN 8wt%/PVP 13wt% – All ethanol solvent.

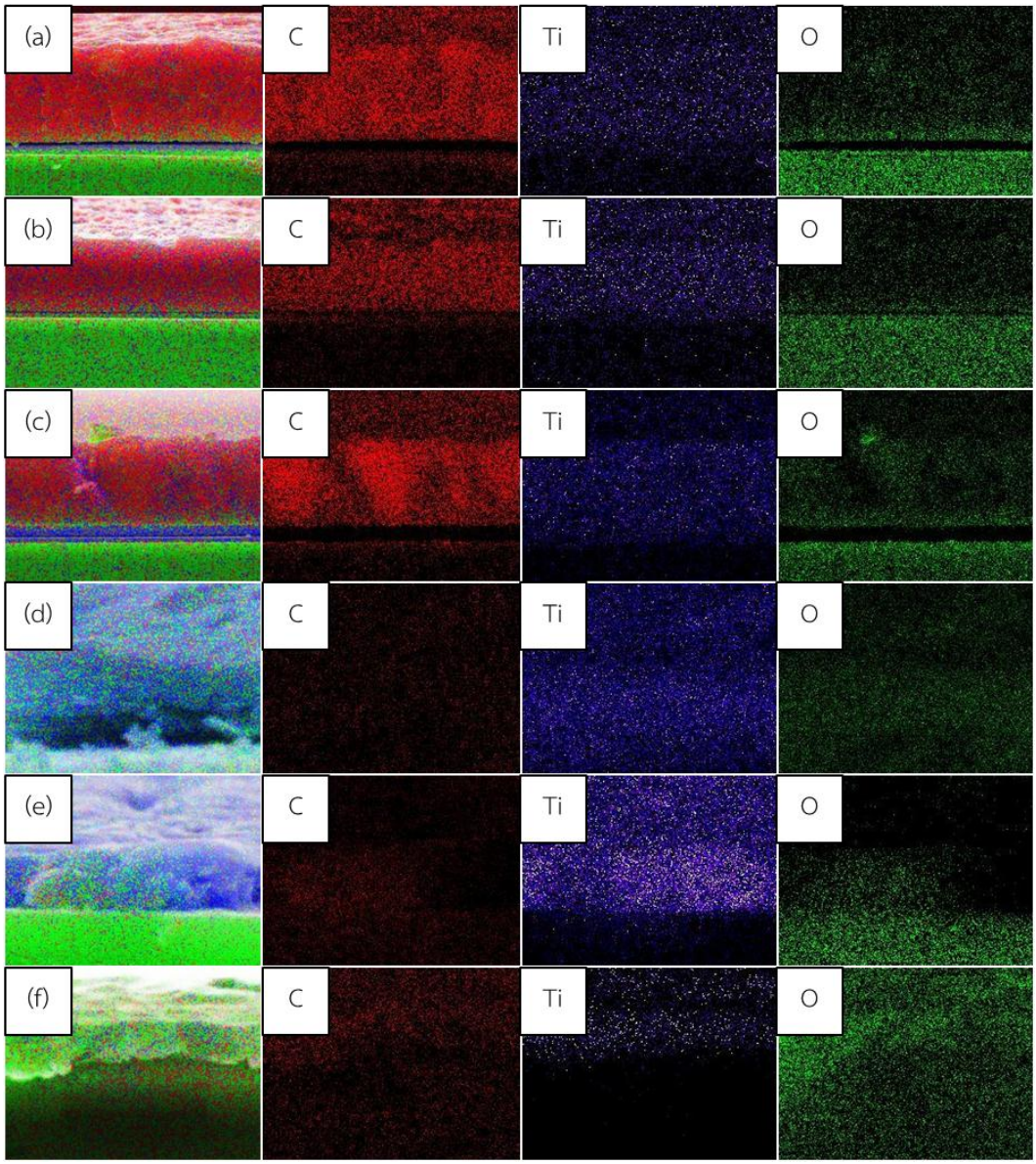

Figure C.3. SEM-EDX mapping of resultant core/sheath films (a) PAN 8wt%/TTIP 11vol%, (b) PAN 8wt%/TTIP 15.5vol%, (c) PAN 8wt%/TTIP 20vol%, (d) calcined PAN 8wt%/TTIP 11vol%, (e) calcined PAN 8wt%/TTIP 15.5vol% and (f) calcined PAN 8wt%/TTIP 20vol% – All DMF solvent.

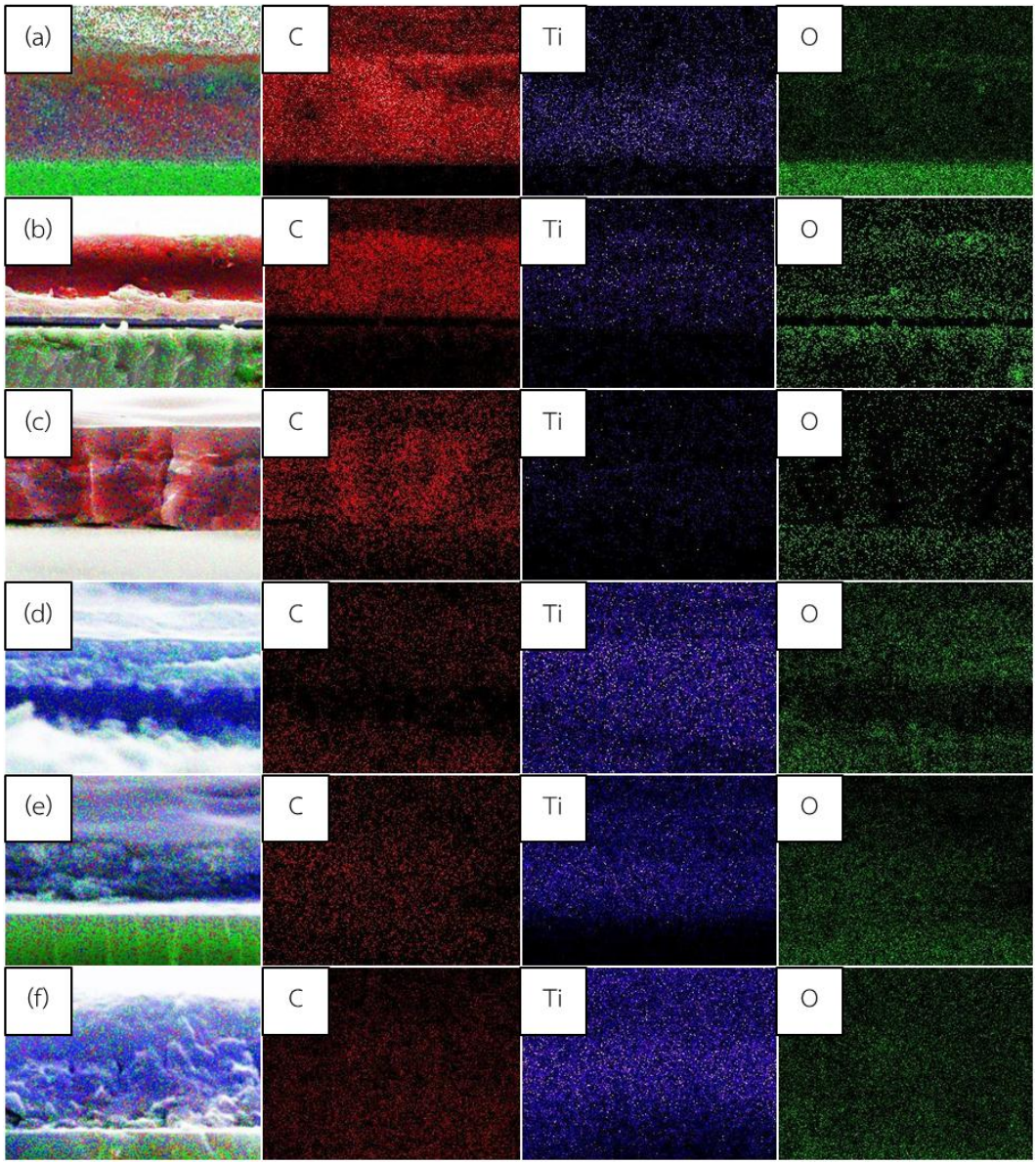

Figure C.4. SEM-EDX mapping of resultant core/sheath films (a) PAN 8wt%/TTIP 11vol%, (b) PAN 8wt%/TTIP 15.5vol%, (c) PAN 8wt%/TTIP 20vol%, (d) calcined PAN 8wt%/TTIP 11vol%, (e) calcined PAN 8wt%/TTIP 15.5vol% and (f) calcined PAN 8wt%/TTIP 20vol% – All ethanol solvent.

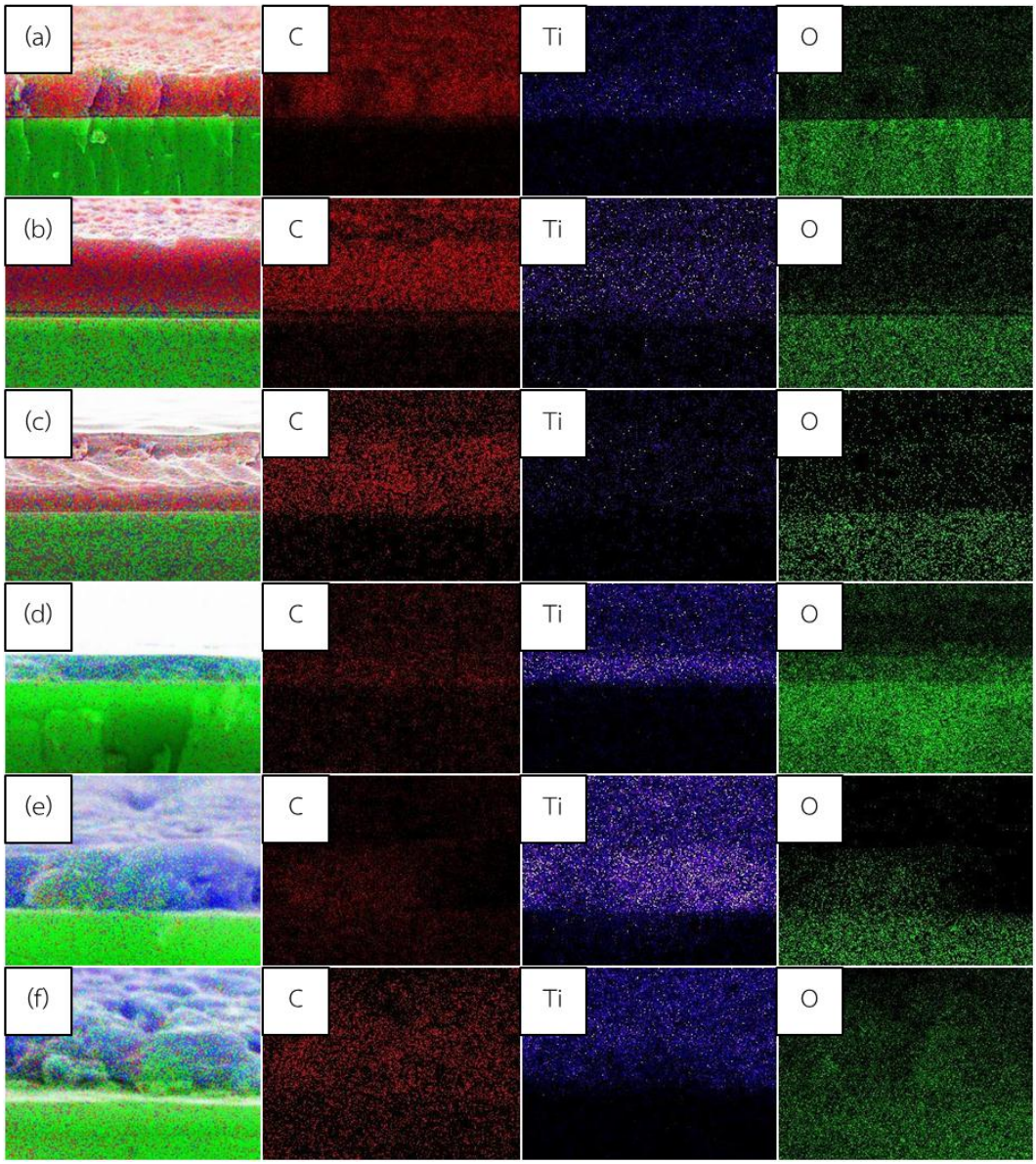

Figure C.5. SEM-EDX mapping of resultant core/sheath films (a) PAN 8wt%/age 0 min, (b) PAN 8wt%/age 15 min, (c) PAN 8wt%/age 30 min, (d) calcined PAN 8wt%/age 0 min, (e) calcined PAN 8wt%/age 15 min and (f) calcined PAN 8wt%/age 30 min – All DMF solvent.

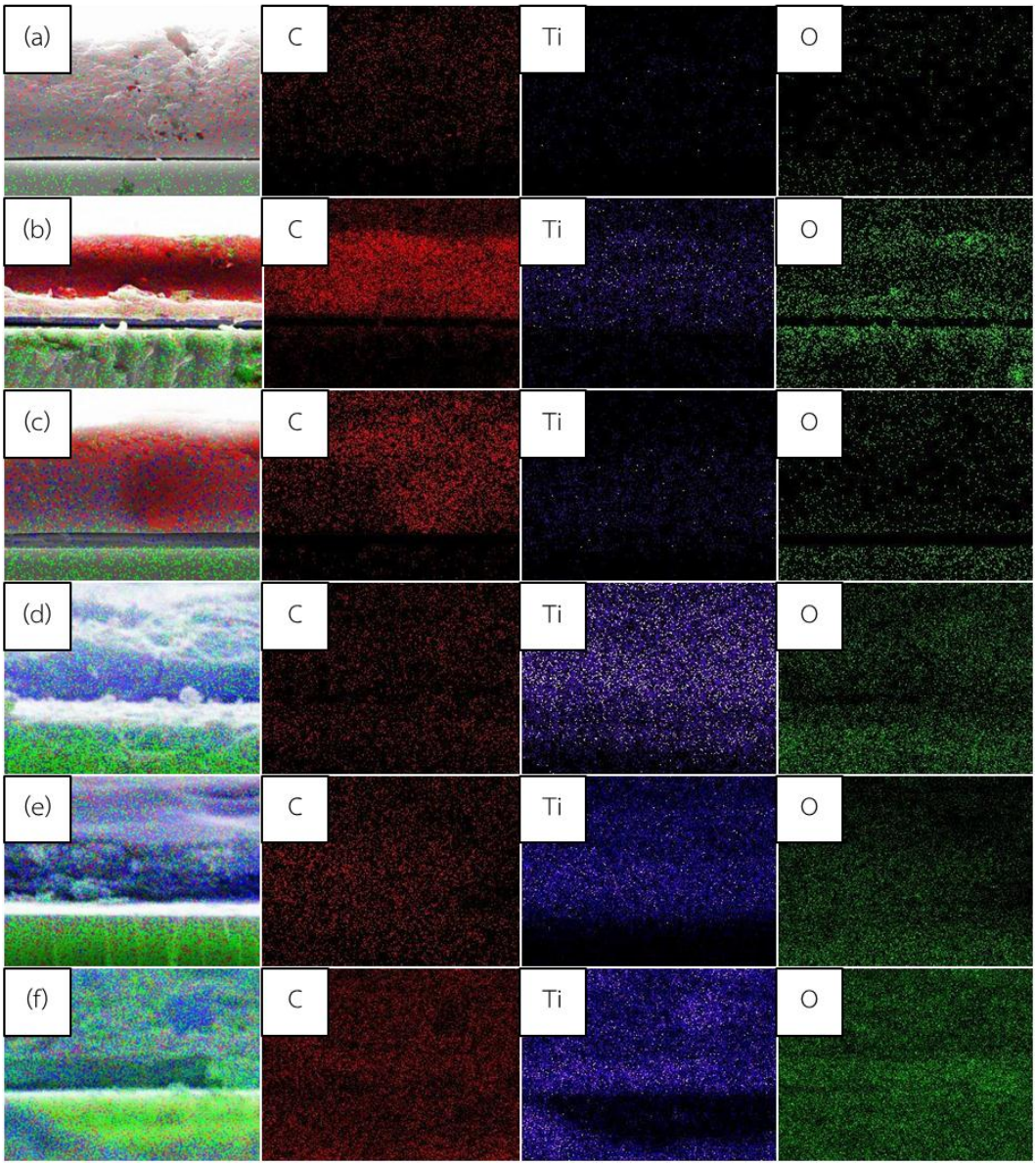

Figure C.6. SEM-EDX mapping of resultant core/sheath films (a) PAN 8wt%/age 0 min, (b) PAN 8wt%/age 15 min, (c) PAN 8wt%/age 30 min, (d) calcined PAN 8wt%/age 0 min, (e) calcined PAN 8wt%/age 15 min and (f) calcined PAN 8wt%/age 30 min – All ethanol solvent.

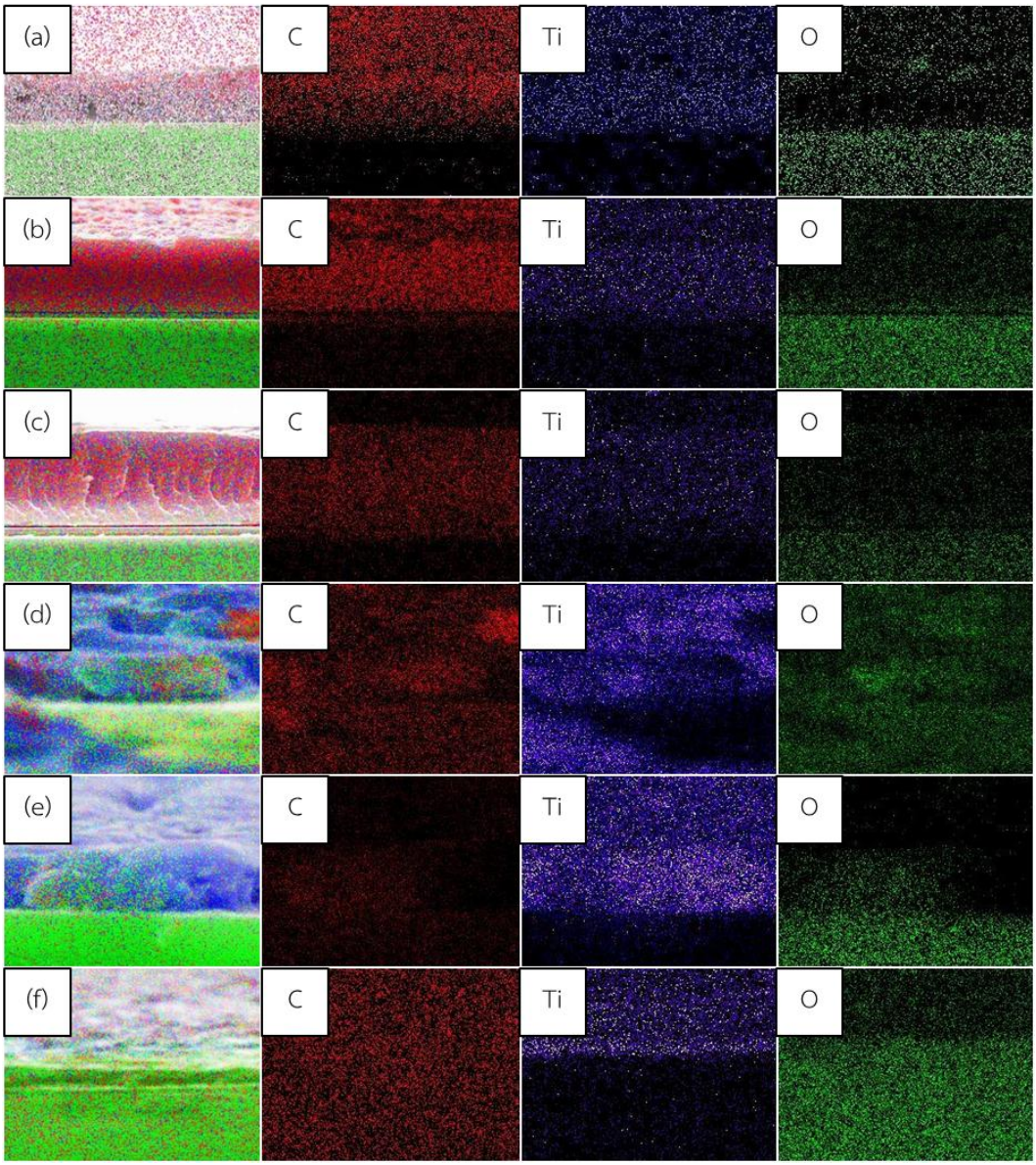

Figure C.7. SEM-EDX mapping of resultant core/sheath films (a) PAN 8wt%/3 V, (b) PAN 8wt%/5 V, (c) PAN 8wt%/7 V, (d) calcined PAN 8wt%/3 V, (e) calcined PAN 8wt%/5 V and (f) calcined PAN 8wt%/7 V – All DMF solvent.

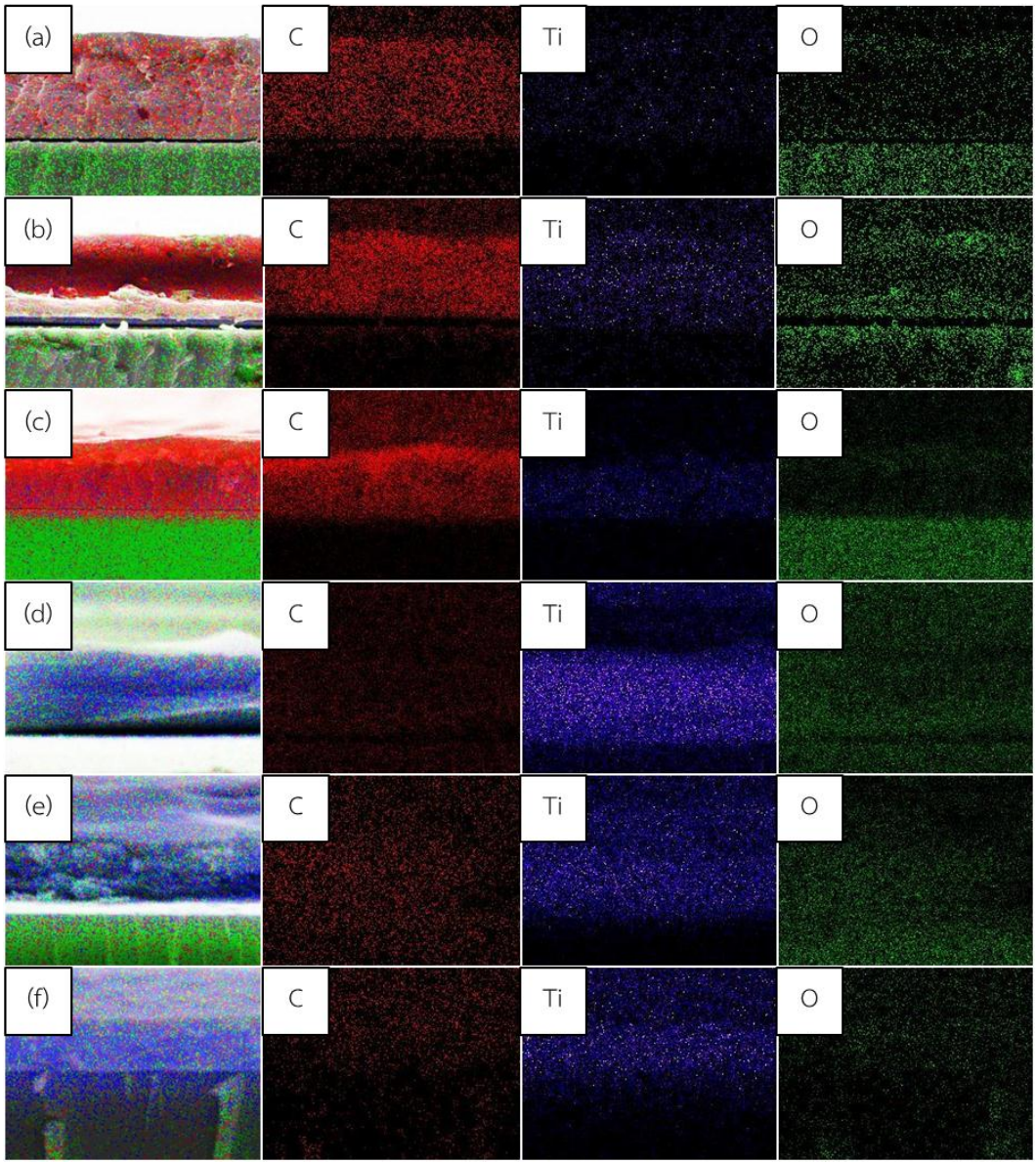

Figure C.8. SEM-EDX mapping of resultant core/sheath films (a) PAN 8wt%/3 V, (b) PAN 8wt%/5 V, (c) PAN 8wt%/7 V, (d) calcined PAN 8wt%/3 V, (e) calcined PAN 8wt%/5 V and (f) calcined PAN 8wt%/7 V – All ethanol solvent.

APPENDIX D

EDX PATTERNS AND ATOMIC PERCENTAGE OF BOTH FILMS AND CALCINED FILMS.

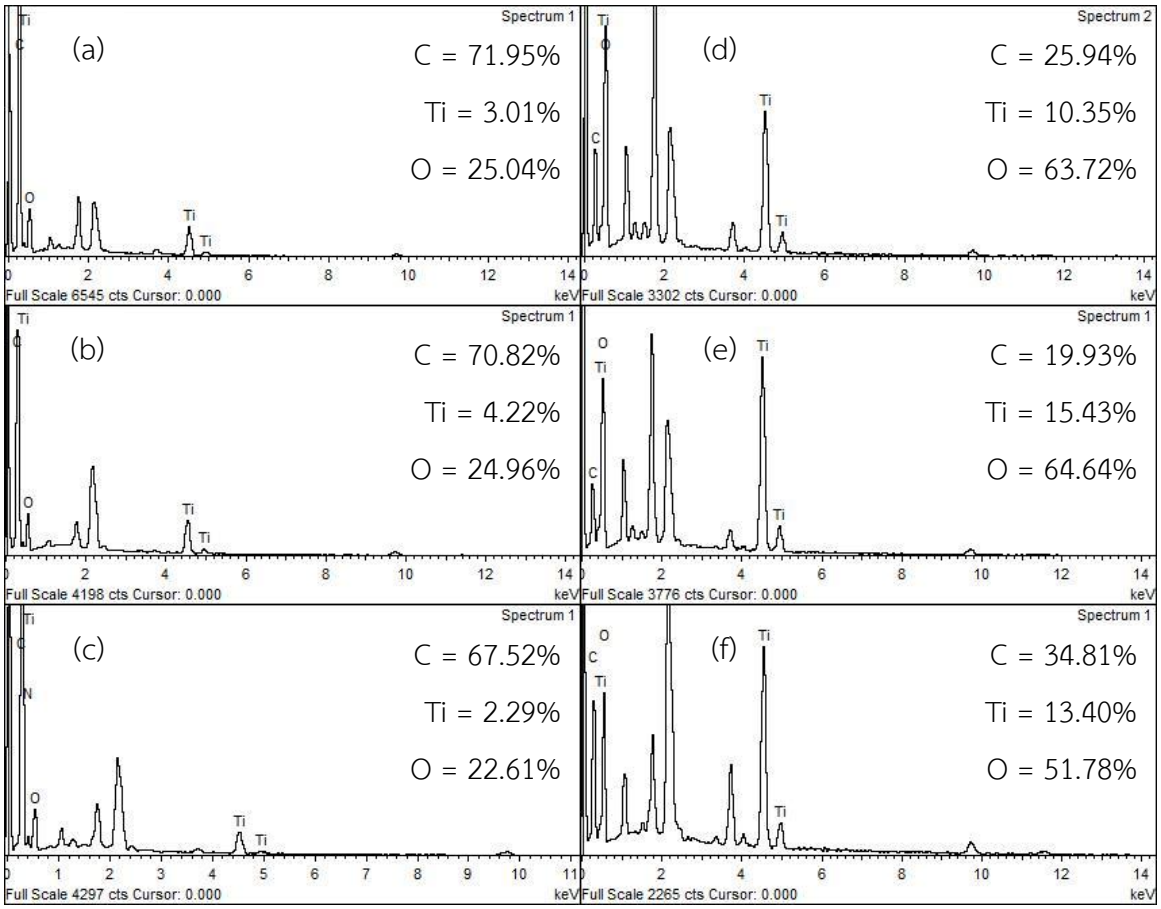

Figure D.1. EDX patterns and atomic percentage of resultant core/sheath films (a) PAN 8wt%/PVP 10wt%, (b) PAN 8wt%/PVP 11.5wt%, (c) PAN 8wt%/PVP 13wt%, (d) calcined PAN 8wt%/PVP 10wt%, (e) calcined PAN 8wt%/PVP 11.5wt% and (f) calcined PAN 8wt%/PVP 13wt% – All DMF solvent.

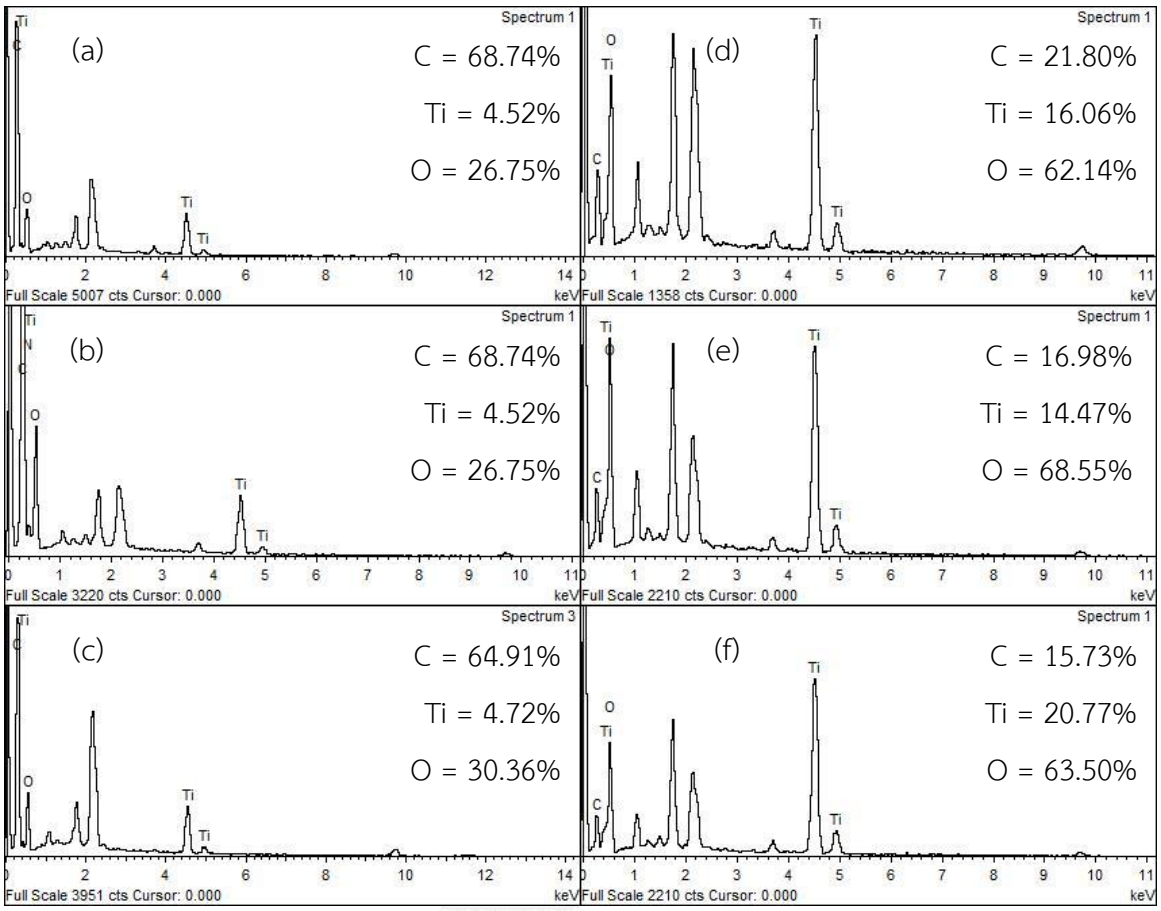

Figure D.2. EDX patterns and atomic percentage of resultant core/sheath films (a) PAN 8wt%/PVP 10wt%, (b) PAN 8wt%/PVP 11.5wt%, (c) PAN 8wt%/PVP 13wt%, (d) calcined PAN 8wt%/PVP 10wt%, (e) calcined PAN 8wt%/PVP 11.5wt% and (f) calcined PAN 8wt%/PVP 13wt% – All ethanol solvent.

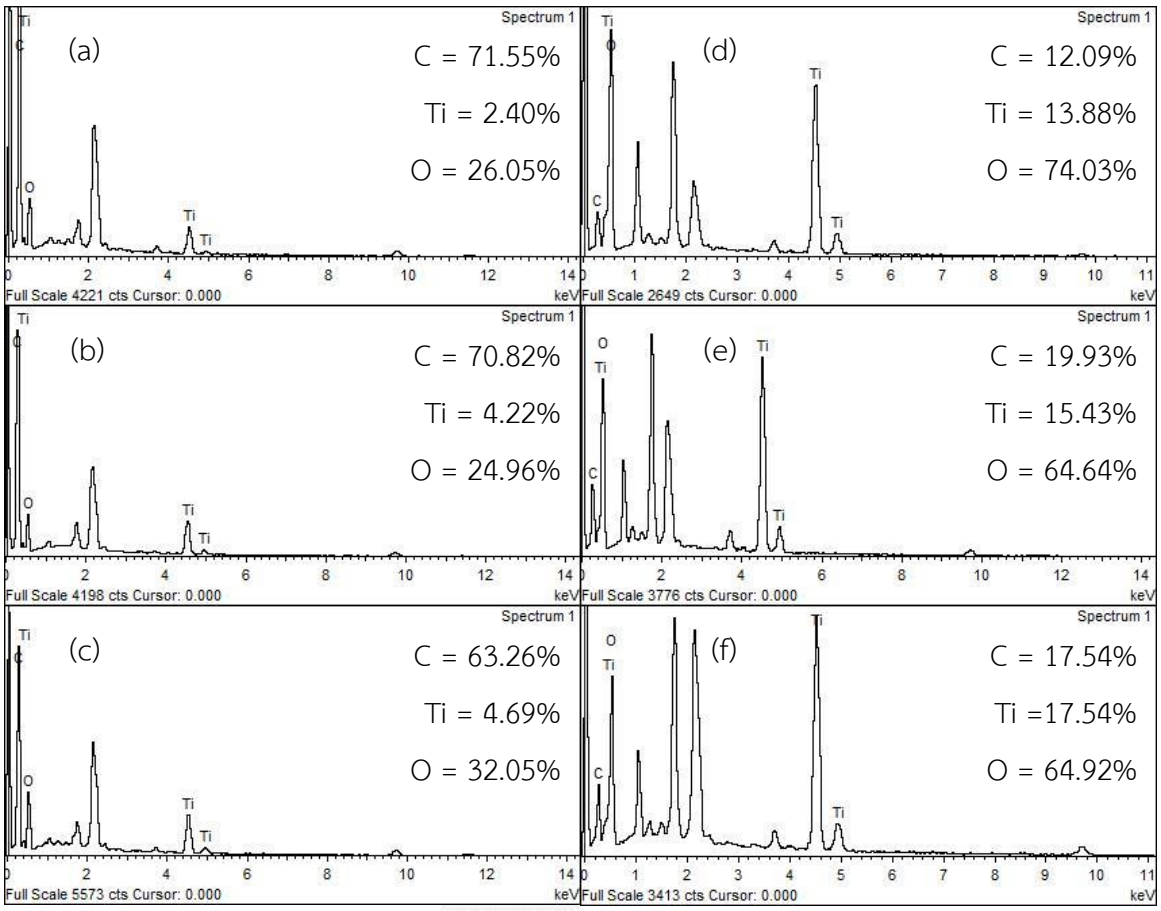

Figure D.3. EDX patterns and atomic percentage of resultant core/sheath films (a) PAN 8wt%/TTIP 11vol%, (b) PAN 8wt%/TTIP 15.5vol%, (c) PAN 8wt%/TTIP 20vol%, (d) calcined PAN 8wt%/TTIP 11vol%, (e) calcined PAN 8wt%/TTIP 15.5vol% and (f) calcined PAN 8wt%/TTIP 20vol% – All DMF solvent.

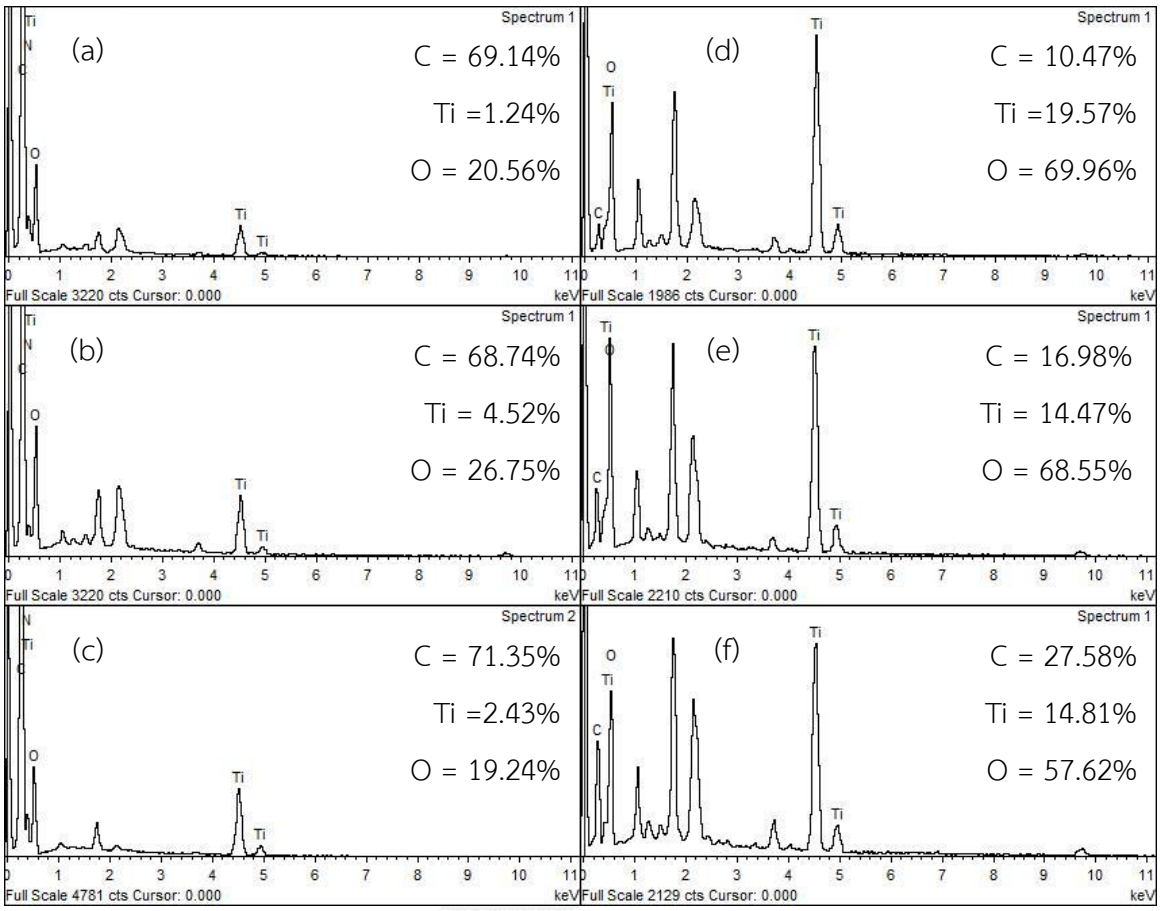

Figure D.4. EDX patterns and atomic percentage of resultant core/sheath films (a) PAN 8wt%/TTIP 11vol%, (b) PAN 8wt%/TTIP 15.5vol%, (c) PAN 8wt%/TTIP 20vol%, (d) calcined PAN 8wt%/TTIP 11vol%, (e) calcined PAN 8wt%/TTIP 15.5vol% and (f) calcined PAN 8wt%/TTIP 20vol% – All ethanol solvent.

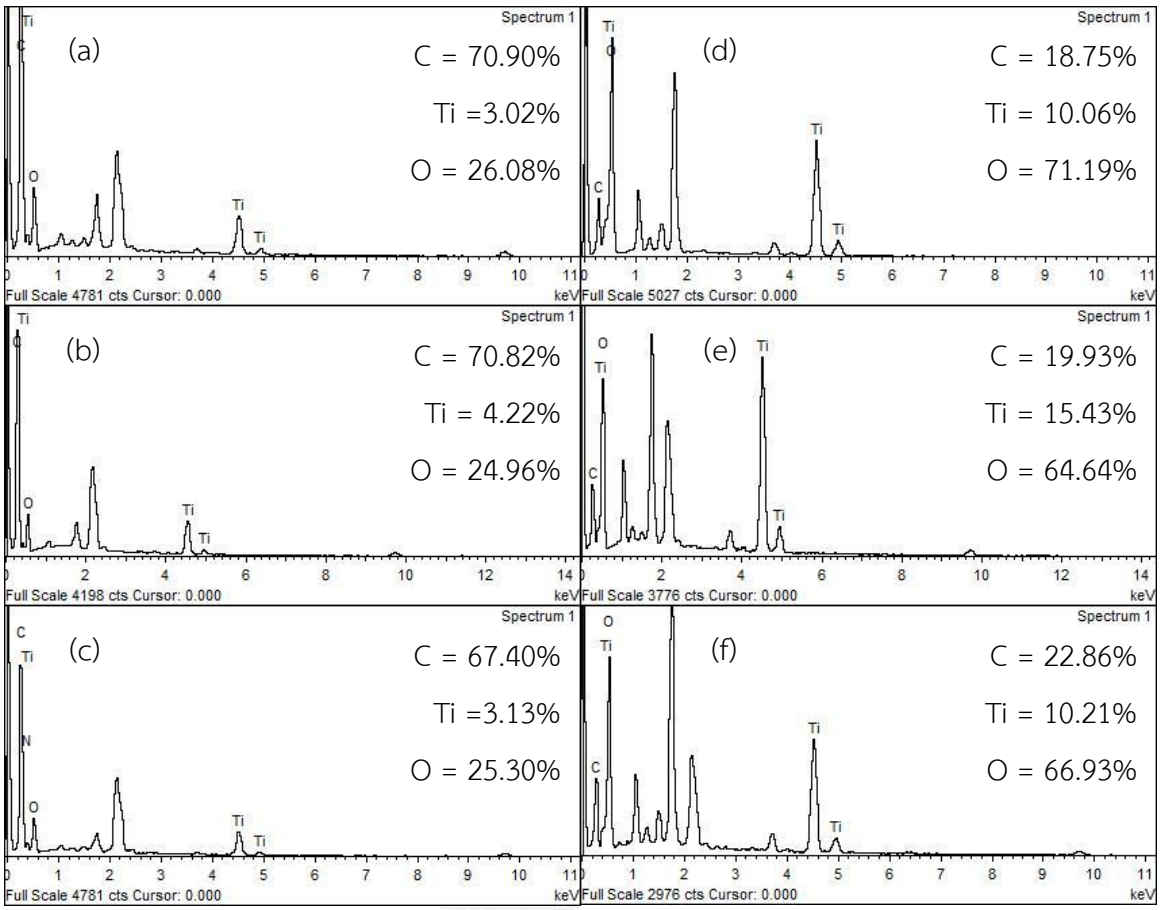

Figure D.5. EDX patterns and atomic percentage of resultant core/sheath films (a) PAN 8wt%/age 0 min, (b) PAN 8wt%/age 15 min, (c) PAN 8wt%/age 30 min, (d) calcined PAN 8wt%/age 0 min, (e) calcined PAN 8wt%/age 15 min and (f) calcined PAN 8wt%/age 30 min – All DMF solvent.

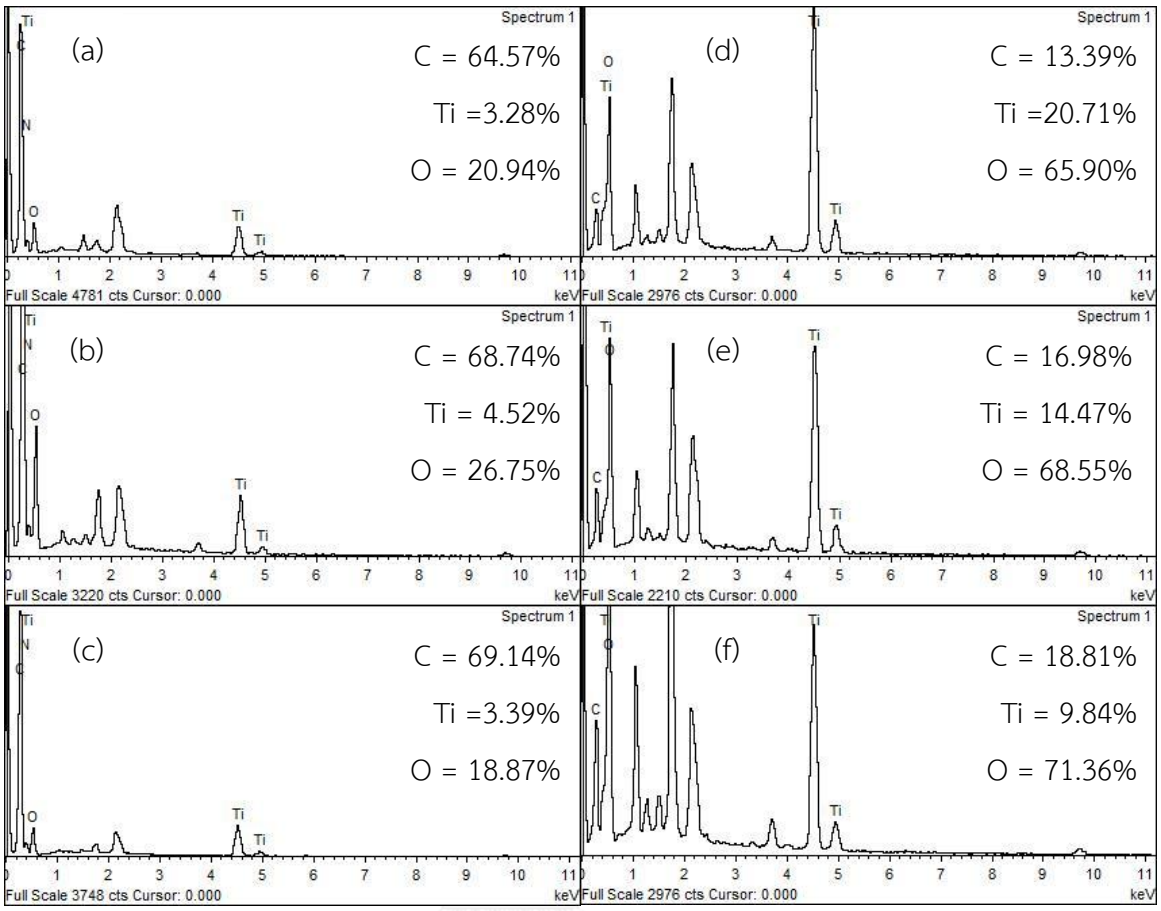

Figure D.6. EDX patterns and atomic percentage of resultant core/sheath films (a) PAN 8wt%/age 0 min, (b) PAN 8wt%/age 15 min, (c) PAN 8wt%/age 30 min, (d) calcined PAN 8wt%/age 0 min, (e) calcined PAN 8wt%/age 15 min and (f) calcined PAN 8wt%/age 30 min – All ethanol solvent.

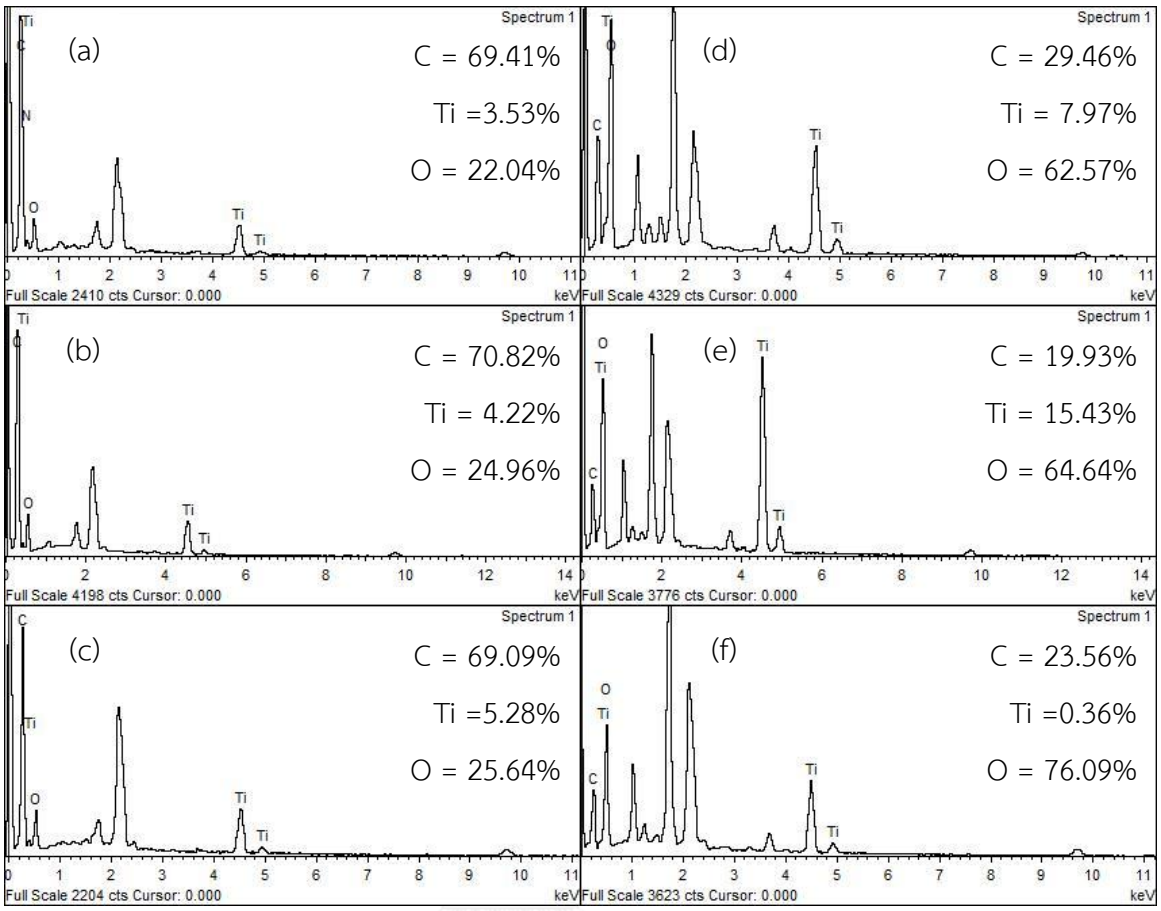

Figure D.7. EDX patterns and atomic percentage of resultant core/sheath films (a) PAN 8wt%/3 V, (b) PAN 8wt%/5 V, (c) PAN 8wt%/7 V, (d) calcined PAN 8wt%/3 V, (e) calcined PAN 8wt%/5 V and (f) calcined PAN 8wt%/7 V – All DMF solvent.

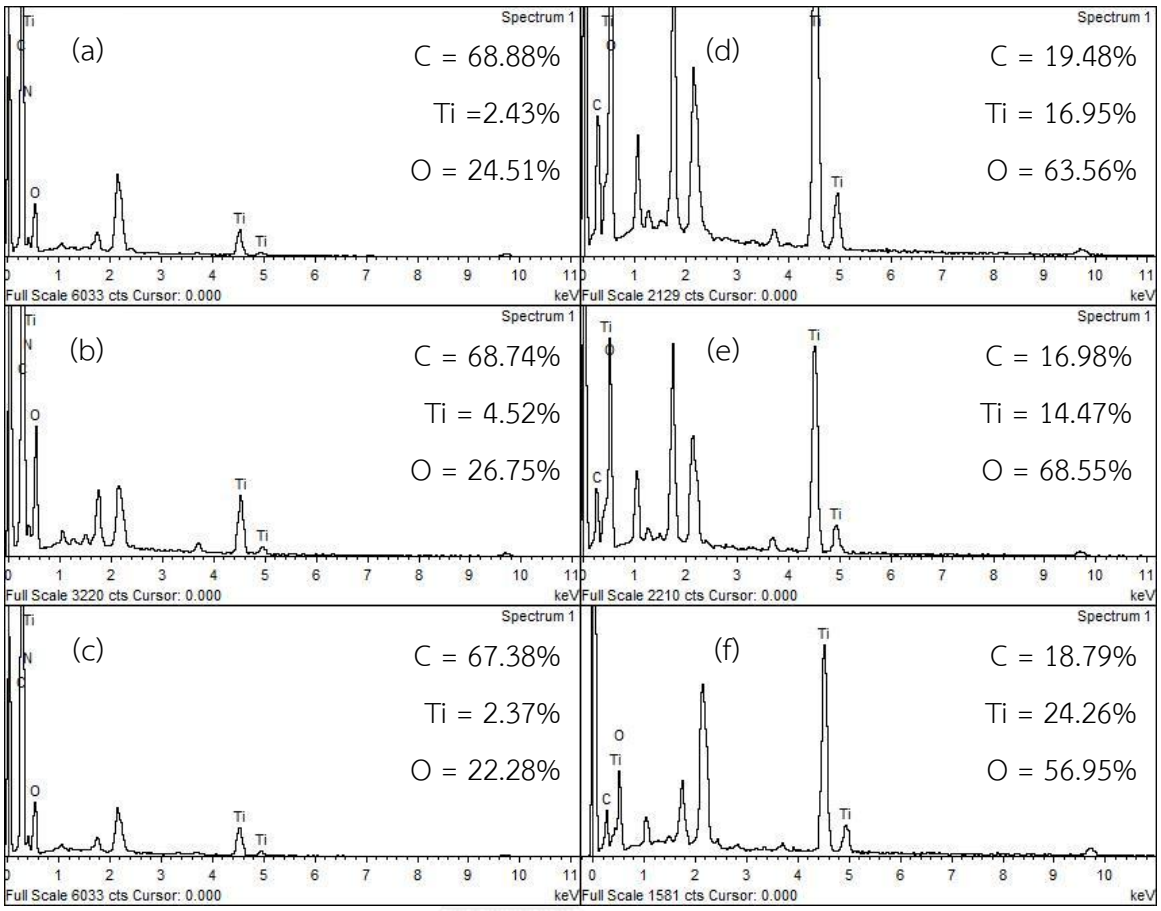

Figure D.8. EDX patterns and atomic percentage of resultant core/sheath films (a) PAN 8wt%/3 V, (b) PAN 8wt%/5 V, (c) PAN 8wt%/7 V, (d) calcined PAN 8wt%/3 V, (e) calcined PAN 8wt%/5 V and (f) calcined PAN 8wt%/7 V – All ethanol solvent.

APPENDIX E

LIST OF PUBLICATION

Veronica Winoto, Varong Pavarajarn, “Interaction at the Core/Sheath Interface in TiO_2-PVP/PAN Flexible Nanofibers”, The 3rd Joint Conference on Renewable Energy and Nanotechnology (JCREN) 2014, Mahidol University, Kanchanaburi Campus, Kanchanaburi, Thailand, December 21-23, 2014.

Interaction at the Core/Sheath Interface in TiO_2-PVP/PAN Flexible Nanofibers

Veronica Winoto and Varong Pavarajarn*
Center of Excellence in Particle Technology, Faculty of Engineering,
Chulalongkorn University, Bangkok, THAILAND
* Corresponding author: Varong.P@chula.ac.th

Abstract

Flexible polyacrylonitrile (PAN)/titanium dioxide (TiO_2) photocatalyst in a form of nanofiber can be fabricated from co-axially electrospun TiO_2-poly vinyl pyrolidone (PVP)/PAN core/sheath fibers. However, interaction at the core/sheath interface greatly affects properties of the final product. In this work, such interaction was investigated. In the fabrication of the TiO_2-PVP/PAN nanofiber, a solution of PAN in N,N'-dimethylformamide (DMF) was supplied to the center of a coaxial electrospinning nozzle, while a mixture of PVP, titanium (IV) isopropoxide (TTIP), acetic acid in DMF or ethanol was fed into the annulus of the nozzle. The electrical potential of 25 kV was applied to initiate the electrospinning of the fibers. The resultant fibers were characterized by Transmission electron microscope (TEM), Scanning electron microscopy with energy-dispersive x-ray (SEM-EDX) and Fourier transform infrared spectroscopy (FTIR).

1. Introduction

TiO_2 is one of the most common semiconductor photocatalysts. It has been used in many forms including nanoparticles, thin film and nanofibers. The use of TiO_2 in the form of nanofiber has an advantage in the ease of the removal of the catalyst from the fluid after being used. Unfortunately, TiO_2 nanofibers are easily crumbled into powder after repeated use. Recently, our group proposed a novel approach to fabricate flexible TiO_2 nanofiber using co-axial electrospinning [1]. PAN was used as core of the fiber because PAN can withstand high temperature required for phase transformation of TiO_2 to anatase form, while PVP was used as a spinning aid in the sheath side. Unfortunately, PAN can be dissolved only in limited number of polar solvents such as DMF [2]. On the other hand, PVP is compatible with wider range of solvent including DMF and ethanol. Using the same solvent in both core and sheath parts during electrospinning may result in transfer of TiO_2 sol from the sheath into the core, which renders TiO_2 to be ineffective as the photocatalyst. However, using different solvent may cause rapid solidification of PAN, hence inhibits electrospinning. This work therefore focuses on an interaction at core/sheath interface so that fabrication of the flexible TiO_2 nanofiber can be improved.

2. Experimental

2.1 Preparation of electrospinning solutions

In the co-axial electrospinning, core and sheath solutions are supplied to the electrospinning nozzle separately. In this work, the core solution was prepared by mixing PAN in DMF and stirred at 60°C until the mixture became homogeneous. The concentration of PAN was fixed at 8%wt. To prepare the sheath solution, 10%wt PVP solution in either ethanol or DMF was first prepared in similar manner as the PAN solution. At the same time, 3 ml of TTIP, 6 ml of acetic acid and 6 ml of the solvent were mixed for 15 min. The PVP solution were then mixed with the TTIP solution

and further stirred at room temperature for another 70 min. It should be noted that when ethanol was used as solvent, amount of PVP, TTIP, ethanol and acetic acid were adjusted to 13%wt, 1.6 ml, 10.5 ml and 3 ml, respectively.

2.2 Fabrication of core/sheath nanofibers

Both core and sheath solutions were separately supplied to a co-axial nozzle via syringe pumps. A high voltage power supply with electric potential of 25 kV was connected to the nozzle, while a grounding electrode was connected to a collector drum rotating at 400 rpm. The distance between the nozzle and the collector was fixed at 25 cm. The obtained fibers were calcined in a furnace at 500°C for 2 hr, with a heating rate of 10°C/min. The core/sheath structure of both as-spun and calcined nanofibers was investigated by TEM.

2.3 Investigation of interaction

Interaction between the core solution and the sheat solution was investigated by spin coating one solution on top of the other. Before the spin coating, a glass slide was sonicated and cleaned with deionized water, ethanol 95.5% and acetone. Morphology of the film as well as the qualitative elemental information were investigated by SEM-EDX. The change in chemical functional group as a result of the interaction was identified using FTIR.

3. Results and Discussion

The structures of core/sheath nanofibers observed by transmission electron microscope (TEM) are shown in **Fig. 1.** All resultant nanofibers were confirmed to be core/sheath structure. The rough surface was found in as-spun nanofiber formed when ethanol was used as solvent in sheath solution (Fig. 1d). After calcination, the surface of the nanofiber becomes smooth (see Fig. 1e-f). It should be noted that the type of solvent in the sheath solution does not significantly affect diameter of the obtained fibers. Nevertheless, the electrospinning condition was fixed in this work.

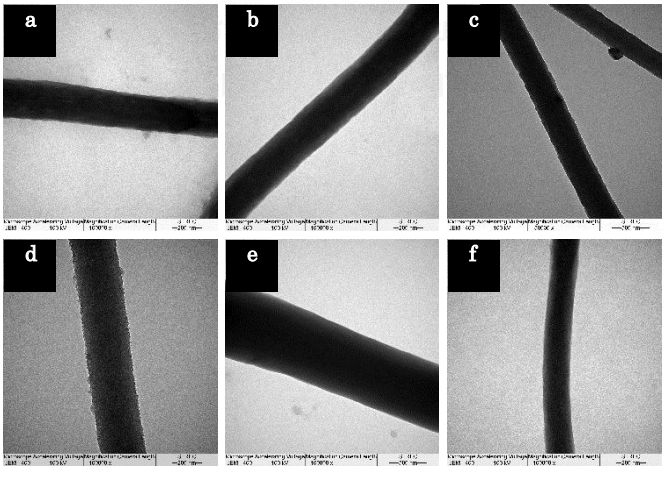

Fig. 1 TEM micrographs of: (a) as-spun fiber formed by using DMF as the solvent in sheath solution; (b) the fiber in a) after being calcined using heating rate of 10°C/min; (c) the fiber in a) after being calcined using heating rate of 60°C/min; (d) as-spun fiber formed by using ethanol as the solvent in sheath solution; (e) the fiber in d) after being calcined using heating rate of 10°C/min; (f) the fiber in d) after being calcined using heating rate of 60°C/min.

Morphology and elemental mapping of the cross-sectioned films of the core

solution and the sheath solution are shown **Fig. 2**. The films in Fig. 2a, 2b and 2d become uniformly one layer, while the films in Fig. 2c and 2e are divided into two separated layers. The separation is clearer in Fig. 2e, whereas ethanol was used as the solvent in the sheath layer. The Ti signal in Fig. 2e shows that TiO_2 sols from the sheath solution can disperse into the layer of core solution although the solvents in the core and the sheath layers are different. Nevertheless, it should be noted that the interaction between PAN and ethanol is strong, which causes rapid solidification of PAN and results in very rough surface (Fig. 2f).

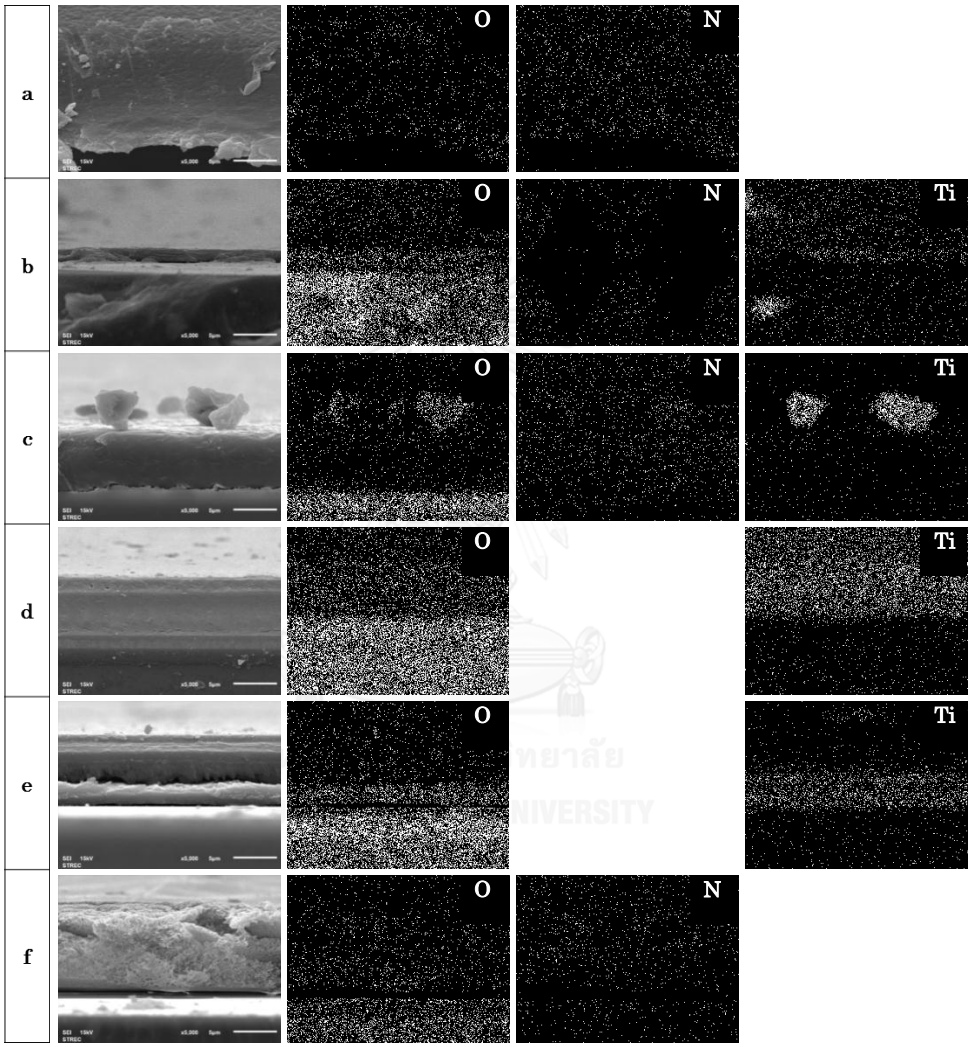

Fig. 2 Morphology and elemental mapping of different spin coating films formed by: (a) core solution; (b) sheath solution using DMF as solvent; (c) solution in b) on top of solution in a); (d) sheath solution using ethanol as solvent; (e) solution in d) on top of solution in a); (f) ethanol on top of solution in a).

The chemical interaction between the core and sheath solutions were also observed by Fourier transform infrared spectroscopy (FTIR) as shown in **Fig. 3**. The FTIR spectra of the core solution shows a signal corresponding to C≡N groups at wavenumber around 2242 cm^{-1} [5]. The C=C groups are shown at wavenumber 1635 cm^{-1} [6]. The bands at wavenumber around 1439, 1388, 1257, 1063 and 865 cm^{-1} are assigned to CH_3 asymmetric deformation mode, N-C-H bending mode, C-N asymmetric stretching, CH_3 rocking mode and C-N symmetric stretching,

respectively [7]. The spectra of core/sheath mixture and sheath solution with DMF as the solvent present the same bands as the core solution at wavenumber 1388, 1257, 1063 and 865 cm^{-1}. After mixing the core solution and the sheath solution with ethanol as the solvent, the mixture separates into two phases, i.e., solid and liquid phases, immediately. The spectra of the solid phase shows the bands at wavenumber around 1257, 1093, 1063, 866 and 659 cm^{-1} which can be assigned to C-N asymmetric stretching, CH_3 rocking mode (for 1093 and 1063 cm^{-1}), C-N symmetric stretching and O=C-N stretching mode. On the other hand, the liquid phase shows the bands at wavenumber around 2960, 1660, 1439 and 1257 cm^{-1} which are assigned to stretching and bending vibrations of C-H bonds [5], C=O stretching [6], CH_3 asymmetric deformation and C-N symmetric stretching [7].

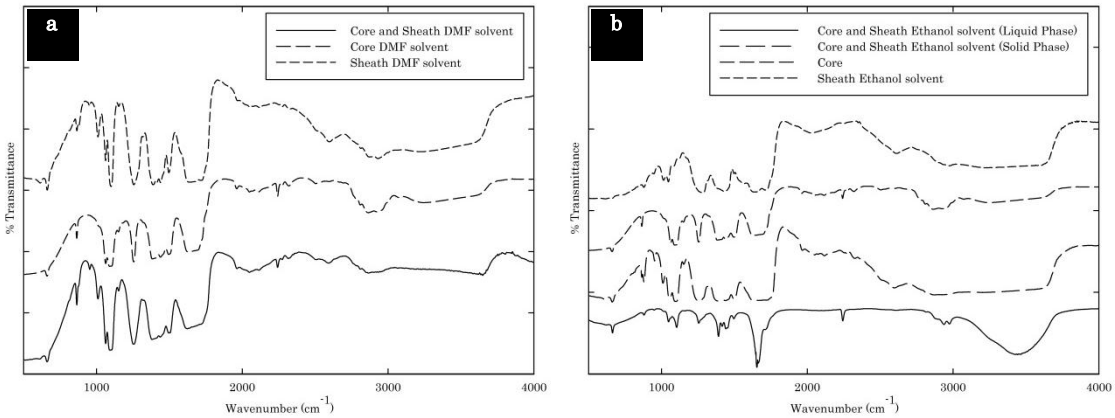

Fig. 3 The FTIR spectra of core solution with different sheath solvent solution: (a) DMF as solvent for sheath solution; (b) ethanol as solvent for sheath solution.

4. Conclusion

The results show that although ethanol is a good solvent for PVP, its interaction with PAN is too strong to cause rapid solidification at the core/sheath interface, which prevents electrospinning of the fibers. Therefore, sheath solution with DMF solvent is more stable and compatible with core solution.

References

[1] Duriyasart, F.; Masayoshi, F.; Takashi, S.; Chika, T.; Pavarajarn, V., The 4th KKU International Engineering Conference, May 10-12, 2012, Khon Kaen, Thailand.

[2] Nataraj, S.K.; Yang, K.S.; Aminabhavi, T.M., Progress in Polymer Science, **37**, 487-513 (2012)

[3] Cheng, C.; Wu, J.; Xiao, Y.; Chen, Y.; Fan, L.; Huang, M.; Ling, J.; Wang, J.; Tang, Z.; Yue, G., Electrochimica Acta, **56**, 7256-7260 (2011)

[4] Biswas, A.; Park, H.; Sigmund, W.M., Ceramics International, **38**, 883-886 (2012)

[5] Govindaraj, P.; Kandasubramanian, B.; Kodam, K.M., Materials Chemistry and Physics, **147**, 934-941 (2014)

[6] Ouyang, Q.; Cheng, L.; Wang, H.; Li, K., Polymer Degradation and Stability, **93**, 1415-1421 (2008)

[7] Jacob, M.M.E.; Arof, A.K., Electrochimica Acta, **45**, 1701-1706 (2000)

VITA

Miss Veronica Winoto was born in April, 20th 1991 in Jakarta, Indonesia. She finished her high school from Sai Nam Pheung, Bangkok in 2009. She graduated the Bachelor's Degree in Chemical Engineering from Thammasat University, Rangsit Campus, Pathumthani in 2013. She continued her Master study in Chemical Engineering at Chulalongkorn University, Bangkok, Thailand in 2013.